Published for SISSA by Springer

Received: *September 15, 2017*
Revised: *February 5, 2018*
Accepted: *March 18, 2018*
Published: *March 27, 2018*

Search for electroweak production of charginos and neutralinos in multilepton final states in proton-proton collisions at $\sqrt{s} = 13\,\text{TeV}$



The CMS collaboration

E-mail: cms-publication-committee-chair@cern.ch

Abstract: Results are presented from a search for the direct electroweak production of charginos and neutralinos in signatures with either two or more leptons (electrons or muons) of the same electric charge, or with three or more leptons, which can include up to two hadronically decaying tau leptons. The results are based on a sample of proton-proton collision data collected at $\sqrt{s} = 13\,\text{TeV}$, recorded with the CMS detector at the LHC, corresponding to an integrated luminosity of $35.9\,\text{fb}^{-1}$. The observed event yields are consistent with the expectations based on the standard model. The results are interpreted in simplified models of supersymmetry describing various scenarios for the production and decay of charginos and neutralinos. Depending on the model parameters chosen, mass values between 180 GeV and 1150 GeV are excluded at 95% CL. These results significantly extend the parameter space probed for these particles in searches at the LHC. In addition, results are presented in a form suitable for alternative theoretical interpretations.

Keywords: Hadron-Hadron scattering (experiments), Supersymmetry

ArXiv ePrint: 1709.05406

Open Access, Copyright CERN,
for the benefit of the CMS Collaboration.
Article funded by SCOAP^3.

https://doi.org/10.1007/JHEP03(2018)166

JHEP03(2018)166

Contents

1 Introduction 1

2 Supersymmetric models 2

3 The CMS detector 5

4 Event selection and Monte Carlo simulation 5

5 Search strategy 8
- 5.1 Two same-sign dilepton category 8
- 5.2 Three or more leptons 9
  - 5.2.1 Three light leptons (signal regions A and B) 10
  - 5.2.2 Three leptons with at least one τ_h (signal regions C to F) 11
  - 5.2.3 More than three leptons (signal regions G to K) 12
- 5.3 Aggregated signal regions 14

6 Backgrounds 14

7 Systematic uncertainties 16

8 Results 19

9 Interpretations of the searches 31

10 Summary 38

The CMS collaboration 44

JHEP03(2018)166

1 Introduction

The standard model (SM) describes the vast majority of particle physics phenomena. So far, it has withstood a multitude of challenges from precision measurements. Searches for physics beyond the SM carried out by various experiments also have not revealed convincing evidence for the existence of such phenomena. A recent triumph of the SM is the 2012 discovery of a Higgs boson (H) by the ATLAS and CMS Collaborations at the CERN LHC [1–3]. However, there are several open challenges that cannot be explained by the SM, such as the hierarchy problem [4–6] (and fine tuning), and the absence of a dark matter candidate. Supersymmetry (SUSY) [7–15] is an extension of the SM that introduces an additional symmetry between bosons and fermions, and predicts superpartners, or "sparticles", to the SM particles. This extension offers a solution to several limitations of the SM,

including those cited above. In particular, in the case of conserved R-parity [12], SUSY particles are created in pairs, and the lightest SUSY particle (LSP) is stable, making it a possible dark matter candidate. Furthermore, the existence of relatively light superpartners can lead to the cancellation of the large quantum corrections to the Higgs boson mass, addressing the hierarchy problem.

Thus far, no evidence for such new particles has been found. Constraints have been placed on the masses of the colored superpartners (squarks and gluinos) ranging from several hundred GeV to about 2 TeV, depending on the assumptions entering into the models used for the interpretation of the results [16, 16–20]. The cross sections associated with electroweak production of SUSY particles are far lower than those for strong production. This directly translates into significantly lower exclusion limits, ranging from about 100 to 700 GeV [21–24] on the masses of sparticles produced exclusively via the electroweak interaction. This would be the dominant production mechanism of sparticles if the colored superpartners are too heavy to be produced.

This paper describes a search for direct production of charginos and neutralinos, mixtures of the SUSY partners of the electroweak gauge and Higgs bosons, decaying to two, three, or more charged leptons, and significant missing transverse momentum ($p_{\mathrm{T}}^{\mathrm{miss}}$). In events with two light leptons (electrons or muons), the leptons are required to have the same charge; in events with three or more leptons, up to two may be hadronically decaying tau leptons (τ_{h}). We use a data sample of pp collisions recorded during 2016 with the CMS detector corresponding to an integrated luminosity of 35.9 fb^{-1}. Similar searches have been reported by the CMS and ATLAS collaborations for the lower-energy LHC Run 1 [21–23].

2 Supersymmetric models

This search targets scenarios of direct electroweak production of charginos $\widetilde{\chi}_1^{\pm}$ and neutralinos $\widetilde{\chi}_2^0$, which decay into final states containing two, three, or four charged leptons ($\mathrm{e}^{\pm}, \mu^{\pm}, \tau^{\pm}$). The results are interpreted using simplified models [24, 25]. In such models, the masses and the decay modes of the relevant particles are the only free parameters.

In the case of $\widetilde{\chi}_1^{\pm}\widetilde{\chi}_2^0$ production, the $\widetilde{\chi}_1^{\pm}$ and $\widetilde{\chi}_2^0$ are assumed to be mass-degenerate and wino-like, i.e. superpartners of the $\mathrm{SU}(2)_L$ gauge fields, and the $\widetilde{\chi}_1^0$ is set to be bino-like, i.e. a superpartner of the $\mathrm{U}(1)_Y$ gauge field [26]. The masses of the pure wino-like and bino-like gauginos are governed by two complex gaugino Majorana mass parameters, M_2 and M_1, and can assume any values. In this scenario, the $\widetilde{\chi}_1^0$ is the lightest SUSY particle (LSP).

For the effective $\widetilde{\chi}_1^0\widetilde{\chi}_1^0$ production, the $\widetilde{\chi}_2^0$, $\widetilde{\chi}_1^{\pm}$, and $\widetilde{\chi}_1^0$ are assumed to be higgsino-like, i.e. are superpartners of the Higgs doublets. In this case, scenarios in which the $\widetilde{\chi}_1^0$ is next-to-LSP (NLSP) are considered.

Production of $\widetilde{\chi}_1^{\pm}\widetilde{\chi}_2^0$ with 2-body decays through sleptons. In the first scenario considered, the charginos and neutralinos decay to leptons via intermediate sleptons or sneutrinos, the SUSY partners of charged leptons and neutrinos, as shown in figure 1. The combination of gauge eigenstates that make up the neutralinos, charginos, and their masses, will determine whether their decays through sleptons and sneutrinos (which are

JHEP03(2018)166

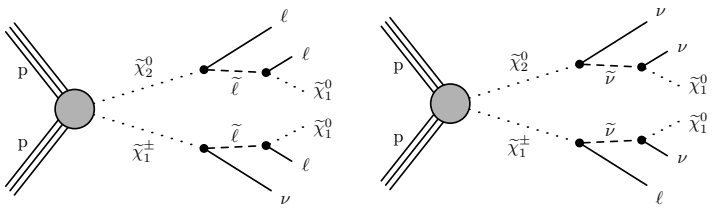


Figure 1. Chargino and neutralino pair production with decays mediated by sleptons and sneutrinos.

assumed to be mass-degenerate) lead to all three lepton flavors with equal probability, or if they prefer to decay to τ leptons. Three different scenarios for the decays are considered:

- $\widetilde{\chi}_1^\pm\widetilde{\chi}_2^0$ production with $\widetilde{\ell}_L$-mediated decays: the chargino and neutralino decay via sleptons or sneutrinos to all lepton flavors with the same branching fraction ("flavor-democratic" scenario). As the decay through sleptons or sneutrinos happens with equal probability, only 50% of the decays will lead to three-lepton final states.

- $\widetilde{\chi}_1^\pm\widetilde{\chi}_2^0$ production with $\widetilde{\ell}_R$-mediated decays: in this case, because the $\widetilde{\ell}_R$ couples to the chargino via its higgsino component, chargino decays to $\widetilde{\ell}_R$ strongly favor the production of a τ lepton ("τ-enriched" scenario). The neutralino still decays to all three flavors. In this model, both left-handed sleptons and sneutrinos are considered to be heavy and decoupled; they do not participate in this process.

- $\widetilde{\chi}_1^\pm\widetilde{\chi}_2^0$ production with $\widetilde{\tau}$-mediated decays: the first- and second-generation sleptons and sneutrinos are decoupled and the chargino and neutralino only decay via a $\widetilde{\tau}_R$. We will refer to this model as the "τ-dominated" scenario. Left-handed sleptons and sneutrinos are considered to be heavy and decoupled; they do not participate in this process.

In these simplified models, the slepton mass is assumed to lie between the common $\widetilde{\chi}_1^\pm$ and $\widetilde{\chi}_2^0$ masses, and that of the $\widetilde{\chi}_1^0$. In addition, the branching fraction to leptons is taken to be 100%. Three different mass assumptions are considered: $m_{\widetilde{\ell}} = m_{\widetilde{\nu}} = m_{\widetilde{\chi}_1^0} + x\,(m_{\widetilde{\chi}_2^0} - m_{\widetilde{\chi}_1^0})$, with $x = 0.05$, 0.5 and 0.95. When $x = 0.05$ or 0.95, one of the three leptons is very soft and may escape detection. The same-sign (SS) final state is used in these cases to recover some of these events without the penalty of increasing the SM background.

Production of $\widetilde{\chi}_1^\pm\widetilde{\chi}_2^0$ with 2-body decays to W, Z, and Higgs bosons. In the second scenario, we assume that the sleptons are too heavy and that the $\widetilde{\chi}_1^\pm$ and $\widetilde{\chi}_2^0$ undergo direct decay to the LSP via the emission of a W boson, Z boson, or Higgs boson as depicted in figure 2. The chargino decays to a W and the $\widetilde{\chi}_1^0$, while the neutralino can decay either to a Z or a Higgs boson and the $\widetilde{\chi}_1^0$. The Higgs boson is expected to have SM-like properties and branching fraction if all the other Higgs bosons are much heavier [15]. If the Higgs boson decays to WW, ZZ, or $\tau\tau$, and each W or Z decays leptonically, one can expect multiple leptons in the final state. However, compared to the other models included in this

JHEP03(2018)166

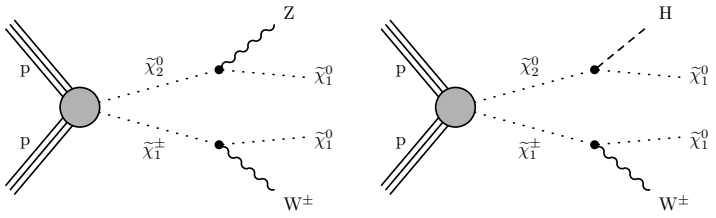


Figure 2. Chargino and neutralino pair production with the chargino decaying to a W boson and the LSP and the neutralino decaying to (left) a Z boson and the LSP or (right) a Higgs boson and the LSP.

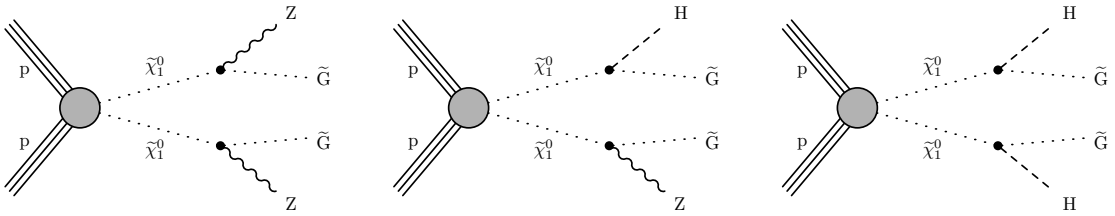


Figure 3. A GMSB model with higgsino pair production. The $\widetilde{\chi}_2^0$, $\widetilde{\chi}_1^\pm$, and $\widetilde{\chi}_1^0$ are nearly mass-degenerate with $\widetilde{\chi}_1^0$ decaying to Z or Higgs bosons and $\widetilde{G}$ LSP.

analysis, the leptonic branching fractions are rather small, namely 3.3% for WZ to three leptons and 2.9% for WH to three leptons, including taus.

Production of $\widetilde{\chi}_1^0\widetilde{\chi}_1^0$ in models with four higgsinos. Finally we consider the production of pairs of neutralinos that decay via a Z or a Higgs boson. As for the pair of neutralinos ($\widetilde{\chi}_2^0\widetilde{\chi}_2^0$ or $\widetilde{\chi}_1^0\widetilde{\chi}_1^0$) the production cross section is vanishingly small [27–29], we consider a specific gauge-mediated SUSY breaking (GMSB) model with four higgsinos ($\widetilde{\chi}_2^0$, $\widetilde{\chi}_1^\pm$, $\widetilde{\chi}_1^0$) and an effectively massless gravitino $\widetilde{G}$ as the LSP [30–32].

The cross sections for higgsino pair production are computed at NLO plus next-to-leading-log (NLL) precision in a limit of mass-degenerate higgsino states $\widetilde{\chi}_2^0$, $\widetilde{\chi}_1^\pm$, and $\widetilde{\chi}_1^0$, with all the other sparticles assumed to be heavy and decoupled. Following the convention of real mixing matrices and signed neutralino masses [33], we set the sign of the mass of $\widetilde{\chi}_1^0$ ($\widetilde{\chi}_2^0$) to +1 (−1). The lightest two neutralino states are defined as symmetric (anti-symmetric) combinations of higgsino states by setting the product of the elements N_{i3} and N_{i4} of the neutralino mixing matrix N to +0.5 (−0.5) for $i = 1$ (2). The elements U_{12} and V_{12} of the chargino mixing matrices U and V are set to 1.

Since the $\widetilde{\chi}_2^0$, $\widetilde{\chi}_1^\pm$, and $\widetilde{\chi}_1^0$ are nearly mass degenerate, the heavier higgsinos $\widetilde{\chi}_1^\pm$ and $\widetilde{\chi}_2^0$ decay to the $\widetilde{\chi}_1^0$ via soft particles which escape detection. Therefore the sum of the various possible production processes of higgsinos ($\widetilde{\chi}_1^\pm\widetilde{\chi}_2^0$, $\widetilde{\chi}_1^0\widetilde{\chi}_2^0$, $\widetilde{\chi}_1^\pm\widetilde{\chi}_1^\mp$, $\widetilde{\chi}_1^\pm\widetilde{\chi}_1^0$) describes an effective $\widetilde{\chi}_1^0\widetilde{\chi}_1^0$ production mechanism at the LHC. In the considered scenario, each $\widetilde{\chi}_1^0$ promptly decays to a Z or a Higgs boson and the gravitino LSP. Different final states depending on the assumptions on the NLSP are possible, as shown in figure 3.

JHEP03(2018)166

3 The CMS detector

The central feature of the CMS apparatus is a superconducting solenoid of 6 m internal diameter, providing a magnetic field of 3.8 T. Within the solenoid volume are a silicon pixel and strip tracker, a lead tungstate crystal electromagnetic calorimeter, and a brass scintillator hadron calorimeter, each composed of a barrel and two endcap sections. Forward calorimeters extend the pseudorapidity (η) [34] coverage provided by the barrel and endcap detectors. Muons are measured in gas-ionization detectors embedded in the steel flux-return yoke outside the solenoid. The first level of the CMS trigger system, composed of custom hardware processors, uses information from the calorimeters and muon detectors to select events of interest in a fixed time interval of less than 4 μs. The high-level trigger processor farm further decreases the event rate from around 100 kHz to around 1 kHz, before data storage. A more detailed description of the CMS detector, together with a definition of the coordinate system used and the relevant kinematic variables, can be found in ref. [34].

4 Event selection and Monte Carlo simulation

The events are recorded if they satisfy the requirements of the CMS two-level trigger system. As we consider different lepton multiplicities in the final state, a combination of several trigger algorithms is required to cover all possible cases and to maximize the acceptance. Events with at least two light-flavor leptons (e or μ) rely mostly on dilepton triggers with transverse momentum (p_{T}) >23 (17) GeV for the leading electron (muon) and $p_{\mathrm{T}} > 12\,(8)$ GeV for the subleading electron (muon). For events with at least two leptons, the double lepton triggers are not fully efficient. Single lepton triggers are used to increase the acceptance for these events.

For the final state with two τ_{h}s and one electron or muon, we use single lepton triggers requiring an isolated e (μ) with $p_{\mathrm{T}} > 27\,(24)$ GeV. Typical trigger efficiencies for leptons satisfying the offline selection criteria described below are 98% (92%) per electron (muon). In final states with three or more leptons, the total trigger efficiency is close to 100%.

In the offline analysis, the information from all subdetectors is combined by the CMS particle-flow algorithm [35]. The particle flow algorithm provides a global interpretation of the event and reconstructs and identifies individual particles. The particles are classified into charged hadrons, neutral hadrons, photons, electrons, and muons.

We require electrons to have $|\eta| < 2.5$ to ensure that they are within the tracking volume, and $p_{\mathrm{T}} > 10$ GeV. The particle flow algorithm for electrons uses a multivariate discriminant, built from variables that characterize the shower shape and track quality [36]. To exclude electrons from photon conversions, we reject candidates that have missing measurements in the innermost layers of the tracking system or are matched to a secondary conversion vertex candidate [36].

Muon candidates are reconstructed by combining the information from the silicon tracker and the muon spectrometer in a global fit [37]. An identification selection is performed using the quality of the geometrical matching between the tracker and the muon

JHEP03(2018)166

system measurements. Only muons within the muon system acceptance $|\eta| < 2.4$ having a minimum p_{T} of 10 GeV are considered.

Light lepton candidates are required to be consistent with originating from the primary vertex, defined as the one with the largest p_{T}^2 sum of the tracks pointing to that vertex [38]. The transverse impact parameter d_0 of a lepton track with respect to this vertex must not exceed 0.5 mm, and the longitudinal displacement d_z of that impact point must not exceed 1.0 mm. Additionally they must satisfy a requirement on the impact parameter significance $S_{\mathrm{IP3D}} \equiv |d_{\mathrm{3D}}|/\sigma(d_{\mathrm{3D}}) < 8$, where d_{3D} is the three-dimensional displacement with respect to the primary vertex and $\sigma(d_{\mathrm{3D}})$ is its uncertainty as estimated from the track fit. Furthermore, leptons are required to be isolated. An isolation variable I_{mini} [39, 40] is computed as the ratio of the scalar p_{T} sum of charged hadrons, neutral hadrons, and photons within a cone around the lepton candidate direction at the vertex to the transverse momentum $p_{\mathrm{T}}(\ell)$ of the lepton candidate. The cone radius $\Delta R = \sqrt{(\Delta\eta)^2 + (\Delta\phi)^2}$ (where ϕ is the azimuthal angle in radians) depends on $p_{\mathrm{T}}(\ell)$ as:

$$\Delta R\left(p_{\mathrm{T}}(\ell)\right) = \frac{10\,\mathrm{GeV}}{\min\left[\max\left(p_{\mathrm{T}}(\ell), 50\,\mathrm{GeV}\right), 200\,\mathrm{GeV}\right]}. \tag{4.1}$$

The varying isolation cone definition takes into account the increased collimation of the decay products of a particle as its p_{T} increases, and it reduces the inefficiency from accidental overlap between the lepton and other objects in an event. Loosely isolated leptons are required to have $I_{\mathrm{mini}} < 0.4$. Electrons and muons that pass all the aforementioned requirements are referred to as *loose* in this analysis.

In order to discriminate between leptons ("prompt" leptons) originating from decays of heavy particles, such as W and Z bosons, or SUSY particles, and those produced in hadron decays or in photon conversions, as well as misidentified hadrons ("nonprompt" leptons), we use a multivariate discriminator based on a boosted decision tree (BDT) [41, 42]. This BDT takes the following variables as inputs: d_0, d_z, S_{IP3D}, and I_{mini}; variables related to the jet closest to the lepton, such as the ratio between the p_{T} of the lepton and the p_{T} of the jet ($p_{\mathrm{T}}^{\mathrm{ratio}}$), the b tagging discriminator value of the jet, the number of charged particles in the jet, and the $p_{\mathrm{T}}^{\mathrm{rel}}$ variable:

$$p_{\mathrm{T}}^{\mathrm{rel}} = \frac{|(\vec{p}(\mathrm{jet}) - \vec{p}(\ell)) \times \vec{p}(\ell)|}{|\vec{p}(\mathrm{jet}) - \vec{p}(\ell)|}. \tag{4.2}$$

Other identification variables, such as the muon segment compatibility and the electron identification multivariate discriminant are also included. The BDT is trained using simulation with prompt leptons from $\mathrm{t\bar{t}Z}$ and with nonprompt leptons from $\mathrm{t\bar{t}}$ processes. Leptons satisfying a requirement on this discriminant in addition to the loose requirements are referred to as *tight* leptons. Two working points are defined, one with higher efficiency for the three or more lepton channel and one with high nonprompt background rejection for the SS dilepton channel. The identification efficiency measured in data for electrons passing tight criteria varies between 40 (20)% for tracks with $p_{\mathrm{T}} < 20\,\mathrm{GeV}$ in the barrel (endcap) region and the plateau efficiency of 90 (80)% for those with $p_{\mathrm{T}} > 50\,\mathrm{GeV}$ in the barrel (endcap) region, while the misidentification rate for non-prompt electrons is between

JHEP03(2018)166

3% and 7% depending on the p_T. For muons, the efficiency is between 82% for $p_T < 20\,\text{GeV}$ and 100% for $p_T > 40\,\text{GeV}$, the misidentification rate for non-prompt muons goes from 2% up to 10% depending on p_T.

The τ_h candidates are reconstructed with the hadron-plus-strips algorithm [43]. They are required to pass the "decay mode finding" discriminator [43], selecting one- or three-prong decay modes, with or without additional π^0 particles. In addition, they must fulfill $p_T > 20\,\text{GeV}$, $|\eta| < 2.3$, and isolation requirements computed in a cone defined by $\Delta R = 0.5$ centered on the τ_h direction. The typical τ_h identification efficiency of these selection requirements is 50%, while the jet misidentification rate is well below 0.1% [44].

Particle-flow candidates are clustered into jets using the anti-k_T algorithm [45] with a distance parameter of 0.4, as implemented in the FastJet package [46, 47]. Jets are required to satisfy quality requirements [48] to remove those likely arising from anomalous energy deposits. Charged hadrons are not considered if they do not originate from the selected primary vertex. After the estimated contribution of neutral particles from additional pp interactions in the same beam crossing (pileup) is subtracted by using the average p_T in the event per unit area [49], jet energies are corrected for residual nonuniformity and nonlinearity of the detector response using simulation and data [48, 50]. Only jets with $p_T > 25\,\text{GeV}$, $|\eta| < 2.4$, and separated from any lepton candidate by $\Delta R > 0.4$ are retained.

To identify jets originating from b quarks, the combined secondary vertex algorithm [51, 52] is used. Jets with $p_T > 25\,\text{GeV}$ and $|\eta| < 2.4$ are considered b quark jets ("b jets") if they satisfy the requirements of the medium working point of the algorithm. These requirements result in an efficiency of approximately 63% for tagging a bottom quark jet, and a mistagging rate of 1.5% for light-flavor jets, as measured in $\mathrm{t\bar{t}}$ events in data. Simulated events are corrected for the differences in the performance of the algorithm between data and simulation. Events with at least one identified b jet are rejected in the analysis to reduce the $\mathrm{t\bar{t}}$ background.

The missing transverse momentum p_T^{miss} is obtained as the magnitude of the negative vector sum $\vec{p}_T^{\text{miss}}$ of the transverse momenta of all reconstructed particle-flow candidates consistent with originating from the primary vertex and is further adjusted to account for jet energy corrections applied to the event [53]. This quantity is used in the definitions of the search regions presented in the following sections.

The Monte Carlo (MC) simulated samples, which include the effects of pileup, are used to estimate the background from SM processes with prompt leptons (see section 6) and to calculate the selection efficiency for various new-physics scenarios. The samples are reweighted to match the pileup profile in the data. The SM background samples are produced with the MadGraph5_aMC@NLO v2.2.2 or v2.3.3 generator [54] at leading-order (LO) [55] or next-to-leading-order (NLO) [56] accuracy in perturbative quantum chromodynamics, including up to one or two additional partons in the matrix element calculations. The exceptions are the diboson samples, which are produced with the powheg v2.0 [57, 58] generator without additional partons in the matrix element calculations. The NNPDF3.0LO [59] parton distribution functions (PDFs) are used for the simulated samples generated at LO and the NNPDF3.0NLO [59] PDFs for those generated at NLO. Parton showering and hadronization are described using the pythia 8.212 gener-

JHEP03(2018)166

ator [60] with the CUETP8M1 tune [61, 62]. A double counting of the partons generated with MadGraph5_aMC@NLO and those with pythia is removed using the MLM [55] and the FXFX [56] matching schemes, in the LO and NLO samples, respectively. The CMS detector response for the background samples is modelled with the Geant4 package [63].

Signal samples are generated with MadGraph5_aMC@NLO at LO precision, including up to two additional partons in the matrix element calculations. The NNPDF3.0LO [59] parton distribution functions (PDFs) are used. Parton showering and hadronization are modelled with pythia as described above. SUSY particles, are also modelled with pythia, while the detector simulation is performed with the CMS fast simulation package [64]. Any residual differences in the detector response description between the Geant4 and fast simulation are corrected for, with corresponding uncertainties in the signal acceptance taken into account.

5 Search strategy

This search is designed to target the scenarios described in section 2 of direct electroweak production of charginos $\widetilde{\chi}_1^{\pm}$ and neutralinos $\widetilde{\chi}_2^0$ leading to final states with either two, three, or four leptons and little hadronic activity. The specific strategy of the analysis is guided by the assumption that R-parity is conserved, hence leading to the presence of particles in the final states that evade detection, yielding a sizable $p_{\mathrm{T}}^{\mathrm{miss}}$.

The small cross section of the electroweak production drives the analysis design, which includes all the possible final states to enhance the discovery potential. Therefore, the analysis is subdivided into several categories defined by the number of leptons in the event, their flavors, and their charges. Each of these categories is further subdivided into bins defined by the kinematic variables that enhance the discrimination against SM backgrounds and the sensitivity to possible mass hierarchies of new particles.

Among the SM processes yielding the same final states as those targeted in this search there are WZ production, nonprompt leptons, external and internal (where the emitted photon is virtual) conversions, rare SM processes (i.e., multiboson production or single-boson production in association with a $\mathrm{t\bar{t}}$ pair), and charge misidentification. The dominant source of background varies depending on the considered category and thus the search strategy is tailored accordingly.

5.1 Two same-sign dilepton category

Although most of the targeted models naturally yield three charged lepton final states, for compressed-spectrum scenarios, e.g. when the mass splitting between the next-to-lightest SUSY particle and the LSP is small, one of the leptons from the decay chain of a neutralino can be very soft, such that it may not fulfill the selection requirements. By accepting events with two SS leptons, we recover some of these missing events while keeping the SM background under control.

We require two SS leptons with $p_{\mathrm{T}} > 25\,(20)$ GeV for the leading and $p_{\mathrm{T}} > 15\,(10)$ GeV for the trailing electron (muon), no third lepton with $p_{\mathrm{T}} > 20, 10, 20$ GeV (e,μ,τ) passing the tight identification criteria, and $p_{\mathrm{T}}^{\mathrm{miss}} > 60$ GeV. To suppress the dominant WZ background,

JHEP03(2018)166

N_{jets}	M_{T} (GeV)	$p_{\text{T}}^{\ell\ell}$ (GeV)	$p_{\text{T}}^{\text{miss}} < 100\,\text{GeV}$	$100 \leq p_{\text{T}}^{\text{miss}} < 150\,\text{GeV}$	$150 \leq p_{\text{T}}^{\text{miss}} < 200\,\text{GeV}$	$p_{\text{T}}^{\text{miss}} \geq 200\,\text{GeV}$
0	<100	<50	SS01	SS02 (++) SS03 (−−)	SS04	SS05
		>50	SS06	SS07 (++) SS08 (−−)	SS09	SS10
	>100		SS11	SS12 (++) SS13 (−−)	SS14	SS15
1	<100	<50	SS16	SS17 (++) SS18 (−−)	SS19	SS20
		>50	SS21	SS22 (++) SS23 (−−)	SS24	SS25
	>100		SS26	SS27 (++) SS28 (−−)	SS29	SS30

Table 1. Search regions for events with two SS light-flavor leptons.

events are vetoed if they contain an opposite-sign same-flavor (OSSF) pair formed from loose electrons or muons within a ±15 GeV window around the Z boson mass, taken to be 91 GeV. To reduce the contribution from the processes with low-mass resonances, events are vetoed if they contain an OSSF pair with an invariant mass below 12 GeV.

The events are first divided into two categories: with and without a jet of $p_{\text{T}} > 40$ GeV. Signal processes would populate the one-jet category when accompanied by initial-state radiation (ISR). In compressed scenarios where the electroweak production and decay of sparticles produces limited $p_{\text{T}}^{\text{miss}}$, the compensating boost to the sparticle system may raise the laboratory $p_{\text{T}}^{\text{miss}}$ above the selection threshold. Further binning is done in $p_{\text{T}}^{\text{miss}}$, the minimum transverse mass ($M_{\text{T}} = \sqrt{2p_{\text{T}}^{\text{miss}}p_{\text{T}}^{\ell}[1-\cos(\Delta\phi)]}$) computed for each lepton, and the p_{T} of the dilepton system ($p_{\text{T}}^{\ell\ell}$). The bins with enough events are also split by charge to help constrain charge-asymmetric backgrounds. This categorization is summarized in table 1.

5.2 Three or more leptons

Most of the targeted models described in section 2 and depicted in figures 1 and 2 yield three isolated leptons and significant $p_{\text{T}}^{\text{miss}}$ in the final state.

Events are selected on the condition that they have $p_{\text{T}}^{\text{miss}} > 50$ GeV and contain at least three leptons, of which at most two are τ_{h} candidates. The leading electron (muon) must satisfy $p_{\text{T}} > 25\,(20)$ GeV, while the subleading electron (muon), if present, must satisfy $p_{\text{T}} > 15\,(10)$ GeV. These criteria are driven by the p_{T} thresholds of the dilepton triggers used in the analysis. If the leading lepton is a muon and the other leptons are electrons or τ_{h} candidates, the muon threshold is increased to $p_{\text{T}} > 25$ GeV. For events with one e or μ and two τ_{h}, all leptons are additionally constrained to have $|\eta| < 2.1$, and the electron (muon) must have $p_{\text{T}} > 30\,(25)$ GeV. These requirements are imposed to ensure that the selected events have a high efficiency with respect to the required triggers. To reduce the contribution from processes with low-mass resonances, events are vetoed if they contain an OSSF loose-lepton pair with an invariant mass below 12 GeV. Additionally, in events with exactly three leptons containing an OSSF pair of two e or μ, the invariant mass of three

JHEP03(2018)166

leptons is required not to be consistent with the mass of a Z boson ($|M_{3\ell} - M_{\mathrm{Z}}| > 15\,\mathrm{GeV}$) in order to suppress contributions from asymmetric photon conversions.

These events are then classified according to the number of identified leptons and their flavor. We distinguish between final states with three and more than three leptons and among final states with differing τ_{h} content as follows:

- Events with three light-flavor leptons (electrons or muons).
- Events with two light-flavor leptons and a τ_{h}.
- Events with one light-flavor lepton and two τ_{h}s.
- Events with at least four light-flavor leptons and no τ_{h}.
- Events with at least three light-flavor leptons and one τ_{h}.
- Events with at least two light-flavor leptons and two τ_{h}.

These categories are then further subdivided according to their kinematic properties to define the different signal regions. Further binning of the events in the aforementioned categories is described in detail in the remainder of this section.

5.2.1 Three light leptons (signal regions A and B)

In most of the cases two out of the three leptons (e or μ) will form an OSSF pair. This is signal region "A". We further divide the events into three bins of invariant mass of the dilepton pair, $M_{\ell\ell}$, in order to separate processes that include a Z boson in the decay chain from those that do not. One of the $M_{\ell\ell}$ bins is defined to be below the Z mass ($M_{\ell\ell} < 75\,\mathrm{GeV}$) and the second one contains the events with $M_{\ell\ell}$ above the Z mass ($M_{\ell\ell} > 105\,\mathrm{GeV}$), which enhances the sensitivity to the scenarios with various mass splittings between the $\widetilde{\chi}_2^0$ and $\widetilde{\chi}_1^0$. The third one is defined as the Z mass window ($75 \leq M_{\ell\ell} < 105\,\mathrm{GeV}$), and it is expected to contain the bulk of the standard model background events. In the case of three same-flavor leptons, the OSSF pair with the invariant mass closest to the mass of the Z boson is used. The transverse mass M_{T} of the third lepton in the event is computed with respect to $p_{\mathrm{T}}^{\mathrm{miss}}$. For the SM WZ $\to 3\ell\nu$ process, the M_{T} variable computed in this way is steeply falling around the W mass, and facilitates discrimination against the dominant background from WZ production in the search. Both variables, M_{T} and $p_{\mathrm{T}}^{\mathrm{miss}}$, are used to further categorize the events with most of the standard model background expected in low M_{T} and $p_{\mathrm{T}}^{\mathrm{miss}}$ bins. These signal regions are summarized in table 2.

Signal region "B" contains the events in which no OSSF pair is found, further sorted into two bins each for $M_{\ell\ell}$ and M_{T}. The low M_{T} bins are then further subdivided into two $p_{\mathrm{T}}^{\mathrm{miss}}$ bins. Most of these events arise from a leptonic decay of Z $\to \tau\tau$; therefore, the $M_{\ell\ell}$ is calculated from the opposite-sign (OS) dilepton pair whose invariant mass is closest to the mean dilepton mass determined from Z $\to \tau\tau$ simulation, which is 50 GeV. An event lacking an OS pair (all three leptons have the same sign) most likely arises from Z $\to \tau\tau$ with one lepton charge misidentified. In this case the event is assigned to the lowest $M_{\ell\ell}$ bin, and the M_{T} is taken to be the minimum M_{T} calculated from any of the three leptons

JHEP03(2018)166

M_{T} (GeV)	$p_{\mathrm{T}}^{\mathrm{miss}}$ (GeV)	$M_{\ell\ell} < 75\,\mathrm{GeV}$	$75 \leq M_{\ell\ell} < 105\,\mathrm{GeV}$	$M_{\ell\ell} \geq 105\,\mathrm{GeV}$
$0-100$	$50-100$	A01	A15†	A32
	$100-150$	A02	A16	A33
	$150-200$	A03	A17	A34
	$200-250$	A04	A18	A35
	$250-400$	A05	A19	A36
	$400-550$		A20	
	$\geq$550		A21	
$100-160$	$50-100$	A06	A22	A37
	$100-150$	A07	A23	A38
	$150-200$	A08	A24	A39
	$\geq$200	A09	A25	A40
$\geq$160	$50-100$	A10	A26	A41
	$100-150$	A11	A27	A42
	$150-200$	A12	A28	A43
	$200-250$	A13	A29	A44
	$250-400$	A14	A30	
	$\geq$400		A31	

Table 2. Search regions corresponding to category A, events with three electrons or muons that form at least one opposite-sign same-flavor (OSSF) pair. Search region A15† overlaps with the WZ control region of the analysis, and is not used in the interpretation.

M_{T} (GeV)	$p_{\mathrm{T}}^{\mathrm{miss}}$ (GeV)	$M_{\ell\ell} < 100\,\mathrm{GeV}$	$M_{\ell\ell} \geq 100\,\mathrm{GeV}$
$0-120$	$50-100$	B01	B04
	>100	B02	B05
>120	>50	B03	B06

Table 3. Search regions corresponding to category B, events with three e or μ that do not form an opposite-sign same-flavor (OSSF) pair.

and the $p_{\mathrm{T}}^{\mathrm{miss}}$. These signal regions are summarized in table 3. For this category, the dominant background arises from nonprompt leptons.

5.2.2 Three leptons with at least one τ_{h} (signal regions C to F)

A third category "C" is built from events with two e or μ forming an OSSF pair and a τ_{h}; it uses the same three $M_{\ell\ell}$ bins as in category "A", again in order to separate off-Z and on-Z regions. For these events, the two-lepton "stransverse mass", M_{T2} [65, 66], replaces M_{T} for the further subdivision of the bins, as M_{T2} is a more powerful discriminator with respect to the dominant $\mathrm{t\bar{t}}$ background containing two leptons and two neutrinos in the final state. M_{T2} is computed with the leptons that are most likely to be the prompt ones from a W boson decay, and in case of $\mathrm{t\bar{t}}$ processes it has an endpoint at the W boson mass;

JHEP03(2018)166

$p_{\mathrm{T}}^{\mathrm{miss}}$ (GeV)	$75 \leq M_{\ell\ell} < 105\,\mathrm{GeV}$	$M_{\mathrm{T2}}(\ell_1, \ell_2)$ (GeV)	$M_{\ell\ell} < 75\,\mathrm{GeV}$	$M_{\ell\ell} \geq 105\,\mathrm{GeV}$
50 – 100	C06	0 – 100	C01	C12
100 – 150	C07		C02	C13
150 – 200	C08		C03	C14
200 – 250	C09		C04	C15
250 – 300			C05	C16
300 – 400	C10			
≥400	C11			
50 – 200		≥100	C17	
≥200			C18	

Table 4. Search region definition corresponding to category C, events with two e or μ forming an opposite-sign same-flavor (OSSF) pair and one τ_{h} candidate. Regions where there is a Z boson candidate are not split into M_{T2} categories.

it is computed as:

$$M_{\mathrm{T2}} = \min_{\vec{p}_{\mathrm{T1}}^{\,\mathrm{miss}} + \vec{p}_{\mathrm{T2}}^{\,\mathrm{miss}} = \vec{p}_{\mathrm{T}}^{\,\mathrm{miss}}} \Big[\max\big\{ M_{\mathrm{T}}(\vec{p}_{\mathrm{T}}^{\,\ell_1}, \vec{p}_{\mathrm{T1}}^{\,\mathrm{miss}}), M_{\mathrm{T}}(\vec{p}_{\mathrm{T}}^{\,\ell_2}, \vec{p}_{\mathrm{T2}}^{\,\mathrm{miss}}) \big\} \Big], \tag{5.1}$$

where the minimization is done over all possible momenta $\vec{p}_{\mathrm{T1}}^{\,\mathrm{miss}}$ and $\vec{p}_{\mathrm{T2}}^{\,\mathrm{miss}}$ summing to the observed $\vec{p}_{\mathrm{T}}^{\,\mathrm{miss}}$. The probability to misidentify τ_{h} is significantly larger than that to misidentify an electron or muon; hence M_{T2} is computed with a pair of light leptons in this category. The M_{T2} bins are defined so that the vast majority of the SM backgrounds are at low M_{T2}, especially the $\mathrm{t\bar{t}}$ contribution. For the signal regions containing a Z boson candidate, the categorization in terms of M_{T2} is not performed. The complete set of requirements defining the signal regions for events in this category is given in table 4.

For events with a τ_{h} and two light leptons that do not form an OSSF pair (i.e., $\mathrm{e^{\pm}e^{\pm}}$, $\mu^{\pm}\mu^{\pm}$, $\mu^{\pm}\mathrm{e}^{\mp}$, $\mu^{\pm}\mathrm{e}^{\pm}$), the OS pair, if present, with the invariant mass closest to the corresponding dilepton mass expected from a $\mathrm{Z} \to \tau\tau$ decay (50 GeV for eμ and 60 GeV for eτ_{h} or $\mu\tau_{\mathrm{h}}$) is used for the event categorization. If no OS pair is present, the event is counted in the lowest $M_{\ell\ell}$ bin. An additional splitting of the regions high in SM background with $M_{\ell\ell} < 100\,\mathrm{GeV}$ is introduced to enhance the sensitivity to various new-particle spectra. Further categorization is performed depending on whether the e or μ form an OS (category "D") or SS (category "E") pair. The final search region binning is shown in tables 5 and 6. The M_{T2} variable is computed with a pair of the OS light leptons if it is present, otherwise a light lepton leading in p_{T} and a τ_{h} is used.

The last category (category "F") includes events with two τ_{h}s and an e or μ, for which the binning is shown in table 7. The M_{T2} variable is computed with the light lepton and the leading τ_{h}. For all these categories ("C" to "F"), the dominant source of background arises from nonprompt leptons.

5.2.3 More than three leptons (signal regions G to K)

The remaining signal regions comprise events with at least four leptons. This category benefits from much lower SM backgrounds compared to the three-lepton category, but suffers from low branching fractions for the signals considered.

JHEP03(2018)166

$M_{T2}(\ell_1, \ell_2)$ (GeV)	p_T^{miss} (GeV)	$M_{\ell\ell} < 60$ GeV	$60 \leq M_{\ell\ell} < 100$ GeV	$M_{\ell\ell} \geq 100$ GeV
$0-100$	$50-100$	D01	D06	D11
	$100-150$	D02	D07	D12
	$150-200$	D03	D08	D13
	$200-250$	D04	D09	D14
	≥ 250	D05	D10	
≥ 100	$50-200$	D15		
	≥ 200	D16		

Table 5. Search region definition corresponding to category D, events with one e and one μ of OS and one τ_h candidate.

$M_{T2}(\ell_1, \tau)$ (GeV)	p_T^{miss} (GeV)	$M_{\ell\ell} < 60$ GeV	$60 \leq M_{\ell\ell} < 100$ GeV	$M_{\ell\ell} \geq 100$ GeV
$0-100$	$50-100$	E01	E06	E11
	$100-150$	E02	E07	
	$150-200$	E03	E08	
	$200-250$	E04	E09	
	≥ 250	E05	E10	
≥ 100	≥ 50	E12		

Table 6. Search region definition corresponding to category E, events with two e or μ of same sign and one τ_h candidate.

$M_{T2}(\ell, \tau_1)$ (GeV)	p_T^{miss} (GeV)	$M_{\ell\ell} < 100$ GeV	$M_{\ell\ell} \geq 100$ GeV
$0-100$	$50-100$	F01	F07
	$100-150$	F02	F08
	$150-200$	F03	F09
	$200-250$	F04	F10
	$250-300$	F05	
	≥ 300	F06	
≥ 100	$50-200$	F11	
	≥ 200	F12	

Table 7. Search region definition corresponding to category F, events with one electron or muon and two τ_h candidates.

The signal regions are formed according to the number of OSSF pairs (with any lepton entering at most one pair) and the number of τ_hs in the event. This separation is motivated by the production of a Z or Higgs boson in the decay chain that would then decay into two light-flavor leptons or two τ_h candidates.

The data are further subdivided in intervals of p_T^{miss} so as to more efficiently discriminate between signal and background. The search region definitions and their notations are summarized in table 8.

JHEP03(2018)166

$p_{\mathrm{T}}^{\mathrm{miss}}$ (GeV)	$0\tau_{\mathrm{h}}$		$1\tau_{\mathrm{h}}$	$2\tau_{\mathrm{h}}$	
	nOSSF ≥ 2	nOSSF < 2	nOSSF ≥ 0	nOSSF ≥ 2	nOSSF < 2
$0-50$	G01	H01	I01	J01	K01
$50-100$	G02	H02	I02	J02	K02
$100-150$	G03	H03	I03	J03	K03
$150-200$	G04	H04	I04	J04	
$\geq$200	G05				

Table 8. Search region definition corresponding to categories G–K, events with four or more leptons. Categorization is made based on the number of OSSF pairs (nOSSF).

Bin	Final state	Definition
1	2 SS leptons	0 jets, $M_{\mathrm{T}} > 100\,\mathrm{GeV}$ and $p_{\mathrm{T}}^{\mathrm{miss}} > 140\,\mathrm{GeV}$
2	2 SS leptons	1 jet , $M_{\mathrm{T}} < 100\,\mathrm{GeV}$, $p_{\mathrm{T}}^{\ell\ell} < 100\,\mathrm{GeV}$ and $p_{\mathrm{T}}^{\mathrm{miss}} > 200\,\mathrm{GeV}$
3	3 light leptons	$M_{\mathrm{T}} > 120\,\mathrm{GeV}$ and $p_{\mathrm{T}}^{\mathrm{miss}} > 200\,\mathrm{GeV}$
4	3 light leptons	$p_{\mathrm{T}}^{\mathrm{miss}} > 250\,\mathrm{GeV}$
5	2 light leptons and 1 tau	$M_{\mathrm{T2}}(\ell_1, \tau) > 50\,\mathrm{GeV}$ and $p_{\mathrm{T}}^{\mathrm{miss}} > 200\,\mathrm{GeV}$
6	1 light lepton and 2 taus	$M_{\mathrm{T2}}(\ell, \tau_1) > 50\,\mathrm{GeV}$ and $p_{\mathrm{T}}^{\mathrm{miss}} > 200\,\mathrm{GeV}$
7	1 light lepton and 2 taus	$p_{\mathrm{T}}^{\mathrm{miss}} > 75\,\mathrm{GeV}$
8	more than 3 leptons	$p_{\mathrm{T}}^{\mathrm{miss}} > 200\,\mathrm{GeV}$

Table 9. Definition of the aggregated regions for multilepton and two SS dilepton final states.

5.3 Aggregated signal regions

To facilitate the use of these results to test models not included in section 2 of this paper, we provide a set of "aggregated signal regions" defined by much simpler selections. Typically, the sensitivity to the signal models obtained by using the aggregate regions is weaker by a factor of two compared with that of the full analysis. The definitions of all aggregated regions are summarized in table 9.

6 Backgrounds

The SM backgrounds leading to the final states under consideration can be divided into the following categories:

- WZ or Wγ^* production: when both W and Z or γ^* bosons decay leptonically, these events produce the same signature as the new physics scenarios targeted by this analysis: three energetic and isolated leptons and a sizable $p_{\mathrm{T}}^{\mathrm{miss}}$ due to a neutrino from the W boson decay. This source is by far the dominant background in the searches with three e or μ, including an OSSF dilepton pair. A SS dilepton signature may also be produced when the W boson is accompanied by a γ^* or off-shell Z boson, when one of the leptons from the Z or γ^* decay fails the applied selection criteria (such as a Z boson mass veto or a minimum p_{T} requirement on a vetoed lepton), or when the Z boson decays to τ leptons yielding a semileptonic (one τ decays hadronically and one decays to leptons) final state.

JHEP03(2018)166

- Nonprompt e, $\boldsymbol{\mu}$, and $\boldsymbol{\tau}_{\mathrm{h}}$: depending on the lepton multiplicity, this background is dominated by W+jets (especially in the SS dilepton regions), $\mathrm{t\bar{t}}$, or Drell-Yan processes. This category contributes the largest background contribution in the trilepton search regions, either that contain a τ_{h} candidate, or that do not contain an OSSF pair.

- External and internal conversions: these processes contribute to the SS dilepton or trilepton final state when the production of a W or a Z boson is accompanied by radiation of an initial- or final-state photon and this photon undergoes an asymmetric internal or external conversion in which one of the leptons has very low p_{T}. This soft lepton has a high probability of failing the selection criteria of the analysis, leading to a reconstructed two- (in case of a W boson) or three-lepton (in case of a Z boson) final state. This background mostly contributes to categories with an OSSF pair and to final states with two SS leptons.

- Rare SM processes with multiple prompt leptons: rare SM processes that yield a SS lepton pair or three or more leptons include multiboson production (two or more bosons, including any combination of W, Z, H, or a prompt γ), single-boson production in association with a $\mathrm{t\bar{t}}$ pair, and double parton scattering. Some of these processes have a very small production rate, and are in some cases further suppressed by the b jet veto. The contribution of such processes is estimated from MC simulation.

- Electron charge misidentification: a background from charge misidentification arises from events with an OS pair of isolated eμ or ee in which the charge of one of the electrons is misreconstructed. In most cases, this arises from severe bremsstrahlung in the tracker material. This is a small background, manifesting itself in the SS dilepton category or in the category with a SS dilepton pair and a τ_{h} candidate.

The WZ background contribution is normalized to data in a dedicated control region containing events with three light leptons: only events with an OSSF pair with an invariant mass of $75 < M_{\ell\ell} < 105\,\mathrm{GeV}$ are selected. Additional requirements on these events are: $M_{\mathrm{T}} < 100\,\mathrm{GeV}$ and $35 < p_{\mathrm{T}}^{\mathrm{miss}} < 100\,\mathrm{GeV}$. The purity of this WZ selection is approximately 86%. This definition overlaps with the search region SR A15 of the trilepton search category. As a consequence, the latter region is not used for the interpretation of the results in terms of new-physics models.

A good description of the M_{T} distribution in our WZ simulation is crucial in this search, especially in the tail where new physics may appear. The tail of the M_{T} distribution is a result of, in order of importance, the accidental usage of a wrong pair of leptons to compute the mass of the Z candidate and the M_{T} of the W candidate ("mispairing" of the leptons), the $p_{\mathrm{T}}^{\mathrm{miss}}$ resolution, and the W boson width. The prediction of lepton mispairing from simulation is confirmed in a control sample in the data similar to the one described above but only allowing events with an OSSF pair of different flavor than the third lepton and using the OS pair of leptons of different flavor in the $M_{\ell\ell}$ computation. More details on these checks can be found in section 7.

JHEP03(2018)166

The background from nonprompt light leptons is estimated using the "tight-to-loose" ratio method, which is described in detail in ref. [40]. The probability for a loosely defined light lepton to pass the full set of selection criteria is measured in a multijet data sample enriched in nonprompt leptons, called the measurement region. Once measured, this probability is applied in a sample of events that pass the full kinematic selection, but where at least one of the leptons fails the nominal selection while passing the loose requirements, in order to predict the number of events from nonprompt leptons entering each search region. The contribution from nonprompt τ_h leptons is estimated in a similar way. This time, the "tight-to-loose" ratio is measured in a Z+jets enriched control sample in data in which a τ_h candidate is required to be present in addition to an OSSF pair consistent with the Z boson decay. The residual contribution from prompt leptons in the measurement and application regions is subtracted using MC simulation. It is verified in both MC simulation and low-p_T^{miss} data control regions that this method describes the background from the nonprompt leptons entering the different search regions within a systematic uncertainty of 30%.

The modelling of the conversion background is verified in a data control region enriched in both external and internal conversions from the Z+jets process with $Z \to \ell\ell\gamma^{(*)}$ and $\gamma^{(*)} \to \ell\ell$, where one of the leptons is out of acceptance. This control region is defined by $|M_{\ell\ell} - M_Z| > 15\,\text{GeV}$, $|M_{3\ell} - M_Z| < 15\,\text{GeV}$, and $p_T^{miss} < 50\,\text{GeV}$. The expected background yields are found to agree with the observed counts in data within the statistical uncertainties. Scale factors are derived for the modelling of the asymmetric conversions to electrons or muons in the $Z\gamma^{(*)}$ process after subtraction of the residual nonprompt lepton and WZ backgrounds. The scale factors are found to be 1.04 ± 0.11 and 1.25 ± 0.24, respectively, and are used to derive the systematic uncertainty on this process.

The charge misidentification background in the SS dilepton channel is estimated by reweighting the events with OS lepton pairs by the charge misidentification probability. For electrons, this probability is obtained from simulation and cross-checked on an on-Z $e^{\pm}e^{\pm}$ control region in data, and is in the range 10^{-5}–10^{-3} depending on the electron's p_T and η. Studies of simulated events indicate that the muon charge misidentification probability is negligible.

7 Systematic uncertainties

The systematic uncertainties in the background estimates and signal acceptance affect both the overall normalization of the yields and the relative populations of processes in the search regions. The systematic uncertainties considered in this analysis are summarized in table 10.

Experimental uncertainties include those in the lepton selection efficiency, the trigger efficiency, the jet energy scale, and the b tag veto efficiency.

Lepton identification efficiencies are computed with the tag-and-probe technique [36, 37], with an uncertainty of 3% per lepton. The τ_h identification efficiency is similarly determined with an uncertainty of 5% [44].

The trigger efficiency uncertainty is obtained from measuring efficiencies of all trigger components with the tag-and-probe technique, and is estimated to be less than 3%.

JHEP03(2018)166

Source	Estimated uncertainty (%)	Treatment
e/μ selection	3	normalization
τ_{h} selection	5	normalization
Trigger efficiency	3	normalization
Jet energy scale	2–10	shape
b tag veto	1–2	shape
Pileup	1–5	shape
Integrated luminosity	2.5	normalization
Scale variations and PDF ($\mathrm{t\bar{t}Z}$ and $\mathrm{t\bar{t}W}$)	15	normalization
Theoretical (ZZ)	25	normalization
Conversions	15	normalization
Other backgrounds	50	normalization
Monte Carlo statistical precision	1–30	normalization
Nonprompt leptons (closure)	30	normalization
Nonprompt leptons (W/Z bkg. subtraction)	5–20	shape
Charge misidentification	20	normalization
WZ normalization	10	normalization
WZ shape	5–50	shape
ISR uncertainty	1–5	shape
Scale variations for signal processes	1–2	shape
Lepton efficiencies	2	normalization
Signal acceptance ($p_{\mathrm{T}}^{\mathrm{miss}}$ modelling)	1–5	shape

Table 10. Summary of systematic uncertainties in the event yields in the search regions and their treatment. Uncertainties are allowed to vary only the normalization of all the bins at once, or both the shape and the normalization (allowing for different correlations across the bins). The upper group lists uncertainties related to experimental effects for all processes whose yield is estimated from simulation; the middle group lists uncertainties in these yields related to the event simulation process itself. The third group lists uncertainties for background processes whose yield is estimated from data. Finally, the last group describes uncertainties related to the extraction of the signal acceptance in MC simulation.

The jet energy scale uncertainty varies between 2 and 10%, depending on the p_{T} and η of the jet. This uncertainty affects other event quantities such as the b tag veto, $p_{\mathrm{T}}^{\mathrm{miss}}$, M_{T}, and M_{T2}, and is computed by shifting the energies of all jets coherently and propagating the variation to all of these kinematic variables. Correlation effects due to the migration of events from one search region to another are taken into account. These variations yield estimated uncertainties ranging from 2 to 10% in the simulated signal and background yields in the different search regions. Similarly, the b jet veto efficiency is corrected for the differences between data and simulation, and an associated uncertainty with this correction is 1–2%, which takes into account the kinematic difference between signal events and those used to measure such efficiency. The uncertainty in the modelling of pileup is computed by

JHEP03(2018)166

modifying slightly the pileup reweighting profile and is measured to be 1–5%, depending on the search region. The uncertainty in the integrated luminosity is 2.5% [67].

The dominant source of background for most of the event categories described in section 5 is WZ production. Systematic uncertainties are derived from detailed evaluation of the modelling of this process. The uncertainty in the normalization of the WZ background is 10%. This includes statistical uncertainties in the yields in the control sample used for normalization, and in the subtraction of the non-WZ contributions to the sample. An additional uncertainty stems from the modelling of the M_{T} shape in the simulation of the WZ process. To estimate the effect of a potentially different $p_{\mathrm{T}}^{\mathrm{miss}}$ resolution and W width in data and simulation on the W boson M_{T} distribution shape, we verify the M_{T} shape prediction from simulation in Wγ and W+jets control samples in data. After applying a threshold $p_{\mathrm{T}} > 40\,\mathrm{GeV}$ on the photon to suppress the contribution of Wγ events produced by final-state radiation (FSR) which influences M_{T}, we find the W boson M_{T} distribution shapes in simulated Wγ, W+jets, and WZ processes to be the same. We thus proceed to measure the Wγ and W+jets M_{T} shape in a dedicated control sample in which an energetic, well-identified, and isolated photon passing the aforementioned p_{T} threshold is required, together with a lepton passing the same criteria as those selected in the trilepton search regions, and $p_{\mathrm{T}}^{\mathrm{miss}} > 50\,\mathrm{GeV}$. A minimum separation of $\Delta R > 0.3$ is required between the lepton and the photon to further reduce the FSR contribution. The residual W+jets contribution in this control sample is about 20%, and consists of events where a jet has very high electromagnetic fraction, and thus is not subject to large mismeasurements that might influence the M_{T} tail. Residual contamination from processes other than Wγ or W+jets is subtracted using MC, and the M_{T} shape measured in this control region is compared to the one predicted by the WZ simulation. The measured shape is found to agree well with the prediction from simulation within the statistical uncertainties, and the precision of this comparison is used to derive systematic uncertainties on the high-M_{T} bins of the trilepton search. This uncertainty is between 5 and 40%, from the comparison of the M_{T} shape in the WZ simulation with the one measured in the Wγ control region. The size of this uncertainty increases for higher M_{T} values and is driven by the statistical uncertainty of the Wγ control sample. Systematic uncertainties on the modelling of $M_{\ell\ell}$ are neglected as lepton momentum scale and resolution effects are too small to have significant effects in this analysis [51, 68].

Further uncertainties in background yields estimated from simulations arise from the unknown higher-order effects in the theoretical calculations of the cross sections, and from uncertainties in the knowledge of the proton PDFs. The uncertainties from the PDFs are estimated by using the envelope of several PDF sets [69]. The effect of these theoretical uncertainties is 15% for $\mathrm{t\bar{t}W}$ and $\mathrm{t\bar{t}Z}$, and 25% for ZZ backgrounds. Theoretical uncertainties are also considered for the remaining minor backgrounds estimated purely from simulation, in which 15% uncertainty is assigned to processes with a prompt γ modelled with NLO accuracy corresponding to the precision of the scale factor measured in a dedicated control region, and 50% to other rare processes.

Other sources of uncertainties are associated with the backgrounds that are derived from, or normalized in, data control samples. The nonprompt background prediction has an uncertainty of 30% assigned to both light-lepton and τ_{h} cases. This uncertainty arises from the performance of the method in the simulation (closure) in various regions of parameter

JHEP03(2018)166

space, and is given by the observed deviations between the estimated and observed yields in the control sample.

The uncertainty in the measurement of the charge misidentification background is derived from the difference between the yields of on-Z $e^{\pm}e^{\pm}$ events in data and simulation. This uncertainty is found to be 20%.

The MadGraph modelling of ISR, which affects the total transverse momentum (p_T^{ISR}) of the system of SUSY particles, is improved by reweighting the p_T^{ISR} distribution in MC SUSY events. This reweighting procedure is based on studies of the transverse momentum of Z events in data [70]. The reweighting factors range between 1.18 at $p_T^{ISR} \approx 125\,GeV$ and 0.78 for $p_T^{ISR} > 600\,GeV$. The deviation of the reweighting factors from 1.0 is taken as the systematic uncertainty on the reweighting procedure.

Additional uncertainties in the signal acceptance extraction are considered for the renormalization and factorization scale variations by simultaneously varying them by a factor of 2 up and down [27–29], p_T^{miss} modelling and lepton efficiencies due to the differences in simulations between signal and background samples.

8 Results

The estimation methods for the dominant background sources, WZ production and nonprompt leptons, have been extensively validated. Such checks are based on both simulation and data control regions as described in sections 6 and 7. In particular, the modelling of the most relevant kinematic distributions used to define the signal regions is validated for each category. Distributions in p_T^{miss} are shown in figure 4 for the SS dilepton channel for events with 0 or 1 jet. Key kinematic distributions for the three-lepton channel are displayed in figure 5 and for three lepton events with at least one τ_h in figure 6. Figure 7 displays the p_T^{miss} for events with four leptons. An example signal mass point in the $\tilde{\chi}_1^{\pm}$-$\tilde{\chi}_1^0$ mass plane for which each category has sensitivity, is also shown in these figures.

The expected and observed yields are summarized in table 11 for the SS dilepton channel, in tables 12–17 for the trilepton channel, and in table 18 for the four-lepton channel. The observed event counts are consistent with those expected from the SM backgrounds.

The comparisons between the expected and observed yields are presented in figure 8 for the SS dilepton channel, in figures 9–11 for the trilepton channel, and in figure 12 for signal regions with at least four leptons. An example signal mass point in the $\tilde{\chi}_1^{\pm}$-$\tilde{\chi}_1^0$ mass plane for which each category has sensitivity, is also shown in these figures. Finally, results for the aggregated signal regions are presented in figure 13 and table 19.

This analysis is mostly statistically limited, as can be seen from the ratio plots of figures 4–12. However, there are search regions for which other sources of uncertainties are also relevant. Such is the case for the on-Z signal regions A, which is dominated by the systematic uncertainty of the WZ normalization for the low-M_T bins and the WZ shape uncertainty for the high-M_T bins. In regions that contain at least one τ_h candidate, the systematic uncertainty on the nonprompt background is comparable to the statistical uncertainty. Finally, the uncertainty on the four-lepton signal regions G–K, is dominated by the ZZ normalization uncertainty.

JHEP03(2018)166

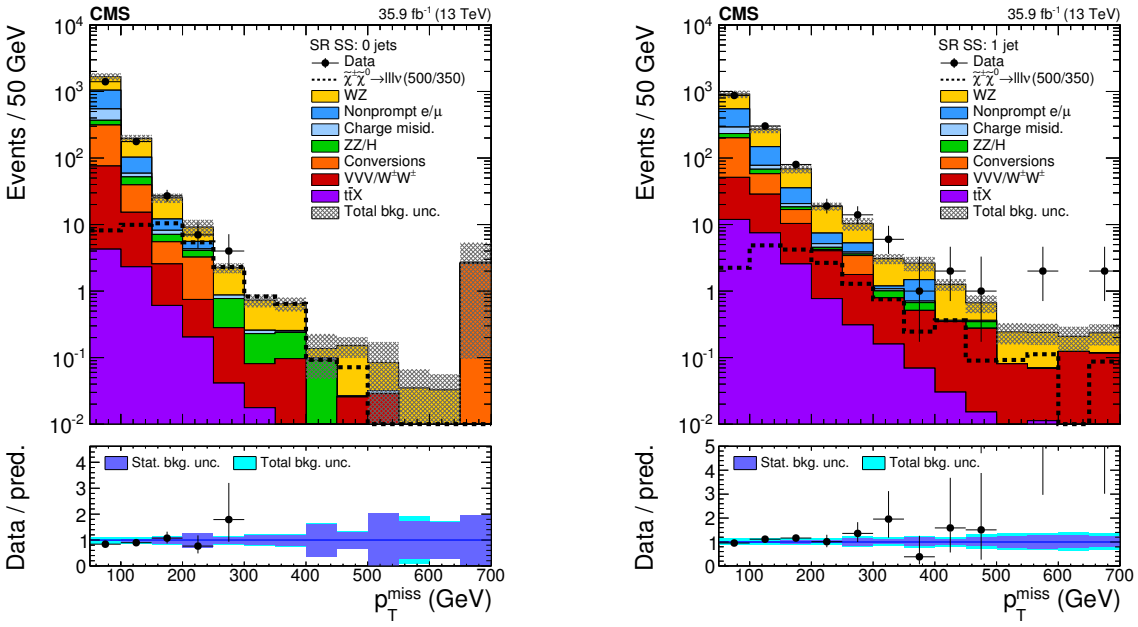


Figure 4. Distribution of $p_{\mathrm{T}}^{\mathrm{miss}}$ for events with 2 SS leptons and 0 jets (left) or 1 jet (right). An example signal mass point in the flavor-democratic model with mass parameter $x = 0.05$ is displayed for illustration. The numbers in the parentheses denote the $\widetilde{\chi}_1^{\pm}$ and $\widetilde{\chi}_1^0$ masses, namely $m_{\widetilde{\chi}_1^{\pm}} = m_{\widetilde{\chi}_2^0} = 500\,\mathrm{GeV}$ and $m_{\widetilde{\chi}_1^0} = 350\,\mathrm{GeV}$. The last bin contains the overflow events.

N_{jets}	M_{T} (GeV)	$p_{\mathrm{T}}^{\ell\ell}$ (GeV)	$p_{\mathrm{T}}^{\mathrm{miss}} < 100\,\mathrm{GeV}$ (exp.)	(obs.)	$100 \le p_{\mathrm{T}}^{\mathrm{miss}} < 150\,\mathrm{GeV}$ (exp.)	(obs.)		$150 \le p_{\mathrm{T}}^{\mathrm{miss}} < 200\,\mathrm{GeV}$ (exp.)	(obs.)	$p_{\mathrm{T}}^{\mathrm{miss}} \ge 200\,\mathrm{GeV}$ (exp.)	(obs.)
0	<100	<50	1430 ± 180	1193	56 ± 9	50	++	5.9 ± 1.2	7	4.5 ± 3.5	2
					36 ± 7	25	−−				
		>50	163 ± 19	143	38 ± 6	41	++	14.4 ± 3.2	11	6.3 ± 0.9	6
					23 ± 4	24	−−				
	>100		82 ± 12	67	27 ± 4	19	++	5.0 ± 0.8	9	5.1 ± 2.6	3
					18 ± 4	18	−−				
1	<100	<50	603 ± 80	591	98 ± 14	116	++	33 ± 6	43	11.4 ± 1.7	13
					66 ± 10	69	−−				
		>50	264 ± 31	232	51 ± 7	52	++	29 ± 5	28	22.2 ± 3.4	27
					31 ± 4	35	−−				
	>100		44 ± 7	49	16.4 ± 2.9	18	++	6.7 ± 1.1	9	3.9 ± 0.8	7
					10.7 ± 1.9	13	−−				

Table 11. SS dilepton category: expected and observed yields in events with two SS light-flavor leptons. For each bin, the first number corresponds to the expected yield (exp.) and its uncertainty, and the second denotes the observed yield (obs.). The uncertainty denotes the total uncertainty in the yield.

JHEP03(2018)166

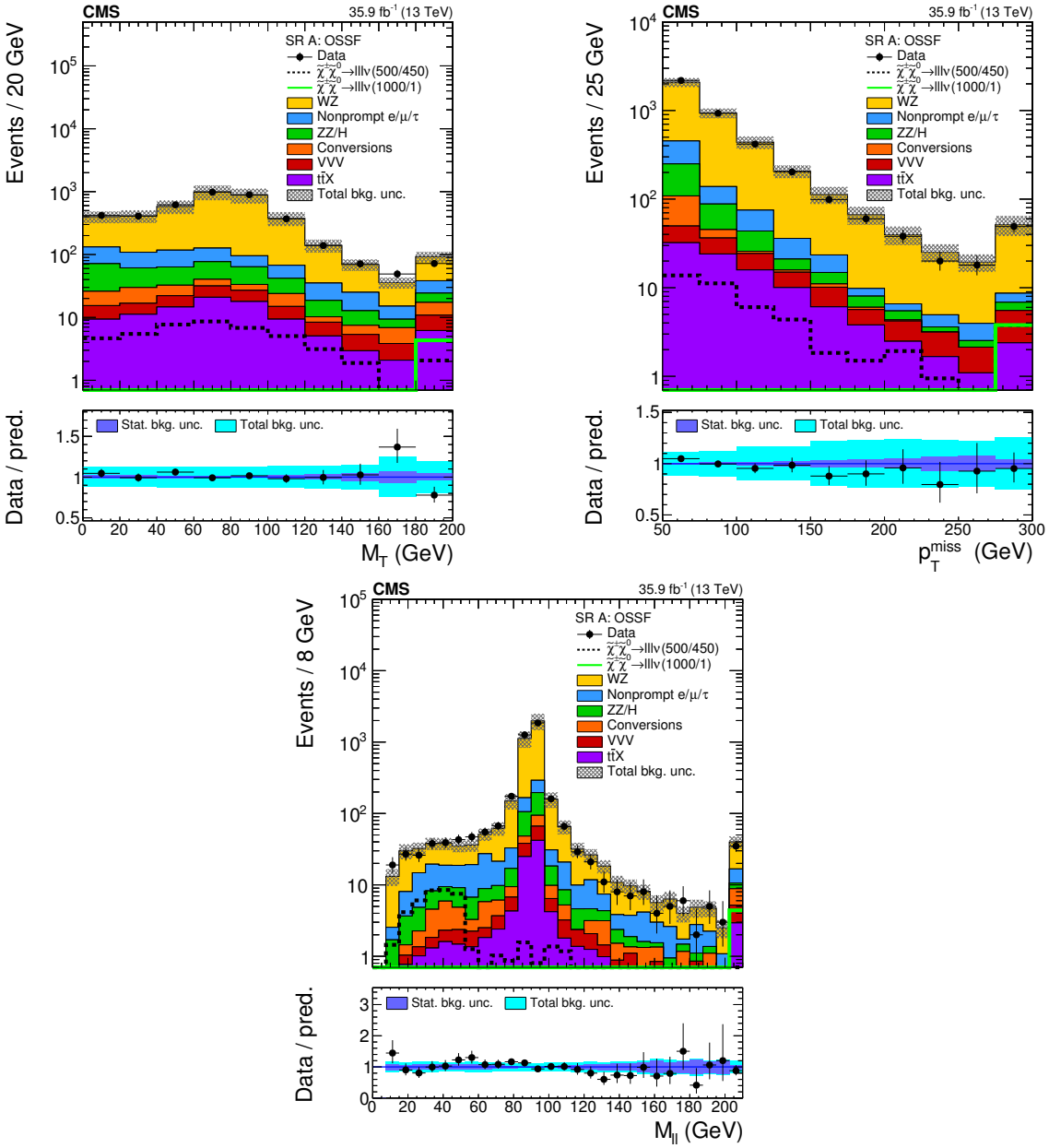


Figure 5. Distribution of kinematical observables used in the event selection for events entering signal regions A: the transverse mass of the third lepton (upper left), the $p_{\mathrm{T}}^{\mathrm{miss}}$ (upper right) and the $M_{\ell\ell}$ of the OSSF pair (lower). Two signal mass points in the flavor-democratic model with mass parameter $x = 0.5$ are displayed for illustration. The notation is analogous to that used in figure 4.

JHEP03(2018)166

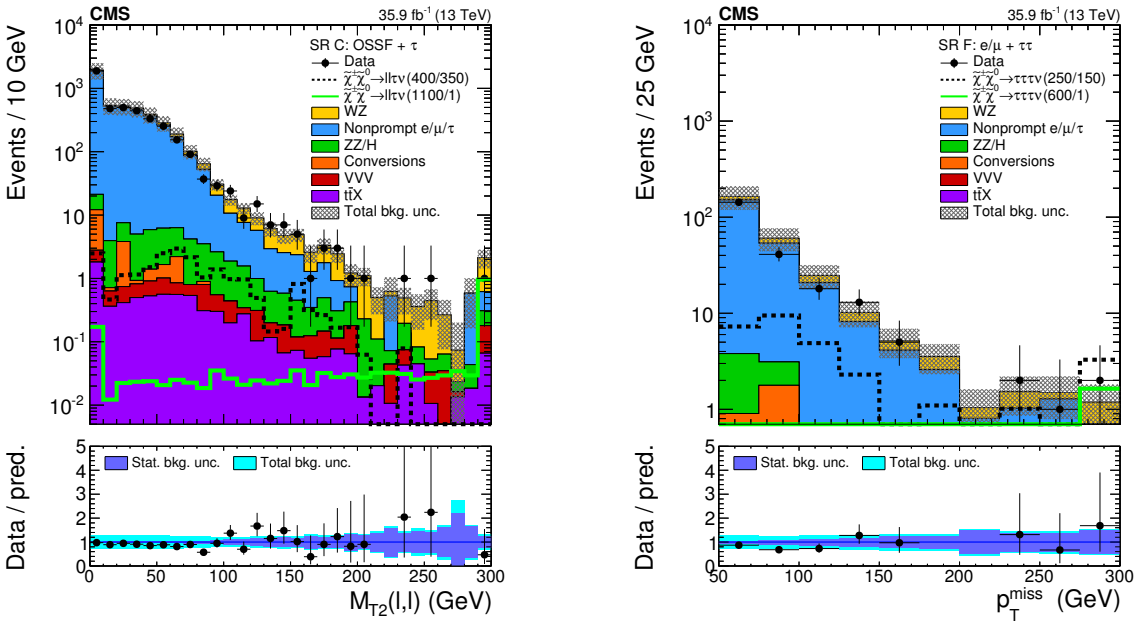


Figure 6. Distributions in the stransverse mass for events with two OSSF light leptons and one τ_h (left) and in p_T^{miss} for events with one light-flavor lepton and two τ_hs. Two signal mass points in the τ-enriched (left) and the τ-dominated (right) scenarios with mass parameter $x = 0.5$ are displayed for illustration. The notation is analogous to that used in figure 4.

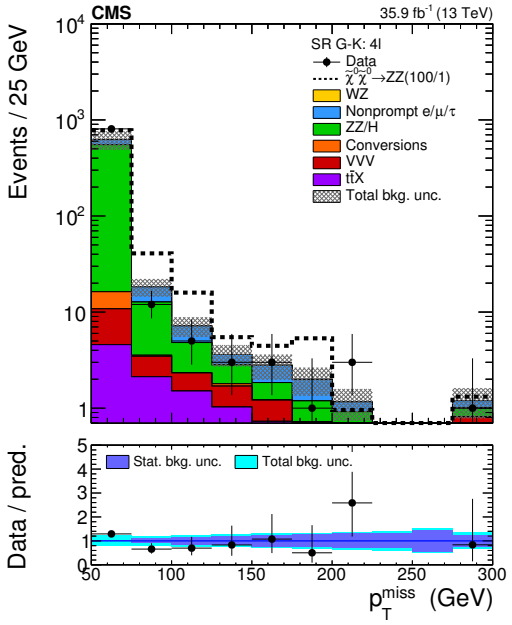


Figure 7. Distribution in p_T^{miss} for events with 4 or more leptons entering search categories G–K. An example signal mass point in the $\widetilde{\chi}_1^0\widetilde{\chi}_1^0$ production GMSB model is displayed for illustration. The numbers in the parenthesis denote the $\widetilde{\chi}_1^0$ and $\widetilde{G}$ masses, namely $m_{\widetilde{\chi}_1^0} = 100\,\text{GeV}$ and $m_{\widetilde{G}} = 1\,\text{GeV}$.

JHEP03(2018)166

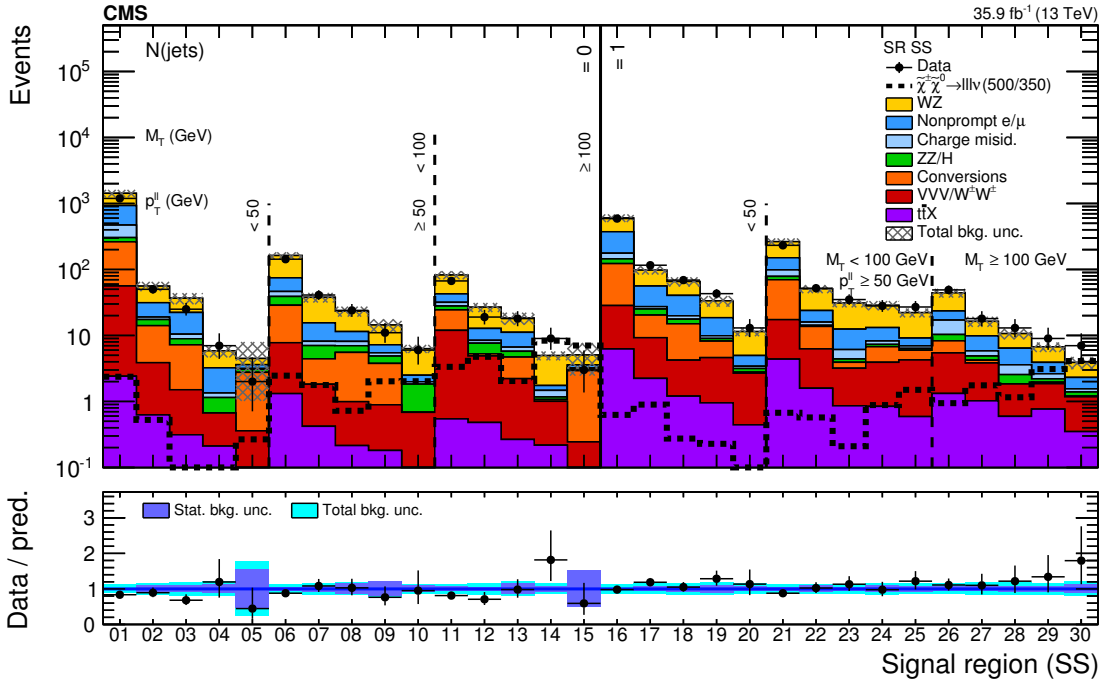


Figure 8. Expected and observed yields comparison in the SS dilepton category. An example signal mass point in the flavor-democratic model with mass parameter $x = 0.05$ is displayed for illustration. The notation is analogous to that used in figure 4.

JHEP03(2018)166

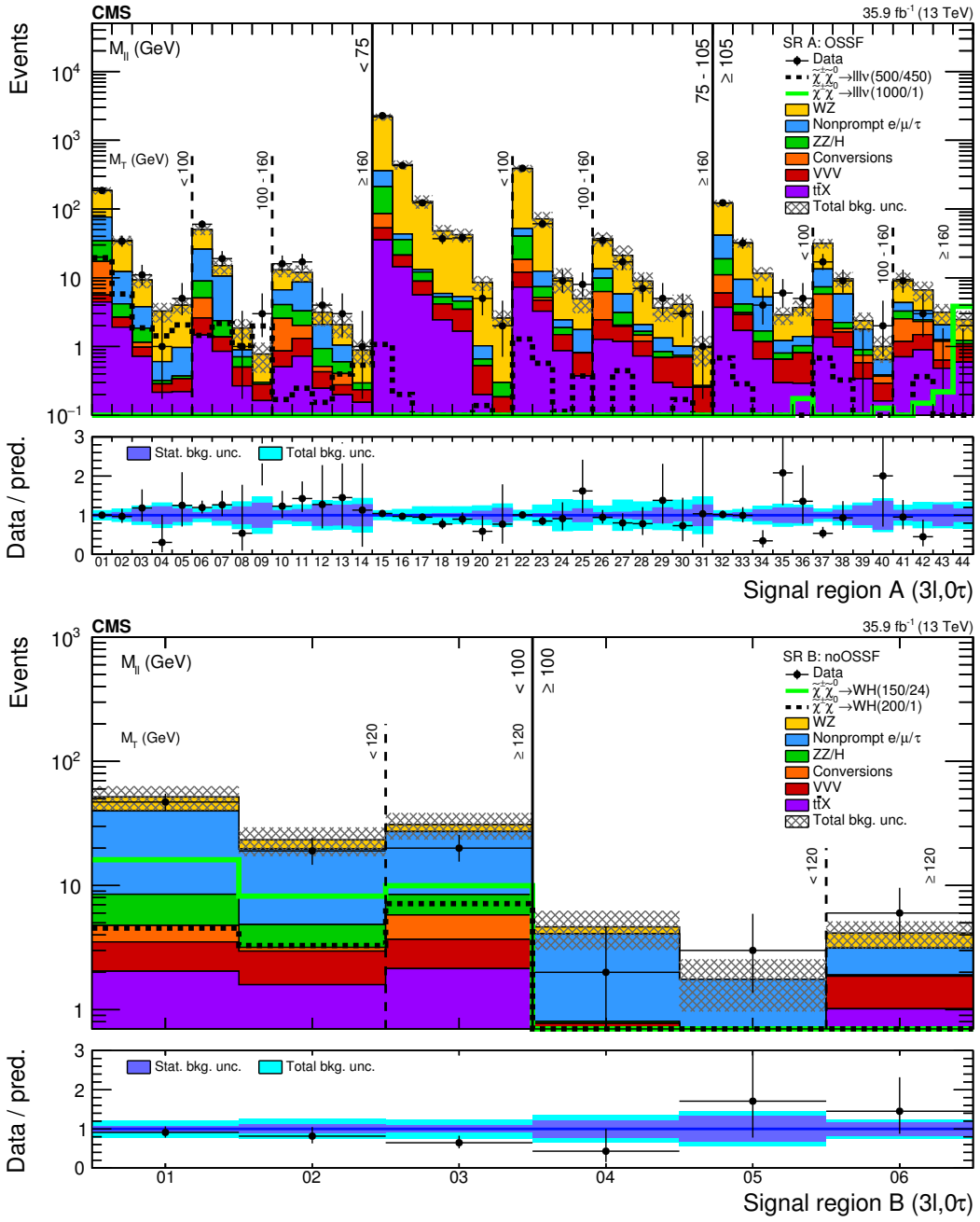


Figure 9. Expected and observed yields comparison in category A (upper) and category B (lower) signal regions, i.e. 3 light flavor leptons including at least one OSSF pair (A) or no OSSF pair (B). SR A15 is replaced by the WZ control region in interpretations of the results. Two signal mass points in the flavor-democratic model with mass parameter $x = 0.5$ are displayed for illustration. The notation is analogous to that used in figure 4.

JHEP03(2018)166

M_{T} (GeV)	$p_{\mathrm{T}}^{\mathrm{miss}}$ (GeV)	$M_{\ell\ell} < 75$ GeV		$75 \leq M_{\ell\ell} < 105$ GeV		$M_{\ell\ell} \geq 105$ GeV	
		(exp.)	(obs.)	(exp.)	(obs.)	(exp.)	(obs.)
$0-100$	$50-100$	185 ± 22	186	2180 ± 260	2278	121 ± 14	123
	$100-150$	35 ± 6	34	440 ± 70	429	32 ± 5	32
	$150-200$	9.3 ± 2.2	11	129 ± 28	123	11.6 ± 2.6	4
	$200-250$	3.3 ± 1.0	1	48 ± 10	37	2.9 ± 0.8	6
	$250-400$	4.0 ± 1.0	5	42 ± 9	38	3.7 ± 1.0	5
	$400-550$			8.5 ± 2.1	5		
	$\geq$550			2.6 ± 0.8	2		
$100-160$	$50-100$	50 ± 8	60	390 ± 50	391	32 ± 5	17
	$100-150$	15 ± 4	19	72 ± 19	61	9.6 ± 2.4	9
	$150-200$	1.9 ± 0.6	1	10 ± 4	9	2.4 ± 0.7	0
	$\geq$200	0.8 ± 0.4	3	4.9 ± 1.9	8	1.0 ± 0.4	2
$\geq$160	$50-100$	13.0 ± 2.8	16	37 ± 9	35	9.4 ± 2.4	9
	$100-150$	11.9 ± 3.2	17	21 ± 8	17	6.6 ± 2.1	3
	$150-200$	3.1 ± 1.2	4	8.9 ± 3.1	7	3.1 ± 1.0	0
	$200-250$	2.1 ± 0.8	3	3.6 ± 1.3	5	2.5 ± 0.8	0
	$250-400$	0.9 ± 0.4	1	4.1 ± 1.6	3		
	$\geq$400			1.0 ± 0.5	1		

Table 12. Category A: expected and observed yields in events with three e or μ that form at least one OSSF pair. For each bin, the first number corresponds to the expected yield (exp.) and its uncertainty, and the second denotes the observed yield (obs.). The uncertainty denotes the total uncertainty in the yield.

M_{T} (GeV)	$p_{\mathrm{T}}^{\mathrm{miss}}$ (GeV)	$M_{\ell\ell} < 100$ GeV		$M_{\ell\ell} \geq 100$ GeV	
		(exp.)	(obs.)	(exp.)	(obs.)
$0-120$	$50-100$	52 ± 11	47	4.6 ± 1.6	2
	$\geq$100	23 ± 6	19	1.8 ± 0.8	3
$\geq$120	≥ 50	31 ± 7	20	4.1 ± 1.0	6

Table 13. Category B: expected and observed yields in events with three e or μ that do not form an OSSF pair. For each bin, the first number corresponds to the expected yield (exp.) and its uncertainty, and the second denotes the observed yield (obs.). The uncertainty denotes the total uncertainty in the yield.

JHEP03(2018)166

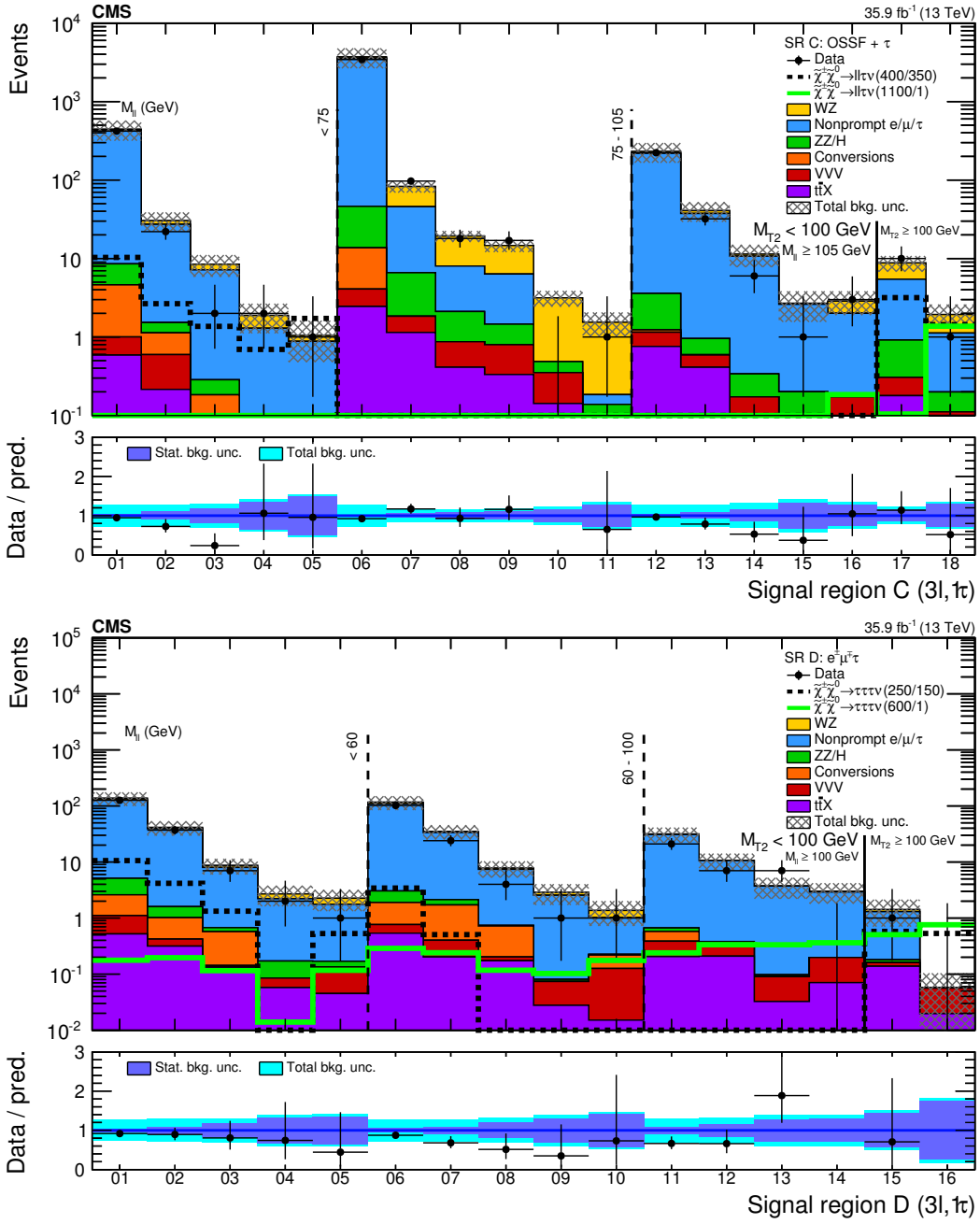


Figure 10. Expected and observed yields comparison in events with one τ_h: categories C (upper) and D (lower). Two signal mass points in the τ-enriched (upper) and the τ-dominated (lower) scenarios with mass parameter $x = 0.5$ are displayed for illustration. The notation is analogous to that used in figure 4.

JHEP03(2018)166

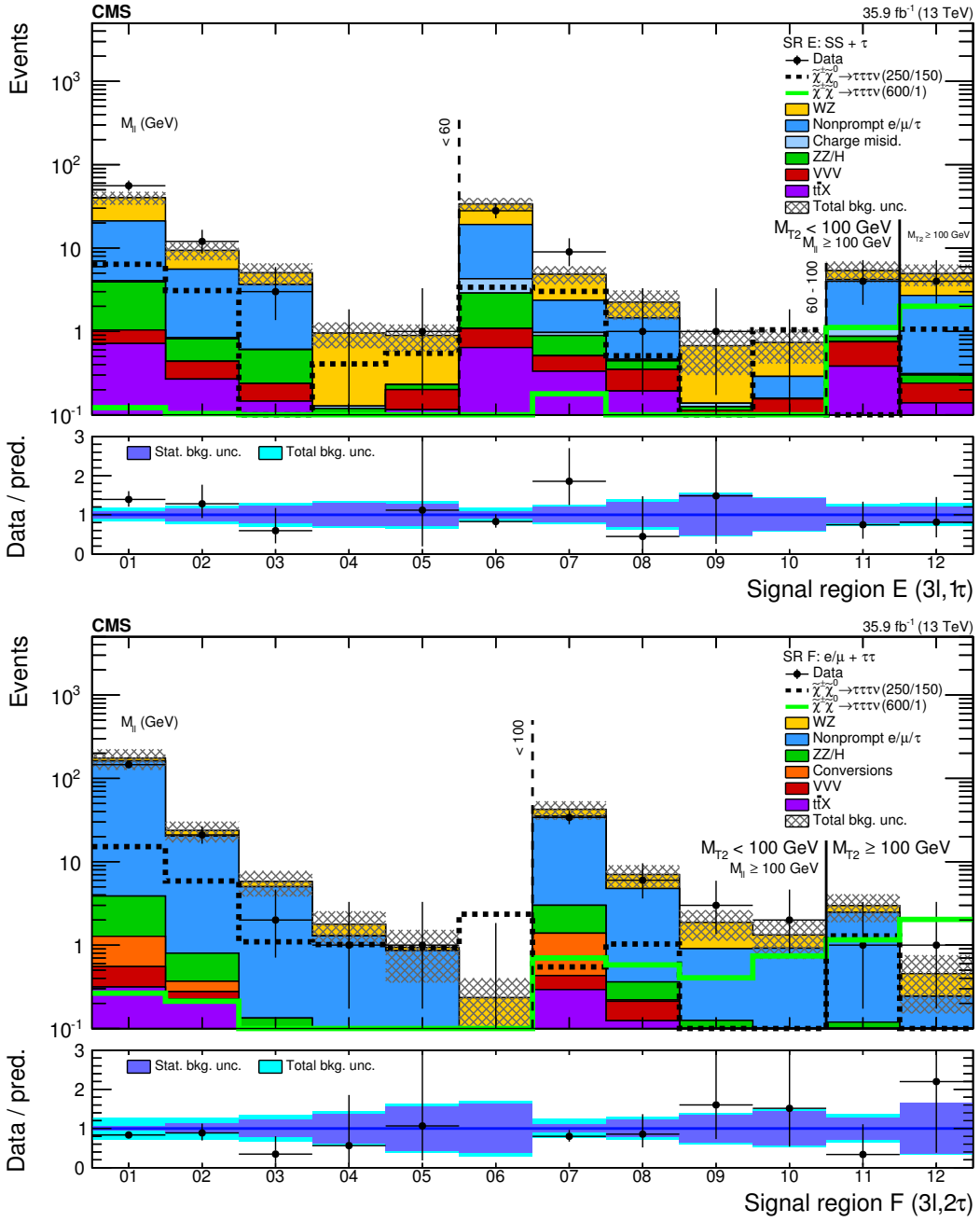


Figure 11. Expected and observed yields comparison in events with one τ_h: category E (upper); and in events with two τ_h: category F (lower). Two signal mass points in the τ-dominated model with mass parameter $x = 0.5$ are displayed for illustration. The notation is analogous to that used in figure 4.

JHEP03(2018)166

$p_{\mathrm{T}}^{\mathrm{miss}}$ (GeV)	$75 \leq M_{\ell\ell} < 105$ GeV		$M_{\mathrm{T2}}(\ell_1, \ell_2)$ (GeV)	$M_{\ell\ell} < 75$ GeV		$M_{\ell\ell} \geq 105$ GeV	
$50-100$	3700 ± 1100	3427	$0-100$	440 ± 130	420	231 ± 65	223
$100-150$	83 ± 14	97		30 ± 8	22	41 ± 11	32
$150-200$	19.4 ± 3.1	18		8.5 ± 2.6	2	11 ± 4	6
$200-250$	14.6 ± 2.6	17		1.9 ± 0.8	2	2.7 ± 1.1	1
$250-300$				1.1 ± 0.6	1	2.9 ± 1.0	3
$300-400$	3.2 ± 0.7	0					
≥ 400	1.5 ± 0.6	1					
$50-200$			≥ 100	8.8 ± 2.0		10	
≥ 200				1.9 ± 0.7		1	

Table 14. Category C: expected and observed yields in events with two e or μ forming and OSSF pair and one τ_{h}. For each bin, the first number corresponds to the expected yield and its uncertainty, and the second denotes the observed yield. The uncertainty denotes the total uncertainty in the yield.

$M_{\mathrm{T2}}(\ell_1, \ell_2)$ (GeV)	$p_{\mathrm{T}}^{\mathrm{miss}}$ (GeV)	$M_{\ell\ell} < 60$ GeV		$60 \leq M_{\ell\ell} < 100$ GeV		$M_{\ell\ell} \geq 100$ GeV	
$0-100$	$50-100$	140 ± 40	126	117 ± 32	102	32 ± 10	21
	$100-150$	41 ± 12	37	35 ± 10	24	11 ± 4	7
	$150-200$	8.7 ± 2.7	7	7.8 ± 2.5	4	3.7 ± 1.5	7
	$200-250$	2.7 ± 1.1	2	2.9 ± 1.2	1	3.0 ± 1.2	0
	≥ 250	2.3 ± 0.9	1	1.4 ± 0.6	1		
≥ 100	$50-200$	1.4 ± 0.7				1	
	≥ 200	0.06 ± 0.05				0	

Table 15. Category D: expected and observed yields in events with an opposite-sign eμ pair and one τ_{h}. For each bin, the first number corresponds to the expected yield and its uncertainty, and the second denotes the observed yield. The uncertainty denotes the total uncertainty in the yield.

$M_{\mathrm{T2}}(\ell_1, \tau_1)$ (GeV)	$p_{\mathrm{T}}^{\mathrm{miss}}$ (GeV)	$M_{\ell\ell} < 60$ GeV		$60 \leq M_{\ell\ell} < 100$ GeV		$M_{\ell\ell} \geq 100$ GeV	
$0-100$	$50-100$	40 ± 7	56	34 ± 6	28	5.4 ± 1.5	4
	$100-150$	9.4 ± 2.2	12	4.8 ± 1.2	9		
	$150-200$	5.0 ± 1.5	3	2.2 ± 0.9	1		
	$200-250$	0.95 ± 0.32	0	0.7 ± 0.4	1		
	≥ 250	0.89 ± 0.32	1	0.73 ± 0.32	0		
≥ 100	≥ 50	4.9 ± 1.4				4	

Table 16. Category E: expected and observed yields in events with one SS e or μ and one τ_{h}. For each bin, the first number corresponds to the expected yield and its uncertainty, and the second denotes the observed yield. The uncertainty denotes the total uncertainty in the yield.

JHEP03(2018)166

$M_{T2}(\ell,\tau_1)$ (GeV)	p_T^{miss} (GeV)	$M_{\ell\ell} < 100$ GeV		$M_{\ell\ell} \geq 100$ GeV	
		(exp.)	(obs.)	(exp.)	(obs.)
0 – 100	50 – 100	170 ± 50	146	42 ± 11	34
	100 – 150	24 ± 7	21	7.0 ± 2.1	6
	150 – 200	5.8 ± 2.0	2	1.9 ± 0.8	3
	200 – 250	1.8 ± 0.8	1	1.3 ± 0.6	2
	250 – 300	0.9 ± 0.6	1		
	≥300	0.23 ± 0.17	0		
≥100	50 – 200	3.0 ± 1.1		1	
	≥200	0.45 ± 0.30		1	

Table 17. Category F: expected and observed yields in events with one e or μ and two τ_h. For each bin, the first number corresponds to the expected yield and its uncertainty, and the second denotes the observed yield. The uncertainty denotes total uncertainty in the yield.

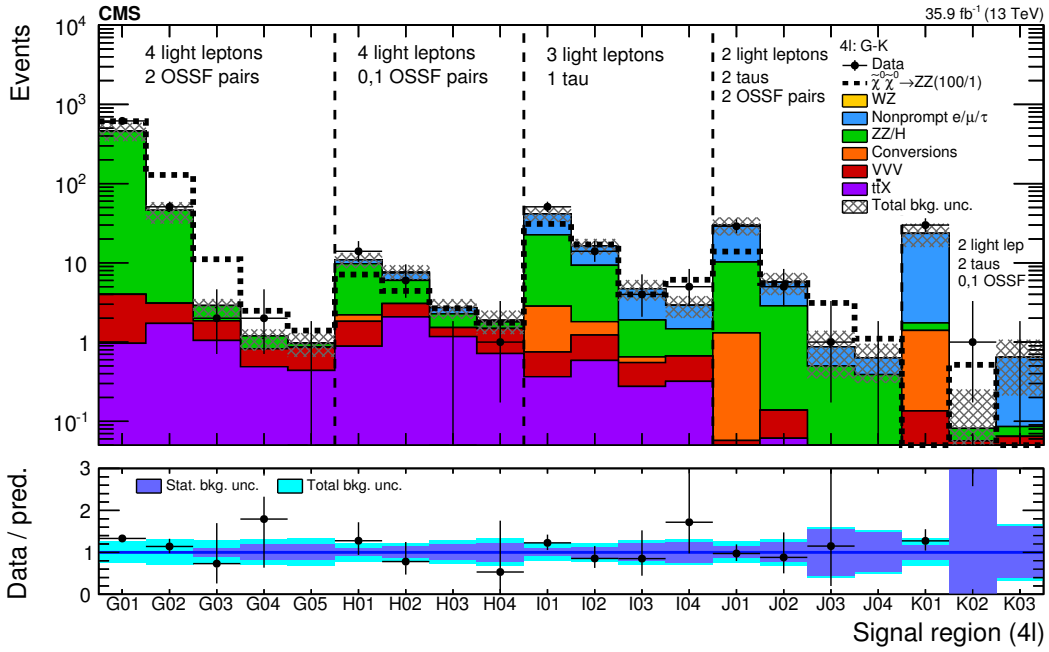


Figure 12. Expected and observed yields comparison in signal regions with at least four leptons (categories G–K). An example mass point in the $\widetilde{\chi}_1^0\widetilde{\chi}_1^0$ production GMSB model is displayed for illustration. The notation is analogous to that used in figure 7.

JHEP03(2018)166

$p_{\mathrm{T}}^{\mathrm{miss}}$ (GeV)	$0\tau_{\mathrm{h}}$				$1\tau_{\mathrm{h}}$		$2\tau_{\mathrm{h}}$			
	nOSSF ≥ 2		nOSSF < 2		nOSSF ≥ 0		nOSSF ≥ 2		nOSSF < 2	
	G		H		I		J		K	
	(exp.)	(obs.)	(exp.)	(obs.)	(exp.)	(obs.)	(exp.)	(obs.)	(exp.)	(obs.)
$0-50$	460 ± 120	619	10.9 ± 2.2	14	42 ± 8	51	30 ± 7	29	24 ± 8	30
$50-100$	45 ± 14	51	7.7 ± 1.5	6	16.4 ± 3.5	14	5.7 ± 1.7	5	$0.07\ ^{+0.18}_{-0.07}$	1
$100-150$	2.7 ± 0.8	2	2.7 ± 0.6	0	4.7 ± 1.4	4	0.9 ± 0.5	1	0.6 ± 0.4	0
$150-200$	1.12 ± 0.33	2	1.9 ± 0.6	1	2.9 ± 0.9	5	0.63 ± 0.32	0		
≥ 200	0.97 ± 0.32	0								

Table 18. Categories G–K: expected and observed yields in the 4ℓ category of the analysis. For each bin, the first number corresponds to the expected yield (exp.) and its uncertainty, and the second denotes the observed yield (obs.). The uncertainty denotes the total uncertainty in the yield.

	Final state	Definition	Event yield	
			(exp.)	(obs.)
1	2 SS leptons	0 jets, $M_{\mathrm{T}} > 100\,\mathrm{GeV}$ and $p_{\mathrm{T}}^{\mathrm{miss}} > 140\,\mathrm{GeV}$	12.5 ± 3.4	13
2	2 SS leptons	1 jets, $M_{\mathrm{T}} < 100\,\mathrm{GeV}$, $p_{\mathrm{T}}^{\ell\ell} < 100\,\mathrm{GeV}$ and $p_{\mathrm{T}}^{\mathrm{miss}} > 200\,\mathrm{GeV}$	18 ± 4	18
3	3 light leptons	$M_{\mathrm{T}} > 120\,\mathrm{GeV}$ and $p_{\mathrm{T}}^{\mathrm{miss}} > 200\,\mathrm{GeV}$	19 ± 4	19
4	3 light leptons	$p_{\mathrm{T}}^{\mathrm{miss}} > 250\,\mathrm{GeV}$	142 ± 34	128
5	2 light leptons and 1 τ_{h}	$M_{\mathrm{T2}}(\ell_1, \tau) > 50\,\mathrm{GeV}$ and $p_{\mathrm{T}}^{\mathrm{miss}} > 200\,\mathrm{GeV}$	22 ± 5	18
6	1 light lepton and 2 τ_{h}s	$M_{\mathrm{T2}}(\ell, \tau_1) > 50\,\mathrm{GeV}$ and $p_{\mathrm{T}}^{\mathrm{miss}} > 200\,\mathrm{GeV}$	1.2 ± 0.6	2
7	1 light lepton and 2 τ_{h}s	$p_{\mathrm{T}}^{\mathrm{miss}} > 75\,\mathrm{GeV}$	109 ± 28	82
8	more than 3 leptons	$p_{\mathrm{T}}^{\mathrm{miss}} > 200\,\mathrm{GeV}$	3.2 ± 0.8	4

Table 19. Expected and observed yields in the aggregated signal regions defined in section 5.3. For each bin, the first number corresponds to the expected yield (exp.) and its uncertainty, and the second denotes the observed yield (obs.). The uncertainty denotes the total uncertainty in the yield.

JHEP03(2018)166

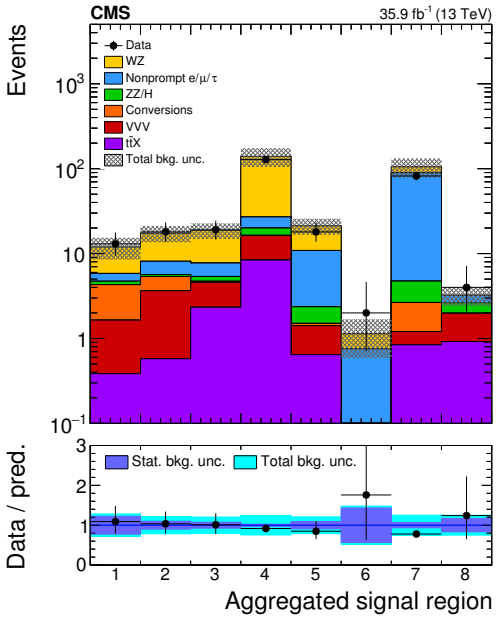


Figure 13. Expected and observed yields comparison in the aggregated signal regions. In this plot, the charge misidentification background prediction from control samples in data (that is only relevant in the first two bins due to the SS dilepton final state) are included in the nonprompt background prediction.

9 Interpretations of the searches

No evidence of any significant deviation with respect to the SM prediction is observed. The results of this search are interpreted in the context of the simplified models covering the scenarios described in section 2.

We compute 95% confidence level (CL) upper limits on the new-physics cross sections using the CL_s method [71–74], incorporating the uncertainties in the signal efficiency and acceptance and the uncertainties in the expected background described in section 7. Lognormal nuisance parameters are used for the signal and background estimate uncertainties. Only the categories with the lepton flavor, multiplicity, and charge requirements corresponding to the topology of the model under consideration are combined to maximize sensitivity to the model in question.

The production cross sections are computed at NLO plus next-to-leading-log (NLL) precision [27–29, 75] in a limit of mass-degenerate wino $\widetilde{\chi}_2^0$ and $\widetilde{\chi}_1^\pm$, light bino $\widetilde{\chi}_1^0$, and with all the other sparticles assumed to be heavy and decoupled. Similarly, for the higgsino models, production cross sections are computed in a limit of mass-degenerate higgsino $\widetilde{\chi}_2^0$, $\widetilde{\chi}_1^\pm$, and $\widetilde{\chi}_1^0$ with all the other sparticles assumed to be heavy and decoupled.

The interpretations of the results are displayed in figures 14–19 for all of the models described in section 2. Each plot shows the 95% CL upper limit on the chargino-neutralino production cross section as a function of the relevant pair of sparticle masses. The observed, $\pm 1\,\sigma_{\text{theory}}$ observed, median expected, and $\pm 1\,\sigma_{\text{experiment}}$ expected contours are also shown. The assumed BR for each model is displayed in each figure. For each interpretation, a

JHEP03(2018)166

Model	Categories used	Figure
$\widetilde{\chi}_1^{\pm}\widetilde{\chi}_2^0$ production, flavor-democratic, $m_{\tilde{\ell}} = m_{\widetilde{\chi}_1^0} + 0.5 \cdot (m_{\widetilde{\chi}_2^0} - m_{\widetilde{\chi}_1^0})$	A	14
$\widetilde{\chi}_1^{\pm}\widetilde{\chi}_2^0$ production, flavor-democratic, $m_{\tilde{\ell}} = m_{\widetilde{\chi}_1^0} + 0.05 \cdot (m_{\widetilde{\chi}_2^0} - m_{\widetilde{\chi}_1^0})$	SS, A	15 (left)
$\widetilde{\chi}_1^{\pm}\widetilde{\chi}_2^0$ production, flavor-democratic, $m_{\tilde{\ell}} = m_{\widetilde{\chi}_1^0} + 0.95 \cdot (m_{\widetilde{\chi}_2^0} - m_{\widetilde{\chi}_1^0})$	SS, A	15 (right)
$\widetilde{\chi}_1^{\pm}\widetilde{\chi}_2^0$ production, τ-enriched, $m_{\tilde{\ell}} = m_{\widetilde{\chi}_1^0} + 0.05 \cdot (m_{\widetilde{\chi}_2^0} - m_{\widetilde{\chi}_1^0})$	A, C	16 (left)
$\widetilde{\chi}_1^{\pm}\widetilde{\chi}_2^0$ production, τ-enriched, $m_{\tilde{\ell}} = m_{\widetilde{\chi}_1^0} + 0.5 \cdot (m_{\widetilde{\chi}_2^0} - m_{\widetilde{\chi}_1^0})$	A, C	16 (center)
$\widetilde{\chi}_1^{\pm}\widetilde{\chi}_2^0$ production, τ-enriched, $m_{\tilde{\ell}} = m_{\widetilde{\chi}_1^0} + 0.95 \cdot (m_{\widetilde{\chi}_2^0} - m_{\widetilde{\chi}_1^0})$	A, C	16 (right)
$\widetilde{\chi}_1^{\pm}\widetilde{\chi}_2^0$ production, τ-dominated, $m_{\tilde{\tau}} = m_{\widetilde{\chi}_1^0} + 0.5 \cdot (m_{\widetilde{\chi}_2^0} - m_{\widetilde{\chi}_1^0})$	B–F	17
$\widetilde{\chi}_1^{\pm}\widetilde{\chi}_2^0$ production, heavy sleptons, $\widetilde{\chi}_1^{\pm}\widetilde{\chi}_2^0 \to$ WZ	A	18 (left)
$\widetilde{\chi}_1^{\pm}\widetilde{\chi}_2^0$ production, heavy sleptons, $\widetilde{\chi}_1^{\pm}\widetilde{\chi}_2^0 \to$ WH	SS, A–K	18 (right)
$\widetilde{\chi}_1^0\widetilde{\chi}_1^0$ production, $\widetilde{\chi}_1^0\widetilde{\chi}_1^0 \to$ ZZ$\widetilde{\mathrm{G}}\widetilde{\mathrm{G}}$	A–K	19 (upper)
$\widetilde{\chi}_1^0\widetilde{\chi}_1^0$ production, $\widetilde{\chi}_1^0\widetilde{\chi}_1^0 \to$ HZ$\widetilde{\mathrm{G}}\widetilde{\mathrm{G}}$	A–K	19 (middle)
$\widetilde{\chi}_1^0\widetilde{\chi}_1^0$ production, $\widetilde{\chi}_1^0\widetilde{\chi}_1^0 \to$ HH$\widetilde{\mathrm{G}}\widetilde{\mathrm{G}}$	A–K	19 (lower)

Table 20. Summary of the interpretations of the results using different models.

combined global fit is performed using only the signal region categories listed in table 20, in order to consider all the correlations across different bins and to constrain the background estimation and uncertainties. No systematic uncertainty gets significantly constrained by the global fit. The figure displaying each interpretation is also cited in the table.

The sensitivity in the flavor-democratic and τ-enriched models, where the mass difference between the $\widetilde{\chi}_1^{\pm}$, $\widetilde{\chi}_2^0$ and the $\widetilde{\chi}_1^0$ is large, is driven by the signal regions A (three e or μ with an OSSF pair) with large $M_{\ell\ell}$, M_{T} and $p_{\mathrm{T}}^{\mathrm{miss}}$ values (SR A42, SR A43, and SR A44). As in these signal regions observed counts in data are below the expected SM background, the observed upper limit on the chargino and neutralino masses with a light $\widetilde{\chi}_1^0$ is stronger than the expected one in figures 14–16.

On the other hand, in the compressed scenarios of the flavor-democratic and τ-enriched models with $x = 0.05$ or $x = 0.95$, where masses of the heavier $\widetilde{\chi}_1^{\pm}$, $\widetilde{\chi}_2^0$ are close to the mass of the $\widetilde{\chi}_1^0$, the analysis sensitivity is dominated by the SS dilepton signal regions with an ISR jet, and large M_{T} and $p_{\mathrm{T}}^{\mathrm{miss}}$ values. Since in these regions the observed yields in data are slightly above the expected SM background, the observed upper limit close to the diagonal is weaker than the expected one in figure 15. To enhance the sensitivity to the τ-dominated model (figure 17), yields from signal regions B to F are used in the interpretation. Among these regions, the ones contributing the most to the total result are signal regions F (one e or μ and two τ_{h} candidates), E (two e or μ of same sign and one τ_{h} candidate), and D (one e and one μ of opposite sign, and one τ_{h} candidate) in order of importance.

In the case in which $\widetilde{\chi}_1^{\pm}$ and $\widetilde{\chi}_2^0$ decay via W and Z bosons, the constraints on the chargino and neutralino masses are weaker (figure 18 left) due to the lower branching fraction to a multilepton final state, and higher WZ SM background in the on-Z signal regions A which drive the sensitivity in this model. In the region where the mass difference between the $\widetilde{\chi}_1^{\pm}$, the $\widetilde{\chi}_2^0$, and the $\widetilde{\chi}_1^0$ is close to the Z boson mass, the analysis sensitivity drops significantly. This happens because the $\widetilde{\chi}_1^{\pm}$ and $\widetilde{\chi}_2^0$ decay products are produced at rest,

JHEP03(2018)166

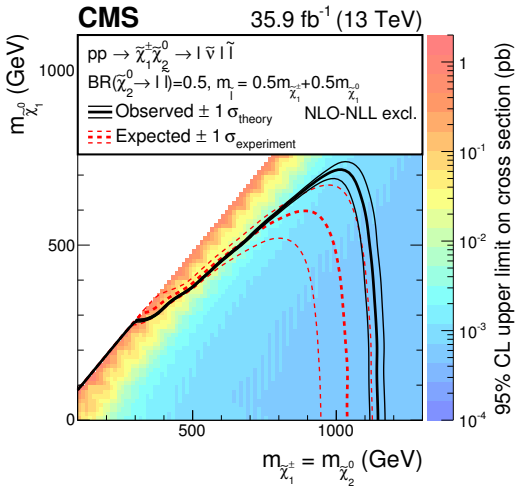


Figure 14. Interpretation of the results in the flavor-democratic model with mass parameter $x = 0.5$ obtained with events of category A. The shading in the $m_{\widetilde{\chi}_1^0}$ versus $m_{\widetilde{\chi}_2^0}$ ($= m_{\widetilde{\chi}_1^\pm}$) plane indicates the 95% CL upper limit on the chargino-neutralino production cross section. The contours bound the mass regions excluded at 95% CL assuming the NLO+NLL cross sections. The observed, $\pm 1\,\sigma_{\text{theory}}$ (± 1 standard deviation of the theoretical cross section) observed, median expected, and $\pm 1\,\sigma_{\text{experiment}}$ expected bounds are shown.

and the $\widetilde{\chi}_1^0$ does not carry large momentum, leading to low additional $p_{\text{T}}^{\text{miss}}$ in the detector. Such a final state is very similar to the SM WZ production, and $M_{\ell\ell}$ variable becomes the only discriminating variable in the signal regions A. In the case of the considered signals, the $M_{\ell\ell}$ has an upper cutoff at $m_{\widetilde{\chi}_2^0} - m_{\widetilde{\chi}_1^0}$ while the SM WZ process does not. This reduces the overall analysis sensitivity in this region and leads to a structure in the mass limit in figure 18 (left).

For the model with $\widetilde{\chi}_1^\pm$ and $\widetilde{\chi}_2^0$ decaying via W and Higgs bosons, all signal regions of the analysis are used. This approach is motivated by the diverse decay modes of the Higgs boson to leptonic final states (via an intermediate W or Z boson, or τ leptons). The most important signal regions in the order of their sensitivity are B (three e or μ that do not form an OSSF pair), A, and to a smaller extent signal regions F, E, D, and SS. The signal regions with more than three leptons (G to K) do not bring any visible improvement to the sensitivity in this scenario.

Finally, in the considered GMSB scenarios leading to the ZZ, HZ, and HH bosons in the final states (figure 19) all trilepton and four-lepton signal regions are used for the interpretation. The sensitivity in the model with two Z bosons in the final state is dominated by the four-lepton signal regions; in the model with two Higgs bosons in the final state by the trilepton signal regions; and in the mixed scenario four-lepton signal regions are more sensitive when the higgsino masses are low, while the trilepton signal regions contribute the most when higgsinos are heavy.

JHEP03(2018)166

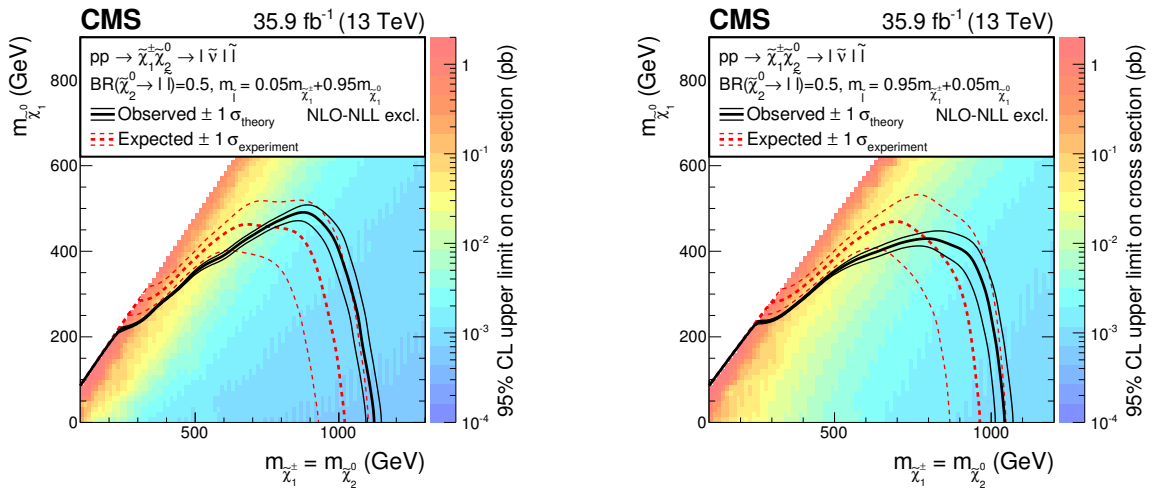


Figure 15. Interpretation of the results in the flavor-democratic model with mass parameter $x = 0.05$ (left) and $x = 0.95$ (right) obtained with the combination of the SS dilepton category and category A. The shading in this figure is as described in figure 14.

JHEP03(2018)166

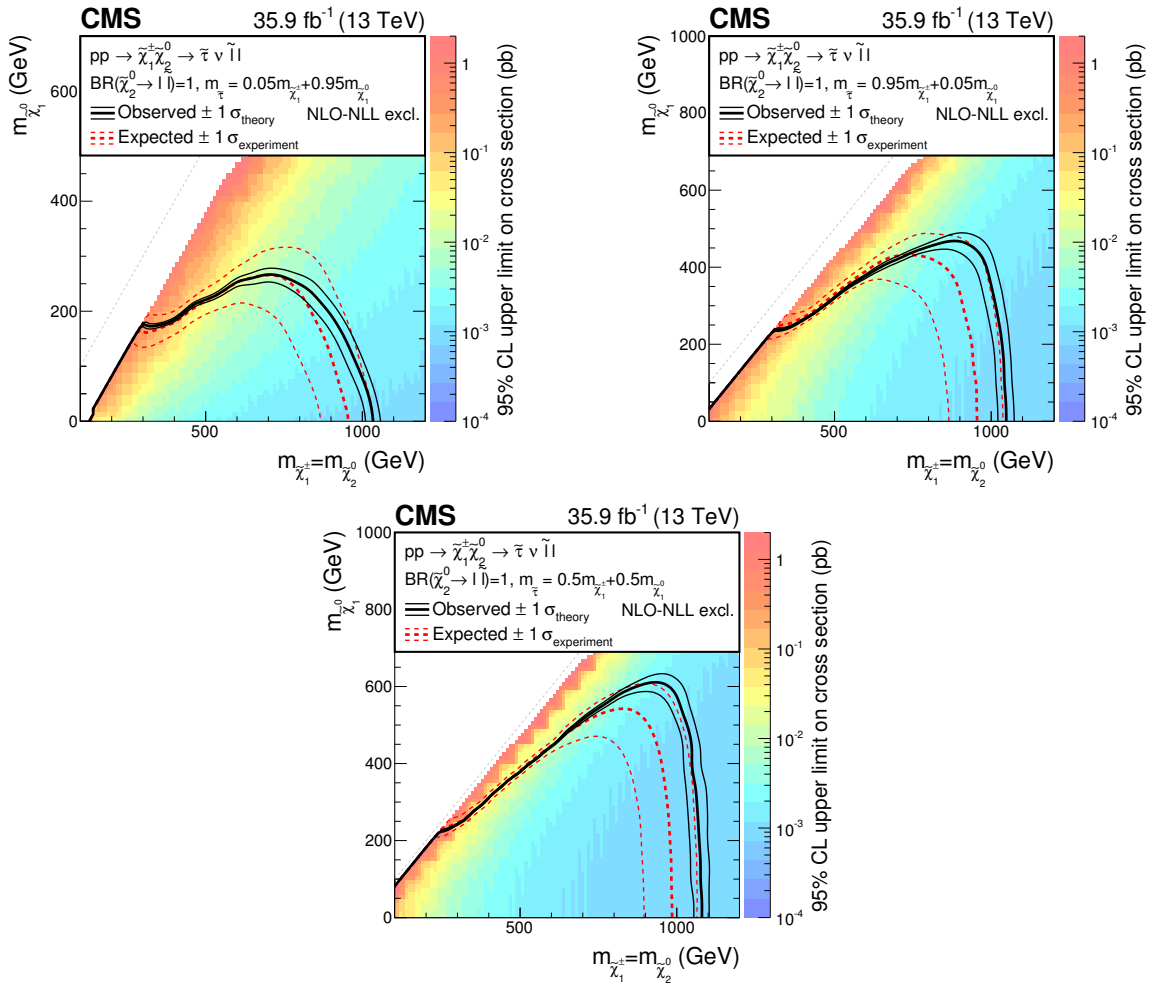


Figure 16. Interpretation of the results in the τ-enriched model with mass parameter $x = 0.05$ (upper-left), $x = 0.95$ (upper-right) and $x = 0.5$ (lower) obtained with events of categories A and C. The shading in this figure is as described in figure 14.

JHEP03(2018)166

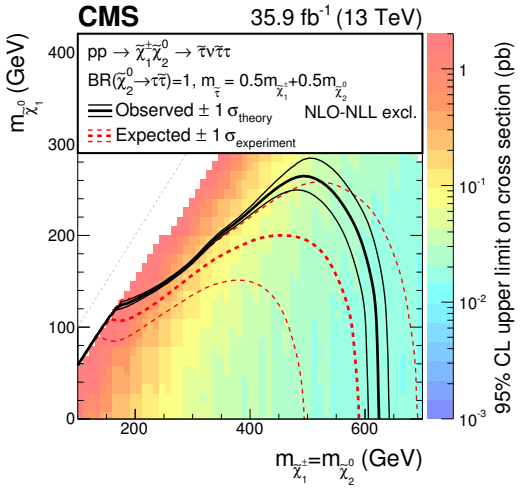


Figure 17. Interpretation of the results in the τ-dominated model with mass parameter $x = 0.5$ obtained with events of category B–F. The shading in this figure is as described in figure 14.

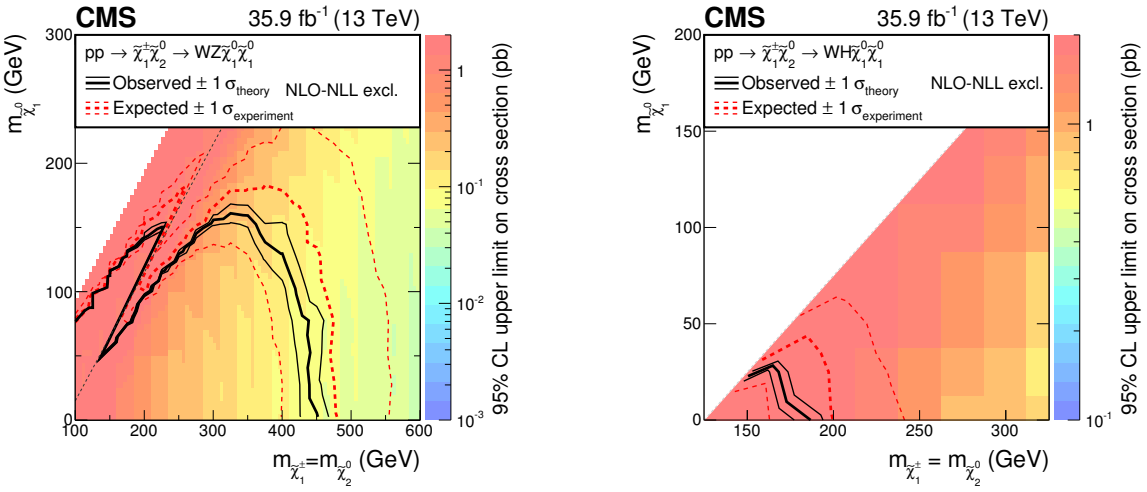


Figure 18. Interpretation of the results in the $\widetilde{\chi}_1^{\pm}\widetilde{\chi}_2^0 \to \mathrm{WZ}\widetilde{\chi}_1^0\widetilde{\chi}_1^0$ (left) model obtained with events of category A and the $\widetilde{\chi}_1^{\pm}\widetilde{\chi}_2^0 \to \mathrm{WH}\widetilde{\chi}_1^0\widetilde{\chi}_1^0$ (right) model obtained with events of all categories (SS dilepton, trilepton, and four-lepton). The shading in this figure is as described in figure 14. The dashed grey line on the left plot corresponds to a mass difference between the $\widetilde{\chi}_1^{\pm}$ and $\widetilde{\chi}_1^0$ equal to the Z mass.

JHEP03(2018)166

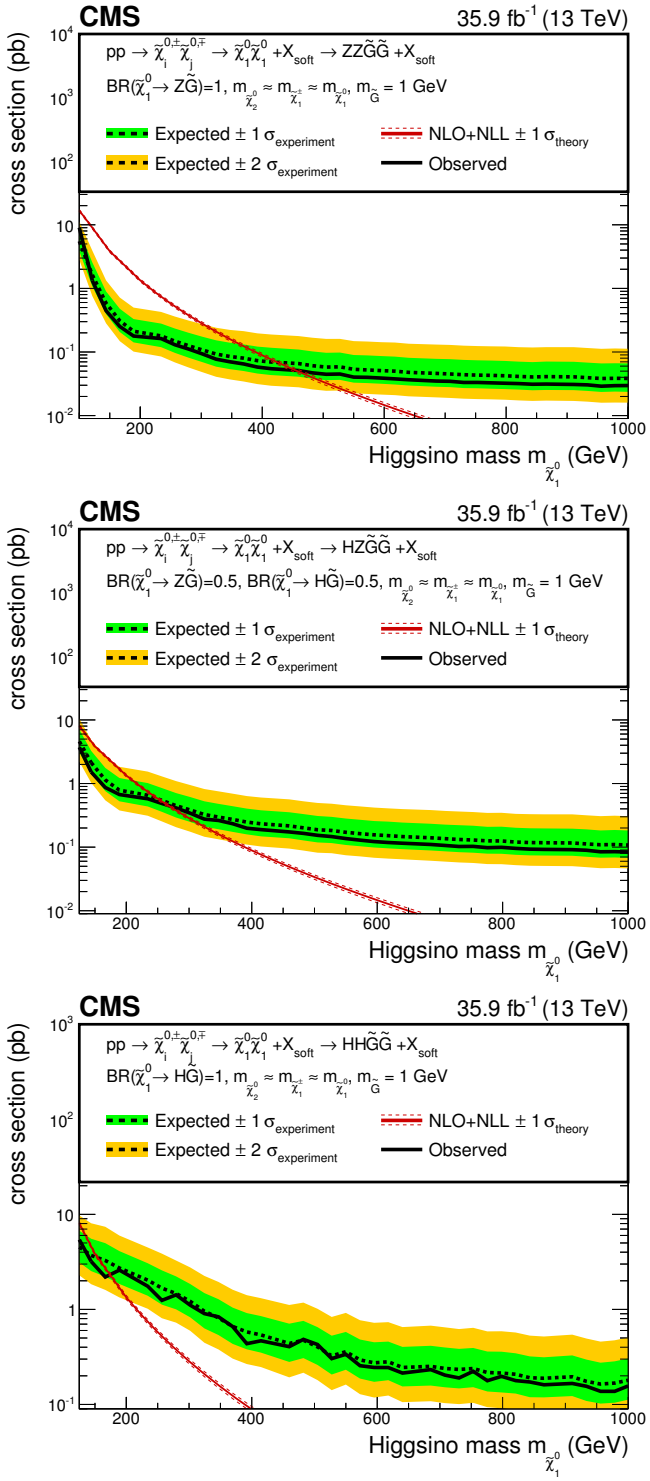


Figure 19. Interpretation of the results in the $\widetilde{\chi}_1^0\widetilde{\chi}_1^0 \to \mathrm{ZZ}\widetilde{\mathrm{G}}\widetilde{\mathrm{G}}$ model (upper), the $\widetilde{\chi}_1^0\widetilde{\chi}_1^0 \to \mathrm{HZ}\widetilde{\mathrm{G}}\widetilde{\mathrm{G}}$ model (middle), and the $\widetilde{\chi}_1^0\widetilde{\chi}_1^0 \to \mathrm{HH}\widetilde{\mathrm{G}}\widetilde{\mathrm{G}}$ model (lower) obtained with events of all trilepton (A–F) and all four-lepton (G–K) categories. The observed, median expected, $\pm 1\,\sigma_{\mathrm{experiment}}$ expected, and $\pm 2\,\sigma_{\mathrm{experiment}}$ expected 95% CL upper limit on the neutralino pair production cross section are compared to the NLO+NLL cross sections $\pm 1\,\sigma_{\mathrm{theory}}$.

JHEP03(2018)166

10 Summary

Results are presented from a search for new physics in same-sign dilepton, trilepton, and four-lepton events containing up to two hadronically decaying τ leptons in proton-proton collision data at $\sqrt{s} = 13\,\text{TeV}$, recorded with the CMS detector at the LHC and corresponding to an integrated luminosity of $35.9\,\text{fb}^{-1}$. The data are categorized based on the number, charge, and flavor of the leptons, and are subdivided into several kinematic regions to be sensitive to a broad range of supersymmetric particles produced via the electroweak interaction.

No significant deviation from the standard model expectations is observed. The results are used to set limits on various simplified models of supersymmetry (SUSY) that entail the production of superpartners of electroweak gauge or Higgs bosons (charginos and neutralinos). Specifically, we consider chargino-neutralino pair production, the electroweak process that is expected to have the largest cross section, and higgsino pair production in a gauge-mediated SUSY breaking inspired SUSY scenario. The resulting signal topologies depend on the masses of the lepton superpartners.

Models with light left-handed sleptons lead to enhanced branching fractions to final states with three leptons. The results imply limits on the masses of charginos and neutralinos up to 1150 GeV at 95% confidence level for the flavor-democratic scenario, extending the reach of our previous search [21] by about 450 GeV. In these models, searches in the same-sign dilepton final state enhance the sensitivity in the experimentally challenging region with small mass difference between the produced gauginos and the lightest supersymmetric particle (LSP) that is inaccessible with the trilepton signature.

Assuming light right-handed sleptons, we consider two scenarios, one in which the chargino decays to τ leptons while the neutralino decays democratically, and another in which both chargino and neutralino decay to τ leptons. For the former we exclude masses of charginos and neutralinos up to 1050 GeV, while for the latter masses up to 625 GeV are excluded.

We also consider scenarios that involve the direct decay of gauginos to the LSP via W and Z or Higgs bosons. For the models with W and Z bosons, chargino masses up to 475 GeV are excluded, improving the previous reach by 200 GeV. In the case of the neutralino decay via a Higgs boson, masses up to 180 GeV are excluded.

In the case of the gauge-mediated SUSY breaking model with four higgsinos and an effectively massless gravitino as the LSP, we exclude higgsino masses up to 450 GeV depending on the assumed next-to-LSP branching fraction to Z or H boson. Finally, results are presented in a form suitable for alternative theoretical interpretations.

Acknowledgments

We congratulate our colleagues in the CERN accelerator departments for the excellent performance of the LHC and thank the technical and administrative staffs at CERN and at other CMS institutes for their contributions to the success of the CMS effort. In addition, we gratefully acknowledge the computing centers and personnel of the Worldwide

JHEP03(2018)166

LHC Computing Grid for delivering so effectively the computing infrastructure essential to our analyses. Finally, we acknowledge the enduring support for the construction and operation of the LHC and the CMS detector provided by the following funding agencies: BMWFW and FWF (Austria); FNRS and FWO (Belgium); CNPq, CAPES, FAPERJ, and FAPESP (Brazil); MES (Bulgaria); CERN; CAS, MoST, and NSFC (China); COLCIENCIAS (Colombia); MSES and CSF (Croatia); RPF (Cyprus); SENESCYT (Ecuador); MoER, ERC IUT, and ERDF (Estonia); Academy of Finland, MEC, and HIP (Finland); CEA and CNRS/IN2P3 (France); BMBF, DFG, and HGF (Germany); GSRT (Greece); OTKA and NIH (Hungary); DAE and DST (India); IPM (Iran); SFI (Ireland); INFN (Italy); MSIP and NRF (Republic of Korea); LAS (Lithuania); MOE and UM (Malaysia); BUAP, CINVESTAV, CONACYT, LNS, SEP, and UASLP-FAI (Mexico); MBIE (New Zealand); PAEC (Pakistan); MSHE and NSC (Poland); FCT (Portugal); JINR (Dubna); MON, RosAtom, RAS, RFBR and RAEP (Russia); MESTD (Serbia); SEIDI, CPAN, PCTI and FEDER (Spain); Swiss Funding Agencies (Switzerland); MST (Taipei); ThEPCenter, IPST, STAR, and NSTDA (Thailand); TUBITAK and TAEK (Turkey); NASU and SFFR (Ukraine); STFC (United Kingdom); DOE and NSF (U.S.A.).

Individuals have received support from the Marie-Curie program and the European Research Council and Horizon 2020 Grant, contract No. 675440 (European Union); the Leventis Foundation; the A. P. Sloan Foundation; the Alexander von Humboldt Foundation; the Belgian Federal Science Policy Office; the Fonds pour la Formation à la Recherche dans l'Industrie et dans l'Agriculture (FRIA-Belgium); the Agentschap voor Innovatie door Wetenschap en Technologie (IWT-Belgium); the Ministry of Education, Youth and Sports (MEYS) of the Czech Republic; the Council of Science and Industrial Research, India; the HOMING PLUS program of the Foundation for Polish Science, cofinanced from European Union, Regional Development Fund, the Mobility Plus program of the Ministry of Science and Higher Education, the National Science Center (Poland), contracts Harmonia 2014/14/M/ST2/00428, Opus 2014/13/B/ST2/02543, 2014/15/B/ST2/03998, and 2015/19/B/ST2/02861, Sonata-bis 2012/07/E/ST2/01406; the National Priorities Research Program by Qatar National Research Fund; the Programa Clarín-COFUND del Principado de Asturias; the Thalis and Aristeia programs cofinanced by EU-ESF and the Greek NSRF; the Rachadapisek Sompot Fund for Postdoctoral Fellowship, Chulalongkorn University and the Chulalongkorn Academic into Its 2nd Century Project Advancement Project (Thailand); the Welch Foundation, contract C-1845; and the Weston Havens Foundation (U.S.A.).

Open Access. This article is distributed under the terms of the Creative Commons Attribution License (CC-BY 4.0), which permits any use, distribution and reproduction in any medium, provided the original author(s) and source are credited.

References

[1] ATLAS collaboration, *Observation of a new particle in the search for the Standard Model Higgs boson with the ATLAS detector at the LHC*, *Phys. Lett.* **B 716** (2012) 1 [arXiv:1207.7214] [INSPIRE].

JHEP03(2018)166

[2] CMS collaboration, *Observation of a new boson at a mass of* 125 *GeV with the CMS experiment at the LHC*, *Phys. Lett.* **B 716** (2012) 30 [arXiv:1207.7235] [INSPIRE].

[3] CMS collaboration, *Observation of a new boson with mass near* 125 *GeV in pp collisions at* $\sqrt{s} = 7$ *and* 8 *TeV*, *JHEP* **06** (2013) 081 [arXiv:1303.4571] [INSPIRE].

[4] R. Barbieri and G.F. Giudice, *Upper bounds on supersymmetric particle masses*, *Nucl. Phys.* **B 306** (1988) 63 [INSPIRE].

[5] E. Witten, *Dynamical breaking of supersymmetry*, *Nucl. Phys.* **B 188** (1981) 513 [INSPIRE].

[6] S. Dimopoulos and H. Georgi, *Softly broken supersymmetry and* SU(5), *Nucl. Phys.* **B 193** (1981) 150 [INSPIRE].

[7] P. Ramond, *Dual theory for free fermions*, *Phys. Rev.* **D 3** (1971) 2415 [INSPIRE].

[8] Yu. A. Golfand and E.P. Likhtman, *Extension of the algebra of Poincaré group generators and violation of p invariance*, *JETP Lett.* **13** (1971) 323 [*Pisma Zh. Eksp. Teor. Fiz.* **13** (1971) 452] [INSPIRE].

[9] A. Neveu and J.H. Schwarz, *Factorizable dual model of pions*, *Nucl. Phys.* **B 31** (1971) 86 [INSPIRE].

[10] D.V. Volkov and V.P. Akulov, *Possible universal neutrino interaction*, *JETP Lett.* **16** (1972) 438 [*Pisma Zh. Eksp. Teor. Fiz.* **16** (1972) 621] [INSPIRE].

[11] J. Wess and B. Zumino, *A Lagrangian model invariant under supergauge transformations*, *Phys. Lett.* **B 49** (1974) 52 [INSPIRE].

[12] J. Wess and B. Zumino, *Supergauge transformations in four-dimensions*, *Nucl. Phys.* **B 70** (1974) 39 [INSPIRE].

[13] P. Fayet, *Supergauge invariant extension of the Higgs mechanism and a model for the electron and its neutrino*, *Nucl. Phys.* **B 90** (1975) 104 [INSPIRE].

[14] H.P. Nilles, *Supersymmetry, supergravity and particle physics*, *Phys. Rept.* **110** (1984) 1 [INSPIRE].

[15] S.P. Martin, *A supersymmetry primer*, *Adv. Ser. Direct. High Energy Phys.* **18** (1998) 1 [*Adv. Ser. Direct. High Energy Phys.* **21** (2010) 1] [hep-ph/9709356] [INSPIRE].

[16] CMS collaboration, *Search for physics beyond the Standard Model in events with two leptons of same sign, missing transverse momentum and jets in proton-proton collisions at* $\sqrt{s} = 13$ *TeV*, *Eur. Phys. J.* **C 77** (2017) 578 [arXiv:1704.07323] [INSPIRE].

[17] CMS collaboration, *Search for new phenomena with the* M_{T2} *variable in the all-hadronic final state produced in proton-proton collisions at* $\sqrt{s} = 13$ *TeV*, *Eur. Phys. J.* **C 77** (2017) 710 [arXiv:1705.04650] [INSPIRE].

[18] CMS collaboration, *Search for supersymmetry in multijet events with missing transverse momentum in proton-proton collisions at* 13 *TeV*, *Phys. Rev.* **D 96** (2017) 032003 [arXiv:1704.07781] [INSPIRE].

[19] ATLAS collaboration, *Search for new phenomena in a lepton plus high jet multiplicity final state with the ATLAS experiment using* $\sqrt{s} = 13$ *TeV proton-proton collision data*, *JHEP* **09** (2017) 088 [arXiv:1704.08493] [INSPIRE].

[20] ATLAS collaboration, *Search for new phenomena in events containing a same-flavour opposite-sign dilepton pair, jets and large missing transverse momentum in* $\sqrt{s} = 13$ *TeV pp collisions with the ATLAS detector*, *Eur. Phys. J.* **C 77** (2017) 144 [arXiv:1611.05791] [INSPIRE].

JHEP03(2018)166

[21] CMS collaboration, *Searches for electroweak production of charginos, neutralinos and sleptons decaying to leptons and W, Z and Higgs bosons in pp collisions at 8 TeV*, *Eur. Phys. J.* **C 74** (2014) 3036 [arXiv:1405.7570] [INSPIRE].

[22] CMS collaboration, *Searches for electroweak neutralino and chargino production in channels with Higgs, Z and W bosons in pp collisions at 8 TeV*, *Phys. Rev.* **D 90** (2014) 092007 [arXiv:1409.3168] [INSPIRE].

[23] ATLAS collaboration, *Search for the electroweak production of supersymmetric particles in $\sqrt{s} = 8$ TeV pp collisions with the ATLAS detector*, *Phys. Rev.* **D 93** (2016) 052002 [arXiv:1509.07152] [INSPIRE].

[24] CMS collaboration, *Interpretation of searches for supersymmetry with simplified models*, *Phys. Rev.* **D 88** (2013) 052017 [arXiv:1301.2175] [INSPIRE].

[25] LHC New Physics Working Group collaboration, D. Alves, *Simplified models for LHC new physics searches*, *J. Phys.* **G 39** (2012) 105005 [arXiv:1105.2838] [INSPIRE].

[26] Particle Data Group collaboration, C. Patrignani et al., *Review of particle physics*, *Chin. Phys.* **C 40** (2016) 100001 [INSPIRE].

[27] W. Beenakker, M. Klasen, M. Krämer, T. Plehn, M. Spira and P.M. Zerwas, *The production of charginos/neutralinos and sleptons at hadron colliders*, *Phys. Rev. Lett.* **83** (1999) 3780 [*Erratum ibid.* **100** (2008) 029901] [hep-ph/9906298] [INSPIRE].

[28] B. Fuks, M. Klasen, D.R. Lamprea and M. Rothering, *Gaugino production in proton-proton collisions at a center-of-mass energy of 8 TeV*, *JHEP* **10** (2012) 081 [arXiv:1207.2159] [INSPIRE].

[29] B. Fuks, M. Klasen, D.R. Lamprea and M. Rothering, *Precision predictions for electroweak superpartner production at hadron colliders with Resummino*, *Eur. Phys. J.* **C 73** (2013) 2480 [arXiv:1304.0790] [INSPIRE].

[30] K.T. Matchev and S.D. Thomas, *Higgs and Z boson signatures of supersymmetry*, *Phys. Rev.* **D 62** (2000) 077702 [hep-ph/9908482] [INSPIRE].

[31] J.T. Ruderman and D. Shih, *General neutralino NLSPs at the early LHC*, *JHEP* **08** (2012) 159 [arXiv:1103.6083] [INSPIRE].

[32] P. Meade, M. Reece and D. Shih, *Prompt decays of general neutralino NLSPs at the Tevatron*, *JHEP* **05** (2010) 105 [arXiv:0911.4130] [INSPIRE].

[33] P.Z. Skands et al., *SUSY Les Houches accord: interfacing SUSY spectrum calculators, decay packages and event generators*, *JHEP* **07** (2004) 036 [hep-ph/0311123] [INSPIRE].

[34] CMS collaboration, *The CMS experiment at the CERN LHC*, 2008 *JINST* **3** S08004 [INSPIRE].

[35] CMS collaboration, *Particle-flow reconstruction and global event description with the CMS detector*, 2017 *JINST* **12** P10003 [arXiv:1706.04965] [INSPIRE].

[36] CMS collaboration, *Performance of electron reconstruction and selection with the CMS detector in proton-proton collisions at $\sqrt{s} = 8$ TeV*, 2015 *JINST* **10** P06005 [arXiv:1502.02701] [INSPIRE].

[37] CMS collaboration, *Performance of CMS muon reconstruction in pp collision events at $\sqrt{s} = 7$ TeV*, 2012 *JINST* **7** P10002 [arXiv:1206.4071] [INSPIRE].

JHEP03(2018)166

[38] CMS collaboration, *Description and performance of track and primary-vertex reconstruction with the CMS tracker*, 2014 *JINST* **9** P10009 [arXiv:1405.6569] [INSPIRE].

[39] K. Rehermann and B. Tweedie, *Efficient identification of boosted semileptonic top quarks at the LHC*, *JHEP* **03** (2011) 059 [arXiv:1007.2221] [INSPIRE].

[40] CMS collaboration, *Search for new physics in same-sign dilepton events in proton-proton collisions at* $\sqrt{s} = 13$ *TeV*, *Eur. Phys. J.* **C 76** (2016) 439 [arXiv:1605.03171] [INSPIRE].

[41] B.P. Roe, H.-J. Yang, J. Zhu, Y. Liu, I. Stancu and G. McGregor, *Boosted decision trees, an alternative to artificial neural networks*, *Nucl. Instrum. Meth.* **A 543** (2005) 577 [physics/0408124] [INSPIRE].

[42] CMS collaboration, *Search for the associated production of the Higgs boson with a top-quark pair*, *JHEP* **09** (2014) 087 [*Erratum ibid.* **10** (2014) 106] [arXiv:1408.1682] [INSPIRE].

[43] CMS collaboration, *Reconstruction and identification of* τ *lepton decays to hadrons and* ν_τ *at CMS*, 2016 *JINST* **11** P01019 [arXiv:1510.07488] [INSPIRE].

[44] CMS collaboration, *Performance of reconstruction and identification of tau leptons in their decays to hadrons and tau neutrino in LHC run-2*, CMS-PAS-TAU-16-002, CERN, Geneva Switzerland, (2016).

[45] M. Cacciari, G.P. Salam and G. Soyez, *The anti-*k_t *jet clustering algorithm*, *JHEP* **04** (2008) 063 [arXiv:0802.1189] [INSPIRE].

[46] M. Cacciari, G.P. Salam and G. Soyez, *FastJet user manual*, *Eur. Phys. J.* **C 72** (2012) 1896 [arXiv:1111.6097] [INSPIRE].

[47] M. Cacciari and G.P. Salam, *Dispelling the* N^3 *myth for the* k_t *jet-finder*, *Phys. Lett.* **B 641** (2006) 57 [hep-ph/0512210] [INSPIRE].

[48] CMS collaboration, *Determination of jet energy calibration and transverse momentum resolution in CMS*, 2011 *JINST* **6** P11002 [arXiv:1107.4277] [INSPIRE].

[49] M. Cacciari and G.P. Salam, *Pileup subtraction using jet areas*, *Phys. Lett.* **B 659** (2008) 119 [arXiv:0707.1378] [INSPIRE].

[50] CMS collaboration, *Jet energy scale and resolution in the CMS experiment in pp collisions at* 8 *TeV*, 2017 *JINST* **12** P02014 [arXiv:1607.03663] [INSPIRE].

[51] CMS collaboration, *Identification of b-quark jets with the CMS experiment*, 2013 *JINST* **8** P04013 [arXiv:1211.4462] [INSPIRE].

[52] CMS collaboration, *Identification of heavy-flavour jets with the CMS detector in pp collisions at* 13 *TeV*, submitted to *JINST* (2017) [arXiv:1712.07158] [INSPIRE].

[53] CMS collaboration, *Performance of the CMS missing transverse momentum reconstruction in pp data at* $\sqrt{s} = 8$ *TeV*, 2015 *JINST* **10** P02006 [arXiv:1411.0511] [INSPIRE].

[54] J. Alwall et al., *The automated computation of tree-level and next-to-leading order differential cross sections and their matching to parton shower simulations*, *JHEP* **07** (2014) 079 [arXiv:1405.0301] [INSPIRE].

[55] J. Alwall et al., *Comparative study of various algorithms for the merging of parton showers and matrix elements in hadronic collisions*, *Eur. Phys. J.* **C 53** (2008) 473 [arXiv:0706.2569] [INSPIRE].

[56] R. Frederix and S. Frixione, *Merging meets matching in MC@NLO*, *JHEP* **12** (2012) 061 [arXiv:1209.6215] [INSPIRE].

JHEP03(2018)166

[57] T. Melia, P. Nason, R. Rontsch and G. Zanderighi, *W^+W^-, WZ and ZZ production in the POWHEG BOX*, *JHEP* **11** (2011) 078 [arXiv:1107.5051] [INSPIRE].

[58] P. Nason and G. Zanderighi, *W^+W^- , WZ and ZZ production in the POWHEG-BOX-V2*, *Eur. Phys. J.* **C 74** (2014) 2702 [arXiv:1311.1365] [INSPIRE].

[59] NNPDF collaboration, R.D. Ball et al., *Parton distributions for the LHC run II*, *JHEP* **04** (2015) 040 [arXiv:1410.8849] [INSPIRE].

[60] T. Sjöstrand, S. Mrenna and P.Z. Skands, *A brief introduction to PYTHIA* 8.1, *Comput. Phys. Commun.* **178** (2008) 852 [arXiv:0710.3820] [INSPIRE].

[61] P. Skands, S. Carrazza and J. Rojo, *Tuning PYTHIA* 8.1*: the Monash* 2013 *tune*, *Eur. Phys. J.* **C 74** (2014) 3024 [arXiv:1404.5630] [INSPIRE].

[62] CMS collaboration, *Event generator tunes obtained from underlying event and multiparton scattering measurements*, *Eur. Phys. J.* **C 76** (2016) 155 [arXiv:1512.00815] [INSPIRE].

[63] GEANT4 collaboration, S. Agostinelli et al., *GEANT4: a simulation toolkit*, *Nucl. Instrum. Meth.* **A 506** (2003) 250 [INSPIRE].

[64] CMS collaboration, S. Abdullin, P. Azzi, F. Beaudette, P. Janot and A. Perrotta, *The fast simulation of the CMS detector at LHC*, *J. Phys. Conf. Ser.* **331** (2011) 032049 [INSPIRE].

[65] C.G. Lester and D.J. Summers, *Measuring masses of semiinvisibly decaying particles pair produced at hadron colliders*, *Phys. Lett.* **B 463** (1999) 99 [hep-ph/9906349] [INSPIRE].

[66] A. Barr, C. Lester and P. Stephens, *m_{T2}: the truth behind the glamour*, *J. Phys.* **G 29** (2003) 2343 [hep-ph/0304226] [INSPIRE].

[67] CMS collaboration, *CMS luminosity measurements for the* 2016 *data taking period*, CMS-PAS-LUM-17-001, CERN, Geneva Switzerland, (2017).

[68] CMS collaboration, *Measurement of inclusive W and Z boson production cross sections in pp collisions at $\sqrt{s} = 8$ TeV*, *Phys. Rev. Lett.* **112** (2014) 191802 [arXiv:1402.0923] [INSPIRE].

[69] J. Butterworth et al., *PDF4LHC recommendations for LHC run II*, *J. Phys.* **G 43** (2016) 023001 [arXiv:1510.03865] [INSPIRE].

[70] CMS collaboration, *Search for top-squark pair production in the single-lepton final state in pp collisions at $\sqrt{s} = 8$ TeV*, *Eur. Phys. J.* **C 73** (2013) 2677 [arXiv:1308.1586] [INSPIRE].

[71] G. Cowan, K. Cranmer, E. Gross and O. Vitells, *Asymptotic formulae for likelihood-based tests of new physics*, *Eur. Phys. J.* **C 71** (2011) 1554 [*Erratum ibid.* **C 73** (2013) 2501] [arXiv:1007.1727] [INSPIRE].

[72] T. Junk, *Confidence level computation for combining searches with small statistics*, *Nucl. Instrum. Meth.* **A 434** (1999) 435 [hep-ex/9902006] [INSPIRE].

[73] A.L. Read, *Presentation of search results: the CL_s technique*, *J. Phys.* **G 28** (2002) 2693 [INSPIRE].

[74] ATLAS, CMS collaborations and the LHC Higgs Combination Group, *Procedure for the LHC Higgs boson search combination in summer* 2011, ATL-PHYS-PUB-2011-11, CERN, Geneva Switzerland, (2011).

[75] B. Fuks, M. Klasen, D.R. Lamprea and M. Rothering, *Revisiting slepton pair production at the Large Hadron Collider*, *JHEP* **01** (2014) 168 [arXiv:1310.2621] [INSPIRE].

JHEP03(2018)166

The CMS collaboration

Yerevan Physics Institute, Yerevan, Armenia

A.M. Sirunyan, A. Tumasyan

Institut für Hochenergiephysik, Wien, Austria

W. Adam, F. Ambrogi, E. Asilar, T. Bergauer, J. Brandstetter, E. Brondolin, M. Dragicevic, J. Erö, M. Flechl, M. Friedl, R. Frühwirth[1], V.M. Ghete, J. Grossmann, J. Hrubec, M. Jeitler[1], A. König, N. Krammer, I. Krätschmer, D. Liko, T. Madlener, I. Mikulec, E. Pree, D. Rabady, N. Rad, H. Rohringer, J. Schieck[1], R. Schöfbeck, M. Spanring, D. Spitzbart, J. Strauss, W. Waltenberger, J. Wittmann, C.-E. Wulz[1], M. Zarucki

Institute for Nuclear Problems, Minsk, Belarus

V. Chekhovsky, V. Mossolov, J. Suarez Gonzalez

Universiteit Antwerpen, Antwerpen, Belgium

E.A. De Wolf, D. Di Croce, X. Janssen, J. Lauwers, H. Van Haevermaet, P. Van Mechelen, N. Van Remortel

Vrije Universiteit Brussel, Brussel, Belgium

S. Abu Zeid, F. Blekman, J. D'Hondt, I. De Bruyn, J. De Clercq, K. Deroover, G. Flouris, D. Lontkovskyi, S. Lowette, S. Moortgat, L. Moreels, A. Olbrechts, Q. Python, K. Skovpen, S. Tavernier, W. Van Doninck, P. Van Mulders, I. Van Parijs

Université Libre de Bruxelles, Bruxelles, Belgium

H. Brun, B. Clerbaux, G. De Lentdecker, H. Delannoy, G. Fasanella, L. Favart, R. Goldouzian, A. Grebenyuk, G. Karapostoli, T. Lenzi, J. Luetic, T. Maerschalk, A. Marinov, A. Randle-conde, T. Seva, C. Vander Velde, P. Vanlaer, D. Vannerom, R. Yonamine, F. Zenoni, F. Zhang[2]

Ghent University, Ghent, Belgium

A. Cimmino, T. Cornelis, D. Dobur, A. Fagot, M. Gul, I. Khvastunov, D. Poyraz, C. Roskas, S. Salva, M. Tytgat, W. Verbeke, N. Zaganidis

Université Catholique de Louvain, Louvain-la-Neuve, Belgium

H. Bakhshiansohi, O. Bondu, S. Brochet, G. Bruno, A. Caudron, S. De Visscher, C. Delaere, M. Delcourt, B. Francois, A. Giammanco, A. Jafari, M. Komm, G. Krintiras, V. Lemaitre, A. Magitteri, A. Mertens, M. Musich, K. Piotrzkowski, L. Quertenmont, M. Vidal Marono, S. Wertz

Université de Mons, Mons, Belgium

N. Beliy

Centro Brasileiro de Pesquisas Fisicas, Rio de Janeiro, Brazil

W.L. Aldá Júnior, F.L. Alves, G.A. Alves, L. Brito, M. Correa Martins Junior, C. Hensel, A. Moraes, M.E. Pol, P. Rebello Teles

JHEP03(2018)166

Universidade do Estado do Rio de Janeiro, Rio de Janeiro, Brazil
E. Belchior Batista Das Chagas, W. Carvalho, J. Chinellato[3], A. Custódio, E.M. Da Costa, G.G. Da Silveira[4], D. De Jesus Damiao, S. Fonseca De Souza, L.M. Huertas Guativa, H. Malbouisson, M. Melo De Almeida, C. Mora Herrera, L. Mundim, H. Nogima, A. Santoro, A. Sznajder, E.J. Tonelli Manganote[3], F. Torres Da Silva De Araujo, A. Vilela Pereira

Universidade Estadual Paulista [a], Universidade Federal do ABC [b], São Paulo, Brazil
S. Ahuja[a], C.A. Bernardes[a], T.R. Fernandez Perez Tomei[a], E.M. Gregores[b], P.G. Mercadante[b], S.F. Novaes[a], Sandra S. Padula[a], D. Romero Abad[b], J.C. Ruiz Vargas[a]

Institute for Nuclear Research and Nuclear Energy of Bulgaria Academy of Sciences
A. Aleksandrov, R. Hadjiiska, P. Iaydjiev, M. Misheva, M. Rodozov, M. Shopova, S. Stoykova, G. Sultanov

University of Sofia, Sofia, Bulgaria
A. Dimitrov, I. Glushkov, L. Litov, B. Pavlov, P. Petkov

Beihang University, Beijing, China
W. Fang[5], X. Gao[5]

Institute of High Energy Physics, Beijing, China
M. Ahmad, J.G. Bian, G.M. Chen, H.S. Chen, M. Chen, Y. Chen, C.H. Jiang, D. Leggat, H. Liao, Z. Liu, F. Romeo, S.M. Shaheen, A. Spiezia, J. Tao, C. Wang, Z. Wang, E. Yazgan, H. Zhang, J. Zhao

State Key Laboratory of Nuclear Physics and Technology, Peking University, Beijing, China
Y. Ban, G. Chen, Q. Li, S. Liu, Y. Mao, S.J. Qian, D. Wang, Z. Xu

Universidad de Los Andes, Bogota, Colombia
C. Avila, A. Cabrera, L.F. Chaparro Sierra, C. Florez, C.F. González Hernández, J.D. Ruiz Alvarez

University of Split, Faculty of Electrical Engineering, Mechanical Engineering and Naval Architecture, Split, Croatia
B. Courbon, N. Godinovic, D. Lelas, I. Puljak, P.M. Ribeiro Cipriano, T. Sculac

University of Split, Faculty of Science, Split, Croatia
Z. Antunovic, M. Kovac

Institute Rudjer Boskovic, Zagreb, Croatia
V. Brigljevic, D. Ferencek, K. Kadija, B. Mesic, A. Starodumov[6], T. Susa

University of Cyprus, Nicosia, Cyprus
M.W. Ather, A. Attikis, G. Mavromanolakis, J. Mousa, C. Nicolaou, F. Ptochos, P.A. Razis, H. Rykaczewski

JHEP03(2018)166

Charles University, Prague, Czech Republic
M. Finger[7], M. Finger Jr.[7]

Universidad San Francisco de Quito, Quito, Ecuador
E. Carrera Jarrin

Academy of Scientific Research and Technology of the Arab Republic of Egypt, Egyptian Network of High Energy Physics, Cairo, Egypt
E. El-khateeb[8], S. Elgammal[9], A. Ellithi Kamel[10]

National Institute of Chemical Physics and Biophysics, Tallinn, Estonia
R.K. Dewanjee, M. Kadastik, L. Perrini, M. Raidal, A. Tiko, C. Veelken

Department of Physics, University of Helsinki, Helsinki, Finland
P. Eerola, J. Pekkanen, M. Voutilainen

Helsinki Institute of Physics, Helsinki, Finland
J. Härkönen, T. Järvinen, V. Karimäki, R. Kinnunen, T. Lampén, K. Lassila-Perini, S. Lehti, T. Lindén, P. Luukka, E. Tuominen, J. Tuominiemi, E. Tuovinen

Lappeenranta University of Technology, Lappeenranta, Finland
J. Talvitie, T. Tuuva

IRFU, CEA, Université Paris-Saclay, Gif-sur-Yvette, France
M. Besancon, F. Couderc, M. Dejardin, D. Denegri, J.L. Faure, F. Ferri, S. Ganjour, S. Ghosh, A. Givernaud, P. Gras, G. Hamel de Monchenault, P. Jarry, I. Kucher, E. Locci, M. Machet, J. Malcles, G. Negro, J. Rander, A. Rosowsky, M.Ö. Sahin, M. Titov

Laboratoire Leprince-Ringuet, Ecole polytechnique, CNRS/IN2P3, Université Paris-Saclay, Palaiseau, France
A. Abdulsalam, I. Antropov, S. Baffioni, F. Beaudette, P. Busson, L. Cadamuro, C. Charlot, R. Granier de Cassagnac, M. Jo, S. Lisniak, A. Lobanov, J. Martin Blanco, M. Nguyen, C. Ochando, G. Ortona, P. Paganini, P. Pigard, S. Regnard, R. Salerno, J.B. Sauvan, Y. Sirois, A.G. Stahl Leiton, T. Strebler, Y. Yilmaz, A. Zabi, A. Zghiche

Université de Strasbourg, CNRS, IPHC UMR 7178, F-67000 Strasbourg, France
J.-L. Agram[11], J. Andrea, D. Bloch, J.-M. Brom, M. Buttignol, E.C. Chabert, N. Chanon, C. Collard, E. Conte[11], X. Coubez, J.-C. Fontaine[11], D. Gelé, U. Goerlach, M. Jansová, A.-C. Le Bihan, N. Tonon, P. Van Hove

Centre de Calcul de l'Institut National de Physique Nucleaire et de Physique des Particules, CNRS/IN2P3, Villeurbanne, France
S. Gadrat

Université de Lyon, Université Claude Bernard Lyon 1, CNRS-IN2P3, Institut de Physique Nucléaire de Lyon, Villeurbanne, France
S. Beauceron, C. Bernet, G. Boudoul, R. Chierici, D. Contardo, P. Depasse, H. El Mamouni, J. Fay, L. Finco, S. Gascon, M. Gouzevitch, G. Grenier, B. Ille, F. Lagarde, I.B. Laktineh,

JHEP03(2018)166

M. Lethuillier, L. Mirabito, A.L. Pequegnot, S. Perries, A. Popov[12], V. Sordini, M. Vander Donckt, S. Viret

Georgian Technical University, Tbilisi, Georgia
A. Khvedelidze[7]

Tbilisi State University, Tbilisi, Georgia
D. Lomidze

RWTH Aachen University, I. Physikalisches Institut, Aachen, Germany
C. Autermann, S. Beranek, L. Feld, M.K. Kiesel, K. Klein, M. Lipinski, M. Preuten, C. Schomakers, J. Schulz, T. Verlage

RWTH Aachen University, III. Physikalisches Institut A, Aachen, Germany
A. Albert, E. Dietz-Laursonn, D. Duchardt, M. Endres, M. Erdmann, S. Erdweg, T. Esch, R. Fischer, A. Güth, M. Hamer, T. Hebbeker, C. Heidemann, K. Hoepfner, S. Knutzen, M. Merschmeyer, A. Meyer, P. Millet, S. Mukherjee, M. Olschewski, K. Padeken, T. Pook, M. Radziej, H. Reithler, M. Rieger, F. Scheuch, D. Teyssier, S. Thüer

RWTH Aachen University, III. Physikalisches Institut B, Aachen, Germany
G. Flügge, B. Kargoll, T. Kress, A. Künsken, J. Lingemann, T. Müller, A. Nehrkorn, A. Nowack, C. Pistone, O. Pooth, A. Stahl[13]

Deutsches Elektronen-Synchrotron, Hamburg, Germany
M. Aldaya Martin, T. Arndt, C. Asawatangtrakuldee, K. Beernaert, O. Behnke, U. Behrens, A. Bermúdez Martínez, A.A. Bin Anuar, K. Borras[14], V. Botta, A. Campbell, P. Connor, C. Contreras-Campana, F. Costanza, C. Diez Pardos, G. Eckerlin, D. Eckstein, T. Eichhorn, E. Eren, E. Gallo[15], J. Garay Garcia, A. Geiser, A. Gizhko, J.M. Grados Luyando, A. Grohsjean, P. Gunnellini, A. Harb, J. Hauk, M. Hempel[16], H. Jung, A. Kalogeropoulos, M. Kasemann, J. Keaveney, C. Kleinwort, I. Korol, D. Krücker, W. Lange, A. Lelek, T. Lenz, J. Leonard, K. Lipka, W. Lohmann[16], R. Mankel, I.-A. Melzer-Pellmann, A.B. Meyer, G. Mittag, J. Mnich, A. Mussgiller, E. Ntomari, D. Pitzl, R. Placakyte, A. Raspereza, B. Roland, M. Savitskyi, P. Saxena, R. Shevchenko, S. Spannagel, N. Stefaniuk, G.P. Van Onsem, R. Walsh, Y. Wen, K. Wichmann, C. Wissing, O. Zenaiev

University of Hamburg, Hamburg, Germany
S. Bein, V. Blobel, M. Centis Vignali, A.R. Draeger, T. Dreyer, E. Garutti, D. Gonzalez, J. Haller, A. Hinzmann, M. Hoffmann, A. Karavdina, R. Klanner, R. Kogler, N. Kovalchuk, S. Kurz, T. Lapsien, I. Marchesini, D. Marconi, M. Meyer, M. Niedziela, D. Nowatschin, F. Pantaleo[13], T. Peiffer, A. Perieanu, C. Scharf, P. Schleper, A. Schmidt, S. Schumann, J. Schwandt, J. Sonneveld, H. Stadie, G. Steinbrück, F.M. Stober, M. Stöver, H. Tholen, D. Troendle, E. Usai, L. Vanelderen, A. Vanhoefer, B. Vormwald

Institut für Experimentelle Kernphysik, Karlsruhe, Germany
M. Akbiyik, C. Barth, S. Baur, E. Butz, R. Caspart, T. Chwalek, F. Colombo, W. De Boer, A. Dierlamm, B. Freund, R. Friese, M. Giffels, A. Gilbert, D. Haitz, F. Hartmann[13],

JHEP03(2018)166

S.M. Heindl, U. Husemann, F. Kassel[13], S. Kudella, H. Mildner, M.U. Mozer, Th. Müller, M. Plagge, G. Quast, K. Rabbertz, M. Schröder, I. Shvetsov, G. Sieber, H.J. Simonis, R. Ulrich, S. Wayand, M. Weber, T. Weiler, S. Williamson, C. Wöhrmann, R. Wolf

Institute of Nuclear and Particle Physics (INPP), NCSR Demokritos, Aghia Paraskevi, Greece

G. Anagnostou, G. Daskalakis, T. Geralis, V.A. Giakoumopoulou, A. Kyriakis, D. Loukas, I. Topsis-Giotis

National and Kapodistrian University of Athens, Athens, Greece

S. Kesisoglou, A. Panagiotou, N. Saoulidou

University of Ioánnina, Ioánnina, Greece

I. Evangelou, C. Foudas, P. Kokkas, S. Mallios, N. Manthos, I. Papadopoulos, E. Paradas, J. Strologas, F.A. Triantis

MTA-ELTE Lendület CMS Particle and Nuclear Physics Group, Eötvös Loránd University, Budapest, Hungary

M. Csanad, N. Filipovic, G. Pasztor

Wigner Research Centre for Physics, Budapest, Hungary

G. Bencze, C. Hajdu, D. Horvath[17], Á. Hunyadi, F. Sikler, V. Veszpremi, G. Vesztergombi[18], A.J. Zsigmond

Institute of Nuclear Research ATOMKI, Debrecen, Hungary

N. Beni, S. Czellar, J. Karancsi[19], A. Makovec, J. Molnar, Z. Szillasi

Institute of Physics, University of Debrecen, Debrecen, Hungary

M. Bartók[18], P. Raics, Z.L. Trocsanyi, B. Ujvari

Indian Institute of Science (IISc), Bangalore, India

S. Choudhury, J.R. Komaragiri

National Institute of Science Education and Research, Bhubaneswar, India

S. Bahinipati[20], S. Bhowmik, P. Mal, K. Mandal, A. Nayak[21], D.K. Sahoo[20], N. Sahoo, S.K. Swain

Panjab University, Chandigarh, India

S. Bansal, S.B. Beri, V. Bhatnagar, U. Bhawandeep, R. Chawla, N. Dhingra, A.K. Kalsi, A. Kaur, M. Kaur, R. Kumar, P. Kumari, A. Mehta, J.B. Singh, G. Walia

University of Delhi, Delhi, India

Ashok Kumar, Aashaq Shah, A. Bhardwaj, S. Chauhan, B.C. Choudhary, R.B. Garg, S. Keshri, A. Kumar, S. Malhotra, M. Naimuddin, K. Ranjan, R. Sharma, V. Sharma

Saha Institute of Nuclear Physics, HBNI, Kolkata, India

R. Bhardwaj, R. Bhattacharya, S. Bhattacharya, S. Dey, S. Dutt, S. Dutta, S. Ghosh, N. Majumdar, A. Modak, K. Mondal, S. Mukhopadhyay, S. Nandan, A. Purohit, A. Roy, D. Roy, S. Roy Chowdhury, S. Sarkar, M. Sharan, S. Thakur

JHEP03(2018)166

Indian Institute of Technology Madras, Madras, India

P.K. Behera

Bhabha Atomic Research Centre, Mumbai, India

R. Chudasama, D. Dutta, V. Jha, V. Kumar, A.K. Mohanty[13], P.K. Netrakanti, L.M. Pant, P. Shukla, A. Topkar

Tata Institute of Fundamental Research-A, Mumbai, India

T. Aziz, S. Dugad, B. Mahakud, S. Mitra, G.B. Mohanty, B. Parida, N. Sur, B. Sutar

Tata Institute of Fundamental Research-B, Mumbai, India

S. Banerjee, S. Bhattacharya, S. Chatterjee, P. Das, M. Guchait, Sa. Jain, S. Kumar, M. Maity[22], G. Majumder, K. Mazumdar, T. Sarkar[22], N. Wickramage[23]

Indian Institute of Science Education and Research (IISER), Pune, India

S. Chauhan, S. Dube, V. Hegde, A. Kapoor, K. Kothekar, S. Pandey, A. Rane, S. Sharma

Institute for Research in Fundamental Sciences (IPM), Tehran, Iran

S. Chenarani[24], E. Eskandari Tadavani, S.M. Etesami[24], M. Khakzad, M. Mohammadi Najafabadi, M. Naseri, S. Paktinat Mehdiabadi[25], F. Rezaei Hosseinabadi, B. Safarzadeh[26], M. Zeinali

University College Dublin, Dublin, Ireland

M. Felcini, M. Grunewald

INFN Sezione di Bari [a], Università di Bari [b], Politecnico di Bari [c], Bari, Italy

M. Abbrescia[a,b], C. Calabria[a,b], C. Caputo[a,b], A. Colaleo[a], D. Creanza[a,c], L. Cristella[a,b], N. De Filippis[a,c], M. De Palma[a,b], F. Errico[a,b], L. Fiore[a], G. Iaselli[a,c], S. Lezki[a,b], G. Maggi[a,c], M. Maggi[a], G. Miniello[a,b], S. My[a,b], S. Nuzzo[a,b], A. Pompili[a,b], G. Pugliese[a,c], R. Radogna[a,b], A. Ranieri[a], G. Selvaggi[a,b], A. Sharma[a], L. Silvestris[a,13], R. Venditti[a], P. Verwilligen[a]

INFN Sezione di Bologna [a], Università di Bologna [b], Bologna, Italy

G. Abbiendi[a], C. Battilana[a,b], D. Bonacorsi[a,b], S. Braibant-Giacomelli[a,b], R. Campanini[a,b], P. Capiluppi[a,b], A. Castro[a,b], F.R. Cavallo[a], S.S. Chhibra[a], G. Codispoti[a,b], M. Cuffiani[a,b], G.M. Dallavalle[a], F. Fabbri[a], A. Fanfani[a,b], D. Fasanella[a,b], P. Giacomelli[a], C. Grandi[a], L. Guiducci[a,b], S. Marcellini[a], G. Masetti[a], A. Montanari[a], F.L. Navarria[a,b], A. Perrotta[a], A.M. Rossi[a,b], T. Rovelli[a,b], G.P. Siroli[a,b], N. Tosi[a]

INFN Sezione di Catania [a], Università di Catania [b], Catania, Italy

S. Albergo[a,b], S. Costa[a,b], A. Di Mattia[a], F. Giordano[a,b], R. Potenza[a,b], A. Tricomi[a,b], C. Tuve[a,b]

INFN Sezione di Firenze [a], Università di Firenze [b], Firenze, Italy

G. Barbagli[a], K. Chatterjee[a,b], V. Ciulli[a,b], C. Civinini[a], R. D'Alessandro[a,b], E. Focardi[a,b], P. Lenzi[a,b], M. Meschini[a], S. Paoletti[a], L. Russo[a,27], G. Sguazzoni[a], D. Strom[a], L. Viliani[a,b,13]

JHEP03(2018)166

INFN Laboratori Nazionali di Frascati, Frascati, Italy

L. Benussi, S. Bianco, F. Fabbri, D. Piccolo, F. Primavera[13]

INFN Sezione di Genova [a], Università di Genova [b], Genova, Italy

V. Calvelli[a,b], F. Ferro[a], E. Robutti[a], S. Tosi[a,b]

INFN Sezione di Milano-Bicocca [a], Università di Milano-Bicocca [b], Milano, Italy

L. Brianza[a,b], F. Brivio[a,b], V. Ciriolo[a,b], M.E. Dinardo[a,b], S. Fiorendi[a,b], S. Gennai[a], A. Ghezzi[a,b], P. Govoni[a,b], M. Malberti[a,b], S. Malvezzi[a], R.A. Manzoni[a,b], D. Menasce[a], L. Moroni[a], M. Paganoni[a,b], K. Pauwels[a,b], D. Pedrini[a], S. Pigazzini[a,b,28], S. Ragazzi[a,b], T. Tabarelli de Fatis[a,b]

INFN Sezione di Napoli [a], Università di Napoli 'Federico II' [b], Napoli, Italy, Università della Basilicata [c], Potenza, Italy, Università G. Marconi [d], Roma, Italy

S. Buontempo[a], N. Cavallo[a,c], S. Di Guida[a,d,13], M. Esposito[a,b], F. Fabozzi[a,c], F. Fienga[a,b], A.O.M. Iorio[a,b], W.A. Khan[a], G. Lanza[a], L. Lista[a], S. Meola[a,d,13], P. Paolucci[a,13], C. Sciacca[a,b], F. Thyssen[a]

INFN Sezione di Padova [a], Università di Padova [b], Padova, Italy, Università di Trento [c], Trento, Italy

P. Azzi[a,13], N. Bacchetta[a], L. Benato[a,b], D. Bisello[a,b], A. Boletti[a,b], R. Carlin[a,b], A. Carvalho Antunes De Oliveira[a,b], P. Checchia[a], P. De Castro Manzano[a], T. Dorigo[a], U. Dosselli[a], F. Gasparini[a,b], U. Gasparini[a,b], A. Gozzelino[a], S. Lacaprara[a], M. Margoni[a,b], A.T. Meneguzzo[a,b], N. Pozzobon[a,b], P. Ronchese[a,b], R. Rossin[a,b], F. Simonetto[a,b], E. Torassa[a], M. Zanetti[a,b], P. Zotto[a,b], G. Zumerle[a,b]

INFN Sezione di Pavia [a], Università di Pavia [b], Pavia, Italy

A. Braghieri[a], F. Fallavollita[a,b], A. Magnani[a,b], P. Montagna[a,b], S.P. Ratti[a,b], V. Re[a], M. Ressegotti, C. Riccardi[a,b], P. Salvini[a], I. Vai[a,b], P. Vitulo[a,b]

INFN Sezione di Perugia [a], Università di Perugia [b], Perugia, Italy

L. Alunni Solestizi[a,b], M. Biasini[a,b], G.M. Bilei[a], C. Cecchi[a,b], D. Ciangottini[a,b], L. Fanò[a,b], P. Lariccia[a,b], R. Leonardi[a,b], E. Manoni[a], G. Mantovani[a,b], V. Mariani[a,b], M. Menichelli[a], A. Rossi[a,b], A. Santocchia[a,b], D. Spiga[a]

INFN Sezione di Pisa [a], Università di Pisa [b], Scuola Normale Superiore di Pisa [c], Pisa, Italy

K. Androsov[a], P. Azzurri[a,13], G. Bagliesi[a], J. Bernardini[a], T. Boccali[a], L. Borrello, R. Castaldi[a], M.A. Ciocci[a,b], R. Dell'Orso[a], G. Fedi[a], L. Giannini[a,c], A. Giassi[a], M.T. Grippo[a,27], F. Ligabue[a,c], T. Lomtadze[a], E. Manca[a,c], G. Mandorli[a,c], L. Martini[a,b], A. Messineo[a,b], F. Palla[a], A. Rizzi[a,b], A. Savoy-Navarro[a,29], P. Spagnolo[a], R. Tenchini[a], G. Tonelli[a,b], A. Venturi[a], P.G. Verdini[a]

JHEP03(2018)166

INFN Sezione di Roma [a], Sapienza Università di Roma [b], Rome, Italy

L. Barone[a,b], F. Cavallari[a], M. Cipriani[a,b], D. Del Re[a,b,13], M. Diemoz[a], S. Gelli[a,b], E. Longo[a,b], F. Margaroli[a,b], B. Marzocchi[a,b], P. Meridiani[a], G. Organtini[a,b], R. Paramatti[a,b], F. Preiato[a,b], S. Rahatlou[a,b], C. Rovelli[a], F. Santanastasio[a,b]

INFN Sezione di Torino [a], Università di Torino [b], Torino, Italy, Università del Piemonte Orientale [c], Novara, Italy

N. Amapane[a,b], R. Arcidiacono[a,c], S. Argiro[a,b], M. Arneodo[a,c], N. Bartosik[a], R. Bellan[a,b], C. Biino[a], N. Cartiglia[a], F. Cenna[a,b], M. Costa[a,b], R. Covarelli[a,b], A. Degano[a,b], N. Demaria[a], B. Kiani[a,b], C. Mariotti[a], S. Maselli[a], E. Migliore[a,b], V. Monaco[a,b], E. Monteil[a,b], M. Monteno[a], M.M. Obertino[a,b], L. Pacher[a,b], N. Pastrone[a], M. Pelliccioni[a], G.L. Pinna Angioni[a,b], F. Ravera[a,b], A. Romero[a,b], M. Ruspa[a,c], R. Sacchi[a,b], K. Shchelina[a,b], V. Sola[a], A. Solano[a,b], A. Staiano[a], P. Traczyk[a,b]

INFN Sezione di Trieste [a], Università di Trieste [b], Trieste, Italy

S. Belforte[a], M. Casarsa[a], F. Cossutti[a], G. Della Ricca[a,b], A. Zanetti[a]

Kyungpook National University, Daegu, Korea

D.H. Kim, G.N. Kim, M.S. Kim, J. Lee, S. Lee, S.W. Lee, C.S. Moon, Y.D. Oh, S. Sekmen, D.C. Son, Y.C. Yang

Chonbuk National University, Jeonju, Korea

A. Lee

Chonnam National University, Institute for Universe and Elementary Particles, Kwangju, Korea

H. Kim, D.H. Moon, G. Oh

Hanyang University, Seoul, Korea

J.A. Brochero Cifuentes, J. Goh, T.J. Kim

Korea University, Seoul, Korea

S. Cho, S. Choi, Y. Go, D. Gyun, S. Ha, B. Hong, Y. Jo, Y. Kim, K. Lee, K.S. Lee, S. Lee, J. Lim, S.K. Park, Y. Roh

Seoul National University, Seoul, Korea

J. Almond, J. Kim, J.S. Kim, H. Lee, K. Lee, K. Nam, S.B. Oh, B.C. Radburn-Smith, S.h. Seo, U.K. Yang, H.D. Yoo, G.B. Yu

University of Seoul, Seoul, Korea

M. Choi, H. Kim, J.H. Kim, J.S.H. Lee, I.C. Park, G. Ryu

Sungkyunkwan University, Suwon, Korea

Y. Choi, C. Hwang, J. Lee, I. Yu

Vilnius University, Vilnius, Lithuania

V. Dudenas, A. Juodagalvis, J. Vaitkus

JHEP03(2018)166

National Centre for Particle Physics, Universiti Malaya, Kuala Lumpur, Malaysia

I. Ahmed, Z.A. Ibrahim, M.A.B. Md Ali[30], F. Mohamad Idris[31], W.A.T. Wan Abdullah, M.N. Yusli, Z. Zolkapli

Centro de Investigacion y de Estudios Avanzados del IPN, Mexico City, Mexico

H. Castilla-Valdez, E. De La Cruz-Burelo, I. Heredia-De La Cruz[32], R. Lopez-Fernandez, J. Mejia Guisao, A. Sanchez-Hernandez

Universidad Iberoamericana, Mexico City, Mexico

S. Carrillo Moreno, C. Oropeza Barrera, F. Vazquez Valencia

Benemerita Universidad Autonoma de Puebla, Puebla, Mexico

I. Pedraza, H.A. Salazar Ibarguen, C. Uribe Estrada

Universidad Autónoma de San Luis Potosí, San Luis Potosí, Mexico

A. Morelos Pineda

University of Auckland, Auckland, New Zealand

D. Krofcheck

University of Canterbury, Christchurch, New Zealand

P.H. Butler

National Centre for Physics, Quaid-I-Azam University, Islamabad, Pakistan

A. Ahmad, M. Ahmad, Q. Hassan, H.R. Hoorani, A. Saddique, M.A. Shah, M. Shoaib, M. Waqas

National Centre for Nuclear Research, Swierk, Poland

H. Bialkowska, M. Bluj, B. Boimska, T. Frueboes, M. Górski, M. Kazana, K. Nawrocki, K. Romanowska-Rybinska, M. Szleper, P. Zalewski

Institute of Experimental Physics, Faculty of Physics, University of Warsaw, Warsaw, Poland

K. Bunkowski, A. Byszuk[33], K. Doroba, A. Kalinowski, M. Konecki, J. Krolikowski, M. Misiura, M. Olszewski, A. Pyskir, M. Walczak

Laboratório de Instrumentação e Física Experimental de Partículas, Lisboa, Portugal

P. Bargassa, C. Beirão Da Cruz E Silva, B. Calpas, A. Di Francesco, P. Faccioli, M. Gallinaro, J. Hollar, N. Leonardo, L. Lloret Iglesias, M.V. Nemallapudi, J. Seixas, O. Toldaiev, D. Vadruccio, J. Varela

Joint Institute for Nuclear Research, Dubna, Russia

S. Afanasiev, P. Bunin, M. Gavrilenko, I. Golutvin, I. Gorbunov, A. Kamenev, V. Karjavin, A. Lanev, A. Malakhov, V. Matveev[34,35], V. Palichik, V. Perelygin, S. Shmatov, S. Shulha, N. Skatchkov, V. Smirnov, N. Voytishin, A. Zarubin

JHEP03(2018)166

Petersburg Nuclear Physics Institute, Gatchina (St. Petersburg), Russia
Y. Ivanov, V. Kim[36], E. Kuznetsova[37], P. Levchenko, V. Murzin, V. Oreshkin, I. Smirnov, V. Sulimov, L. Uvarov, S. Vavilov, A. Vorobyev

Institute for Nuclear Research, Moscow, Russia
Yu. Andreev, A. Dermenev, S. Gninenko, N. Golubev, A. Karneyeu, M. Kirsanov, N. Krasnikov, A. Pashenkov, D. Tlisov, A. Toropin

Institute for Theoretical and Experimental Physics, Moscow, Russia
V. Epshteyn, V. Gavrilov, N. Lychkovskaya, V. Popov, I. Pozdnyakov, G. Safronov, A. Spiridonov, A. Stepennov, M. Toms, E. Vlasov, A. Zhokin

Moscow Institute of Physics and Technology, Moscow, Russia
T. Aushev, A. Bylinkin[35]

National Research Nuclear University 'Moscow Engineering Physics Institute' (MEPhI), Moscow, Russia
M. Chadeeva[38], P. Parygin, D. Philippov, S. Polikarpov, E. Popova, V. Rusinov

P.N. Lebedev Physical Institute, Moscow, Russia
V. Andreev, M. Azarkin[35], I. Dremin[35], M. Kirakosyan[35], A. Terkulov

Skobeltsyn Institute of Nuclear Physics, Lomonosov Moscow State University, Moscow, Russia
A. Baskakov, A. Belyaev, E. Boos, M. Dubinin[39], L. Dudko, A. Ershov, A. Gribushin, V. Klyukhin, O. Kodolova, I. Lokhtin, I. Miagkov, S. Obraztsov, S. Petrushanko, V. Savrin, A. Snigirev

Novosibirsk State University (NSU), Novosibirsk, Russia
V. Blinov[40], Y.Skovpen[40], D. Shtol[40]

State Research Center of Russian Federation, Institute for High Energy Physics, Protvino, Russia
I. Azhgirey, I. Bayshev, S. Bitioukov, D. Elumakhov, V. Kachanov, A. Kalinin, D. Konstantinov, V. Krychkine, V. Petrov, R. Ryutin, A. Sobol, S. Troshin, N. Tyurin, A. Uzunian, A. Volkov

University of Belgrade, Faculty of Physics and Vinca Institute of Nuclear Sciences, Belgrade, Serbia
P. Adzic[41], P. Cirkovic, D. Devetak, M. Dordevic, J. Milosevic, V. Rekovic

Centro de Investigaciones Energéticas Medioambientales y Tecnológicas (CIEMAT), Madrid, Spain
J. Alcaraz Maestre, M. Barrio Luna, M. Cerrada, N. Colino, B. De La Cruz, A. Delgado Peris, A. Escalante Del Valle, C. Fernandez Bedoya, J.P. Fernández Ramos, J. Flix, M.C. Fouz, P. Garcia-Abia, O. Gonzalez Lopez, S. Goy Lopez, J.M. Hernandez, M.I. Josa, A. Pérez-Calero Yzquierdo, J. Puerta Pelayo, A. Quintario Olmeda, I. Redondo, L. Romero, M.S. Soares, A. Álvarez Fernández

JHEP03(2018)166

Universidad Autónoma de Madrid, Madrid, Spain
J.F. de Trocóniz, M. Missiroli, D. Moran

Universidad de Oviedo, Oviedo, Spain
J. Cuevas, C. Erice, J. Fernandez Menendez, I. Gonzalez Caballero, J.R. González Fernández, E. Palencia Cortezon, S. Sanchez Cruz, I. Suárez Andrés, P. Vischia, J.M. Vizan Garcia

Instituto de Física de Cantabria (IFCA), CSIC-Universidad de Cantabria, Santander, Spain
I.J. Cabrillo, A. Calderon, B. Chazin Quero, E. Curras, M. Fernandez, J. Garcia-Ferrero, G. Gomez, A. Lopez Virto, J. Marco, C. Martinez Rivero, P. Martinez Ruiz del Arbol, F. Matorras, J. Piedra Gomez, T. Rodrigo, A. Ruiz-Jimeno, L. Scodellaro, N. Trevisani, I. Vila, R. Vilar Cortabitarte

CERN, European Organization for Nuclear Research, Geneva, Switzerland
D. Abbaneo, E. Auffray, P. Baillon, A.H. Ball, D. Barney, M. Bianco, P. Bloch, A. Bocci, C. Botta, T. Camporesi, R. Castello, M. Cepeda, G. Cerminara, E. Chapon, Y. Chen, D. d'Enterria, A. Dabrowski, V. Daponte, A. David, M. De Gruttola, A. De Roeck, E. Di Marco[42], M. Dobson, B. Dorney, T. du Pree, M. Dünser, N. Dupont, A. Elliott-Peisert, P. Everaerts, G. Franzoni, J. Fulcher, W. Funk, D. Gigi, K. Gill, F. Glege, D. Gulhan, S. Gundacker, M. Guthoff, P. Harris, J. Hegeman, V. Innocente, P. Janot, O. Karacheban[16], J. Kieseler, H. Kirschenmann, V. Knünz, A. Kornmayer[13], M.J. Kortelainen, C. Lange, P. Lecoq, C. Lourenço, M.T. Lucchini, L. Malgeri, M. Mannelli, A. Martelli, F. Meijers, J.A. Merlin, S. Mersi, E. Meschi, P. Milenovic[43], F. Moortgat, M. Mulders, H. Neugebauer, S. Orfanelli, L. Orsini, L. Pape, E. Perez, M. Peruzzi, A. Petrilli, G. Petrucciani, A. Pfeiffer, M. Pierini, A. Racz, T. Reis, G. Rolandi[44], M. Rovere, H. Sakulin, C. Schäfer, C. Schwick, M. Seidel, M. Selvaggi, A. Sharma, P. Silva, P. Sphicas[45], J. Steggemann, M. Stoye, M. Tosi, D. Treille, A. Triossi, A. Tsirou, V. Veckalns[46], G.I. Veres[18], M. Verweij, N. Wardle, W.D. Zeuner

Paul Scherrer Institut, Villigen, Switzerland
W. Bertl†, L. Caminada[47], K. Deiters, W. Erdmann, R. Horisberger, Q. Ingram, H.C. Kaestli, D. Kotlinski, U. Langenegger, T. Rohe, S.A. Wiederkehr

Institute for Particle Physics, ETH Zurich, Zurich, Switzerland
F. Bachmair, L. Bäni, P. Berger, L. Bianchini, B. Casal, G. Dissertori, M. Dittmar, M. Donegà, C. Grab, C. Heidegger, D. Hits, J. Hoss, G. Kasieczka, T. Klijnsma, W. Lustermann, B. Mangano, M. Marionneau, M.T. Meinhard, D. Meister, F. Micheli, P. Musella, F. Nessi-Tedaldi, F. Pandolfi, J. Pata, F. Pauss, G. Perrin, L. Perrozzi, M. Quittnat, M. Schönenberger, L. Shchutska, V.R. Tavolaro, K. Theofilatos, M.L. Vesterbacka Olsson, R. Wallny, A. Zagozdzinska[33], D.H. Zhu

Universität Zürich, Zurich, Switzerland
T.K. Aarrestad, C. Amsler[48], M.F. Canelli, A. De Cosa, S. Donato, C. Galloni, T. Hreus, B. Kilminster, J. Ngadiuba, D. Pinna, G. Rauco, P. Robmann, D. Salerno, C. Seitz,

JHEP03(2018)166

A. Zucchetta

National Central University, Chung-Li, Taiwan

V. Candelise, T.H. Doan, Sh. Jain, R. Khurana, C.M. Kuo, W. Lin, A. Pozdnyakov, S.S. Yu

National Taiwan University (NTU), Taipei, Taiwan

Arun Kumar, P. Chang, Y. Chao, K.F. Chen, P.H. Chen, F. Fiori, W.-S. Hou, Y. Hsiung, Y.F. Liu, R.-S. Lu, M. Miñano Moya, E. Paganis, A. Psallidas, J.f. Tsai

Chulalongkorn University, Faculty of Science, Department of Physics, Bangkok, Thailand

B. Asavapibhop, K. Kovitanggoon, G. Singh, N. Srimanobhas

Çukurova University, Physics Department, Science and Art Faculty, Adana, Turkey

A. Adiguzel[49], F. Boran, S. Damarseckin, Z.S. Demiroglu, C. Dozen, E. Eskut, S. Girgis, G. Gokbulut, Y. Guler, I. Hos[50], E.E. Kangal[51], O. Kara, A. Kayis Topaksu, U. Kiminsu, M. Oglakci, G. Onengut[52], K. Ozdemir[53], S. Ozturk[54], A. Polatoz, B. Tali[55], S. Turkcapar, I.S. Zorbakir, C. Zorbilmez

Middle East Technical University, Physics Department, Ankara, Turkey

B. Bilin, G. Karapinar[56], K. Ocalan[57], M. Yalvac, M. Zeyrek

Bogazici University, Istanbul, Turkey

E. Gülmez, M. Kaya[58], O. Kaya[59], S. Tekten, E.A. Yetkin[60]

Istanbul Technical University, Istanbul, Turkey

M.N. Agaras, S. Atay, A. Cakir, K. Cankocak

Institute for Scintillation Materials of National Academy of Science of Ukraine, Kharkov, Ukraine

B. Grynyov

National Scientific Center, Kharkov Institute of Physics and Technology, Kharkov, Ukraine

L. Levchuk, P. Sorokin

University of Bristol, Bristol, United Kingdom

R. Aggleton, F. Ball, L. Beck, J.J. Brooke, D. Burns, E. Clement, D. Cussans, O. Davignon, H. Flacher, J. Goldstein, M. Grimes, G.P. Heath, H.F. Heath, J. Jacob, L. Kreczko, C. Lucas, D.M. Newbold[61], S. Paramesvaran, A. Poll, T. Sakuma, S. Seif El Nasr-storey, D. Smith, V.J. Smith

Rutherford Appleton Laboratory, Didcot, United Kingdom

K.W. Bell, A. Belyaev[62], C. Brew, R.M. Brown, L. Calligaris, D. Cieri, D.J.A. Cockerill, J.A. Coughlan, K. Harder, S. Harper, E. Olaiya, D. Petyt, C.H. Shepherd-Themistocleous, A. Thea, I.R. Tomalin, T. Williams

JHEP03(2018)166

Imperial College, London, United Kingdom
R. Bainbridge, S. Breeze, O. Buchmuller, A. Bundock, S. Casasso, M. Citron, D. Colling, L. Corpe, P. Dauncey, G. Davies, A. De Wit, M. Della Negra, R. Di Maria, A. Elwood, Y. Haddad, G. Hall, G. Iles, T. James, R. Lane, C. Laner, L. Lyons, A.-M. Magnan, S. Malik, L. Mastrolorenzo, T. Matsushita, J. Nash, A. Nikitenko[6], V. Palladino, M. Pesaresi, D.M. Raymond, A. Richards, A. Rose, E. Scott, C. Seez, A. Shtipliyski, S. Summers, A. Tapper, K. Uchida, M. Vazquez Acosta[63], T. Virdee[13], D. Winterbottom, J. Wright, S.C. Zenz

Brunel University, Uxbridge, United Kingdom
J.E. Cole, P.R. Hobson, A. Khan, P. Kyberd, I.D. Reid, P. Symonds, L. Teodorescu, M. Turner

Baylor University, Waco, U.S.A.
A. Borzou, K. Call, J. Dittmann, K. Hatakeyama, H. Liu, N. Pastika, C. Smith

Catholic University of America, Washington DC, U.S.A.
R. Bartek, A. Dominguez

The University of Alabama, Tuscaloosa, U.S.A.
A. Buccilli, S.I. Cooper, C. Henderson, P. Rumerio, C. West

Boston University, Boston, U.S.A.
D. Arcaro, A. Avetisyan, T. Bose, D. Gastler, D. Rankin, C. Richardson, J. Rohlf, L. Sulak, D. Zou

Brown University, Providence, U.S.A.
G. Benelli, D. Cutts, A. Garabedian, J. Hakala, U. Heintz, J.M. Hogan, K.H.M. Kwok, E. Laird, G. Landsberg, Z. Mao, M. Narain, J. Pazzini, S. Piperov, S. Sagir, R. Syarif, D. Yu

University of California, Davis, Davis, U.S.A.
R. Band, C. Brainerd, D. Burns, M. Calderon De La Barca Sanchez, M. Chertok, J. Conway, R. Conway, P.T. Cox, R. Erbacher, C. Flores, G. Funk, M. Gardner, W. Ko, R. Lander, C. Mclean, M. Mulhearn, D. Pellett, J. Pilot, S. Shalhout, M. Shi, J. Smith, M. Squires, D. Stolp, K. Tos, M. Tripathi, Z. Wang

University of California, Los Angeles, U.S.A.
M. Bachtis, C. Bravo, R. Cousins, A. Dasgupta, A. Florent, J. Hauser, M. Ignatenko, N. Mccoll, D. Saltzberg, C. Schnaible, V. Valuev

University of California, Riverside, Riverside, U.S.A.
E. Bouvier, K. Burt, R. Clare, J. Ellison, J.W. Gary, S.M.A. Ghiasi Shirazi, G. Hanson, J. Heilman, P. Jandir, E. Kennedy, F. Lacroix, O.R. Long, M. Olmedo Negrete, M.I. Paneva, A. Shrinivas, W. Si, L. Wang, H. Wei, S. Wimpenny, B. R. Yates

University of California, San Diego, La Jolla, U.S.A.
J.G. Branson, S. Cittolin, M. Derdzinski, B. Hashemi, A. Holzner, D. Klein, G. Kole, V. Krutelyov, J. Letts, I. Macneill, M. Masciovecchio, D. Olivito, S. Padhi, M. Pieri,

JHEP03(2018)166

M. Sani, V. Sharma, S. Simon, M. Tadel, A. Vartak, S. Wasserbaech[64], J. Wood, F. Würthwein, A. Yagil, G. Zevi Della Porta

University of California, Santa Barbara - Department of Physics, Santa Barbara, U.S.A.

N. Amin, R. Bhandari, J. Bradmiller-Feld, C. Campagnari, A. Dishaw, V. Dutta, M. Franco Sevilla, C. George, F. Golf, L. Gouskos, J. Gran, R. Heller, J. Incandela, S.D. Mullin, A. Ovcharova, H. Qu, J. Richman, D. Stuart, I. Suarez, J. Yoo

California Institute of Technology, Pasadena, U.S.A.

D. Anderson, J. Bendavid, A. Bornheim, J.M. Lawhorn, H.B. Newman, T. Nguyen, C. Pena, M. Spiropulu, J.R. Vlimant, S. Xie, Z. Zhang, R.Y. Zhu

Carnegie Mellon University, Pittsburgh, U.S.A.

M.B. Andrews, T. Ferguson, T. Mudholkar, M. Paulini, J. Russ, M. Sun, H. Vogel, I. Vorobiev, M. Weinberg

University of Colorado Boulder, Boulder, U.S.A.

J.P. Cumalat, W.T. Ford, F. Jensen, A. Johnson, M. Krohn, S. Leontsinis, T. Mulholland, K. Stenson, S.R. Wagner

Cornell University, Ithaca, U.S.A.

J. Alexander, J. Chaves, J. Chu, S. Dittmer, K. Mcdermott, N. Mirman, J.R. Patterson, A. Rinkevicius, A. Ryd, L. Skinnari, L. Soffi, S.M. Tan, Z. Tao, J. Thom, J. Tucker, P. Wittich, M. Zientek

Fermi National Accelerator Laboratory, Batavia, U.S.A.

S. Abdullin, M. Albrow, G. Apollinari, A. Apresyan, A. Apyan, S. Banerjee, L.A.T. Bauerdick, A. Beretvas, J. Berryhill, P.C. Bhat, G. Bolla, K. Burkett, J.N. Butler, A. Canepa, G.B. Cerati, H.W.K. Cheung, F. Chlebana, M. Cremonesi, J. Duarte, V.D. Elvira, J. Freeman, Z. Gecse, E. Gottschalk, L. Gray, D. Green, S. Grünendahl, O. Gutsche, R.M. Harris, S. Hasegawa, J. Hirschauer, Z. Hu, B. Jayatilaka, S. Jindariani, M. Johnson, U. Joshi, B. Klima, B. Kreis, S. Lammel, D. Lincoln, R. Lipton, M. Liu, T. Liu, R. Lopes De Sá, J. Lykken, K. Maeshima, N. Magini, J.M. Marraffino, S. Maruyama, D. Mason, P. McBride, P. Merkel, S. Mrenna, S. Nahn, V. O'Dell, K. Pedro, O. Prokofyev, G. Rakness, L. Ristori, B. Schneider, E. Sexton-Kennedy, A. Soha, W.J. Spalding, L. Spiegel, S. Stoynev, J. Strait, N. Strobbe, L. Taylor, S. Tkaczyk, N.V. Tran, L. Uplegger, E.W. Vaandering, C. Vernieri, M. Verzocchi, R. Vidal, M. Wang, H.A. Weber, A. Whitbeck

University of Florida, Gainesville, U.S.A.

D. Acosta, P. Avery, P. Bortignon, D. Bourilkov, A. Brinkerhoff, A. Carnes, M. Carver, D. Curry, S. Das, R.D. Field, I.K. Furic, J. Konigsberg, A. Korytov, K. Kotov, P. Ma, K. Matchev, H. Mei, G. Mitselmakher, D. Rank, D. Sperka, N. Terentyev, L. Thomas, J. Wang, S. Wang, J. Yelton

Florida International University, Miami, U.S.A.

Y.R. Joshi, S. Linn, P. Markowitz, J.L. Rodriguez

JHEP03(2018)166

Florida State University, Tallahassee, U.S.A.

A. Ackert, T. Adams, A. Askew, S. Hagopian, V. Hagopian, K.F. Johnson, T. Kolberg, G. Martinez, T. Perry, H. Prosper, A. Saha, A. Santra, R. Yohay

Florida Institute of Technology, Melbourne, U.S.A.

M.M. Baarmand, V. Bhopatkar, S. Colafranceschi, M. Hohlmann, D. Noonan, T. Roy, F. Yumiceva

University of Illinois at Chicago (UIC), Chicago, U.S.A.

M.R. Adams, L. Apanasevich, D. Berry, R.R. Betts, R. Cavanaugh, X. Chen, O. Evdokimov, C.E. Gerber, D.A. Hangal, D.J. Hofman, K. Jung, J. Kamin, I.D. Sandoval Gonzalez, M.B. Tonjes, H. Trauger, N. Varelas, H. Wang, Z. Wu, J. Zhang

The University of Iowa, Iowa City, U.S.A.

B. Bilki[65], W. Clarida, K. Dilsiz[66], S. Durgut, R.P. Gandrajula, M. Haytmyradov, V. Khristenko, J.-P. Merlo, H. Mermerkaya[67], A. Mestvirishvili, A. Moeller, J. Nachtman, H. Ogul[68], Y. Onel, F. Ozok[69], A. Penzo, C. Snyder, E. Tiras, J. Wetzel, K. Yi

Johns Hopkins University, Baltimore, U.S.A.

B. Blumenfeld, A. Cocoros, N. Eminizer, D. Fehling, L. Feng, A.V. Gritsan, P. Maksimovic, J. Roskes, U. Sarica, M. Swartz, M. Xiao, C. You

The University of Kansas, Lawrence, U.S.A.

A. Al-bataineh, P. Baringer, A. Bean, S. Boren, J. Bowen, J. Castle, S. Khalil, A. Kropivnitskaya, D. Majumder, W. Mcbrayer, M. Murray, C. Royon, S. Sanders, E. Schmitz, R. Stringer, J.D. Tapia Takaki, Q. Wang

Kansas State University, Manhattan, U.S.A.

A. Ivanov, K. Kaadze, Y. Maravin, A. Mohammadi, L.K. Saini, N. Skhirtladze, S. Toda

Lawrence Livermore National Laboratory, Livermore, U.S.A.

F. Rebassoo, D. Wright

University of Maryland, College Park, U.S.A.

C. Anelli, A. Baden, O. Baron, A. Belloni, B. Calvert, S.C. Eno, C. Ferraioli, N.J. Hadley, S. Jabeen, G.Y. Jeng, R.G. Kellogg, J. Kunkle, A.C. Mignerey, F. Ricci-Tam, Y.H. Shin, A. Skuja, S.C. Tonwar

Massachusetts Institute of Technology, Cambridge, U.S.A.

D. Abercrombie, B. Allen, V. Azzolini, R. Barbieri, A. Baty, R. Bi, S. Brandt, W. Busza, I.A. Cali, M. D'Alfonso, Z. Demiragli, G. Gomez Ceballos, M. Goncharov, D. Hsu, Y. Iiyama, G.M. Innocenti, M. Klute, D. Kovalskyi, Y.S. Lai, Y.-J. Lee, A. Levin, P.D. Luckey, B. Maier, A.C. Marini, C. Mcginn, C. Mironov, S. Narayanan, X. Niu, C. Paus, C. Roland, G. Roland, J. Salfeld-Nebgen, G.S.F. Stephans, K. Tatar, D. Velicanu, J. Wang, T.W. Wang, B. Wyslouch

University of Minnesota, Minneapolis, U.S.A.

A.C. Benvenuti, R.M. Chatterjee, A. Evans, P. Hansen, S. Kalafut, Y. Kubota, Z. Lesko, J. Mans, S. Nourbakhsh, N. Ruckstuhl, R. Rusack, J. Turkewitz

JHEP03(2018)166

University of Mississippi, Oxford, U.S.A.

J.G. Acosta, S. Oliveros

University of Nebraska-Lincoln, Lincoln, U.S.A.

E. Avdeeva, K. Bloom, D.R. Claes, C. Fangmeier, R. Gonzalez Suarez, R. Kamalieddin, I. Kravchenko, J. Monroy, J.E. Siado, G.R. Snow, B. Stieger

State University of New York at Buffalo, Buffalo, U.S.A.

M. Alyari, J. Dolen, A. Godshalk, C. Harrington, I. Iashvili, D. Nguyen, A. Parker, S. Rappoccio, B. Roozbahani

Northeastern University, Boston, U.S.A.

G. Alverson, E. Barberis, A. Hortiangtham, A. Massironi, D.M. Morse, D. Nash, T. Orimoto, R. Teixeira De Lima, D. Trocino, D. Wood

Northwestern University, Evanston, U.S.A.

S. Bhattacharya, O. Charaf, K.A. Hahn, N. Mucia, N. Odell, B. Pollack, M.H. Schmitt, K. Sung, M. Trovato, M. Velasco

University of Notre Dame, Notre Dame, U.S.A.

N. Dev, M. Hildreth, K. Hurtado Anampa, C. Jessop, D.J. Karmgard, N. Kellams, K. Lannon, N. Loukas, N. Marinelli, F. Meng, C. Mueller, Y. Musienko[34], M. Planer, A. Reinsvold, R. Ruchti, G. Smith, S. Taroni, M. Wayne, M. Wolf, A. Woodard

The Ohio State University, Columbus, U.S.A.

J. Alimena, L. Antonelli, B. Bylsma, L.S. Durkin, S. Flowers, B. Francis, A. Hart, C. Hill, W. Ji, B. Liu, W. Luo, D. Puigh, B.L. Winer, H.W. Wulsin

Princeton University, Princeton, U.S.A.

A. Benaglia, S. Cooperstein, O. Driga, P. Elmer, J. Hardenbrook, P. Hebda, S. Higginbotham, D. Lange, J. Luo, D. Marlow, K. Mei, I. Ojalvo, J. Olsen, C. Palmer, P. Piroué, D. Stickland, C. Tully

University of Puerto Rico, Mayaguez, U.S.A.

S. Malik, S. Norberg

Purdue University, West Lafayette, U.S.A.

A. Barker, V.E. Barnes, S. Folgueras, L. Gutay, M.K. Jha, M. Jones, A.W. Jung, A. Khatiwada, D.H. Miller, N. Neumeister, C.C. Peng, J.F. Schulte, J. Sun, F. Wang, W. Xie

Purdue University Northwest, Hammond, U.S.A.

T. Cheng, N. Parashar, J. Stupak

Rice University, Houston, U.S.A.

A. Adair, B. Akgun, Z. Chen, K.M. Ecklund, F.J.M. Geurts, M. Guilbaud, W. Li, B. Michlin, M. Northup, B.P. Padley, J. Roberts, J. Rorie, Z. Tu, J. Zabel

JHEP03(2018)166

University of Rochester, Rochester, U.S.A.
A. Bodek, P. de Barbaro, R. Demina, Y.t. Duh, T. Ferbel, M. Galanti, A. Garcia-Bellido, J. Han, O. Hindrichs, A. Khukhunaishvili, K.H. Lo, P. Tan, M. Verzetti

The Rockefeller University, New York, U.S.A.
R. Ciesielski, K. Goulianos, C. Mesropian

Rutgers, The State University of New Jersey, Piscataway, U.S.A.
A. Agapitos, J.P. Chou, Y. Gershtein, T.A. Gómez Espinosa, E. Halkiadakis, M. Heindl, E. Hughes, S. Kaplan, R. Kunnawalkam Elayavalli, S. Kyriacou, A. Lath, R. Montalvo, K. Nash, M. Osherson, H. Saka, S. Salur, S. Schnetzer, D. Sheffield, S. Somalwar, R. Stone, S. Thomas, P. Thomassen, M. Walker

University of Tennessee, Knoxville, U.S.A.
A.G. Delannoy, M. Foerster, J. Heideman, G. Riley, K. Rose, S. Spanier, K. Thapa

Texas A&M University, College Station, U.S.A.
O. Bouhali[70], A. Castaneda Hernandez[70], A. Celik, M. Dalchenko, M. De Mattia, A. Delgado, S. Dildick, R. Eusebi, J. Gilmore, T. Huang, T. Kamon[71], R. Mueller, Y. Pakhotin, R. Patel, A. Perloff, L. Perniè, D. Rathjens, A. Safonov, A. Tatarinov, K.A. Ulmer

Texas Tech University, Lubbock, U.S.A.
N. Akchurin, J. Damgov, F. De Guio, P.R. Dudero, J. Faulkner, E. Gurpinar, S. Kunori, K. Lamichhane, S.W. Lee, T. Libeiro, T. Peltola, S. Undleeb, I. Volobouev, Z. Wang

Vanderbilt University, Nashville, U.S.A.
S. Greene, A. Gurrola, R. Janjam, W. Johns, C. Maguire, A. Melo, H. Ni, P. Sheldon, S. Tuo, J. Velkovska, Q. Xu

University of Virginia, Charlottesville, U.S.A.
M.W. Arenton, P. Barria, B. Cox, R. Hirosky, A. Ledovskoy, H. Li, C. Neu, T. Sinthuprasith, X. Sun, Y. Wang, E. Wolfe, F. Xia

Wayne State University, Detroit, U.S.A.
R. Harr, P.E. Karchin, J. Sturdy, S. Zaleski

University of Wisconsin - Madison, Madison, WI, U.S.A.
M. Brodski, J. Buchanan, C. Caillol, S. Dasu, L. Dodd, S. Duric, B. Gomber, M. Grothe, M. Herndon, A. Hervé, U. Hussain, P. Klabbers, A. Lanaro, A. Levine, K. Long, R. Loveless, G.A. Pierro, G. Polese, T. Ruggles, A. Savin, N. Smith, W.H. Smith, D. Taylor, N. Woods

†: Deceased
1: Also at Vienna University of Technology, Vienna, Austria
2: Also at State Key Laboratory of Nuclear Physics and Technology, Peking University, Beijing, China
3: Also at Universidade Estadual de Campinas, Campinas, Brazil
4: Also at Universidade Federal de Pelotas, Pelotas, Brazil

JHEP03(2018)166

5: Also at Université Libre de Bruxelles, Bruxelles, Belgium
6: Also at Institute for Theoretical and Experimental Physics, Moscow, Russia
7: Also at Joint Institute for Nuclear Research, Dubna, Russia
8: Now at Ain Shams University, Cairo, Egypt
9: Now at British University in Egypt, Cairo, Egypt
10: Now at Cairo University, Cairo, Egypt
11: Also at Université de Haute Alsace, Mulhouse, France
12: Also at Skobeltsyn Institute of Nuclear Physics, Lomonosov Moscow State University, Moscow, Russia
13: Also at CERN, European Organization for Nuclear Research, Geneva, Switzerland
14: Also at RWTH Aachen University, III. Physikalisches Institut A, Aachen, Germany
15: Also at University of Hamburg, Hamburg, Germany
16: Also at Brandenburg University of Technology, Cottbus, Germany
17: Also at Institute of Nuclear Research ATOMKI, Debrecen, Hungary
18: Also at MTA-ELTE Lendület CMS Particle and Nuclear Physics Group, Eötvös Loránd University, Budapest, Hungary
19: Also at Institute of Physics, University of Debrecen, Debrecen, Hungary
20: Also at Indian Institute of Technology Bhubaneswar, Bhubaneswar, India
21: Also at Institute of Physics, Bhubaneswar, India
22: Also at University of Visva-Bharati, Santiniketan, India
23: Also at University of Ruhuna, Matara, Sri Lanka
24: Also at Isfahan University of Technology, Isfahan, Iran
25: Also at Yazd University, Yazd, Iran
26: Also at Plasma Physics Research Center, Science and Research Branch, Islamic Azad University, Tehran, Iran
27: Also at Università degli Studi di Siena, Siena, Italy
28: Also at INFN Sezione di Milano-Bicocca; Università di Milano-Bicocca, Milano, Italy
29: Also at Purdue University, West Lafayette, U.S.A.
30: Also at International Islamic University of Malaysia, Kuala Lumpur, Malaysia
31: Also at Malaysian Nuclear Agency, MOSTI, Kajang, Malaysia
32: Also at Consejo Nacional de Ciencia y Tecnología, Mexico city, Mexico
33: Also at Warsaw University of Technology, Institute of Electronic Systems, Warsaw, Poland
34: Also at Institute for Nuclear Research, Moscow, Russia
35: Now at National Research Nuclear University 'Moscow Engineering Physics Institute' (MEPhI), Moscow, Russia
36: Also at St. Petersburg State Polytechnical University, St. Petersburg, Russia
37: Also at University of Florida, Gainesville, U.S.A.
38: Also at P.N. Lebedev Physical Institute, Moscow, Russia
39: Also at California Institute of Technology, Pasadena, U.S.A.
40: Also at Budker Institute of Nuclear Physics, Novosibirsk, Russia
41: Also at Faculty of Physics, University of Belgrade, Belgrade, Serbia
42: Also at INFN Sezione di Roma; Sapienza Università di Roma, Rome, Italy
43: Also at University of Belgrade, Faculty of Physics and Vinca Institute of Nuclear Sciences, Belgrade, Serbia
44: Also at Scuola Normale e Sezione dell'INFN, Pisa, Italy
45: Also at National and Kapodistrian University of Athens, Athens, Greece
46: Also at Riga Technical University, Riga, Latvia
47: Also at Universität Zürich, Zurich, Switzerland

JHEP03(2018)166

48: Also at Stefan Meyer Institute for Subatomic Physics (SMI), Vienna, Austria
49: Also at Istanbul University, Faculty of Science, Istanbul, Turkey
50: Also at Istanbul Aydin University, Istanbul, Turkey
51: Also at Mersin University, Mersin, Turkey
52: Also at Cag University, Mersin, Turkey
53: Also at Piri Reis University, Istanbul, Turkey
54: Also at Gaziosmanpasa University, Tokat, Turkey
55: Also at Adiyaman University, Adiyaman, Turkey
56: Also at Izmir Institute of Technology, Izmir, Turkey
57: Also at Necmettin Erbakan University, Konya, Turkey
58: Also at Marmara University, Istanbul, Turkey
59: Also at Kafkas University, Kars, Turkey
60: Also at Istanbul Bilgi University, Istanbul, Turkey
61: Also at Rutherford Appleton Laboratory, Didcot, United Kingdom
62: Also at School of Physics and Astronomy, University of Southampton, Southampton, United Kingdom
63: Also at Instituto de Astrofísica de Canarias, La Laguna, Spain
64: Also at Utah Valley University, Orem, U.S.A.
65: Also at Beykent University, Istanbul, Turkey
66: Also at Bingol University, Bingol, Turkey
67: Also at Erzincan University, Erzincan, Turkey
68: Also at Sinop University, Sinop, Turkey
69: Also at Mimar Sinan University, Istanbul, Istanbul, Turkey
70: Also at Texas A&M University at Qatar, Doha, Qatar
71: Also at Kyungpook National University, Daegu, Korea

JHEP03(2018)166